

Recombinant Expression of the NOD2 CARD2 Domain and Determination of the Solution Structure of Equine Alpha-Defensin 1 (DEFA1)

Dissertation
zur Erlangung des Doktorgrades
der Mathematisch-Naturwissenschaftlichen Fakultät
der Christian-Albrechts-Universität
zu Kiel

von
Mohammad Rasool Shomali

Kiel, 2012

Referent: Prof. Dr. Grötzinger

Korreferent: Prof. Dr. Matthias Leippe

Tag der mündlichen Prüfung: 05.12.2012

Zum Druck genehmigt:

Der Dekan

Table of contents

1	Introduction	1
1.1	The immune System	1
1.1.1	Innate Immune System	1
1.1.2	Pattern-Recognition Receptors	2
1.1.3	Nucleotide-Binding Oligomerization Domain Like Receptors (NLRs)	2
1.1.4	Nucleotide-Binding Oligomerization Domain-Containing Protein 2	3
1.1.5	The Caspase-Activating and Recruitment Domain (CARD)	6
1.2	Effector Substances of the Innate Immune System: Antimicrobial Peptides	8
1.2.1	Antimicrobial Peptides of the Horse	11
1.2.1.1	Equine Beta-Defensins	11
1.2.1.1	Equine Alpha-Defensins	12
1.3	Nuclear Magnetic Resonance Spectroscopy	13
1.3.1	Theory of NMR Spectroscopy	13
1.3.2	Protein NMR Spectroscopy	17
1.3.3	Homonuclear Two Dimensional NMR Spectroscopy	18
1.4	Aim of the Thesis	21
2	Materials and Methods	23
2.1	Cloning of the Human NOD2 CARD2 into pET-32a(+) Expression Vector	23
2.1.1	Restriction Digest	23
2.1.2	Ligation	25
2.1.3	Transformation of Chemically Competent <i>Escherichia coli</i> (<i>E.coli</i>) strain DH5-Alpha	25
2.1.4	PCR Cloning of TEV Protease Cleavage Site	26
2.2	Recombinant Protein Expression	28
2.2.1	Protein Expression of Trx-TEV-NOD2 CARD2 Fusion Protein in <i>E. coli</i> Strain BL21 (DE3)	28
2.2.2	Isolation of Inclusion Bodies	29
2.2.3	Purification and Renaturation of the Fusion Protein	29
2.2.4	Determination of Protein Concentration	30
2.2.5	Discontinuous SDS Polyacrylamide Gel Electrophoresis (SDS-PAGE)	30

2.2.6	Proteolytic Cleavage of Fusion Protein	32
2.2.7	Gradient Reverse Phase-High Performance Liquid Chromatography (RP-HPLC) and Lyophilization.....	32
2.2.8	Circular Dichroism (CD) Spectroscopy	33
2.2.9	Dynamic Light Scattering	34
2.3	NMR Spectroscopy.....	34
2.3.1	Preparation of Equine Alpha-Defensin (DEFA1) Sample for NMR Spectroscopy	34
2.3.2	Performance of 2D- ¹ H Homonuclear TOCSY and NOESY	34
2.3.3	Sequence-Specific Assignment	35
2.3.4	Structure Calculation.....	35
3	Results	37
3.1	NOD2 CARD2.....	37
3.1.1	Protein Expression.....	37
3.1.3	Purification of the Trx-TEV-NOD2 CARD2 Using Ni ²⁺ -NTA Agarose Beads under Denaturing Condition.	38
3.1.5	Renaturation of the Trx-TEV-NOD2 CARD2 Fusion Protein	40
3.1.6	Dynamic Light Scattering (DLS) of Fusion Protein.....	40
3.1.7	Cleavage of the Fusion Protein.....	41
3.1.8	Purification of the 23aa-NOD2 CARD2	44
3.1.9	Determination of the Secondary Structure of the 23-NOD2 CARD2 Using CD-spectroscopy	47
3.1.10	Dynamic Light Scattering of 23aa-NOD2 CARD2	49
3.1.11	NMR-Spectroscopy of the 23aa-CARD2 NOD2.....	51
3.2	Determination of the Three-Dimensional Structure of Equine DEFA1	53
3.2.1	Identification of the Spin Systems of DEFA1	53
3.2.2	Homonuclear Sequential Assignment.....	56
3.2.3	The Secondary Structure Elements of DEFA1.....	59
3.2.4	The Tertiary Structure of DEFA1.....	60
3.2.5	Structural Comparison of DEFA1 with other Alpha-defensin Family Members	66
4	Discussion.....	69

4.1	NOD2 CARD2.....	69
4.2	Equine Alpha-Defensin (DEFA1).....	72
4.3	Prospective	75
4.3.1	NOD2 CARD2.....	75
4.3.2	DEFA1	76
5	Summary.....	77
6	Zusammenfassung	78
7	References.....	80
8	Appendix.....	89
8.1	Abbreviations.....	89
8.2	Curriculum Vita	95
8.3	Posters and Publications.....	96
8.4	Acknowledgments	97
8.5	Declaration.....	98

1 Introduction

1.1 The immune System

The immune system is a system, which is composed of special cells, proteins, tissues, and organs that distinguishes host cells and tissues from foreign substances and provides protection against them.

Pathogens can rapidly change and acclimatize to escape detection and destruction by the immune system. Therefore, the immune system has to continuously evolve, develop and optimize multiple defense mechanisms to identify and neutralize pathogens. One of the systems that evolve is the innate immune system [1].

1.1.1 Innate Immune System

The innate immune system is the first line of defense, which contains many different types of cells, molecules and utilizes various mechanisms to protect host from pathogens and their toxins in a non-specific way [2]. The innate immunity is an evolutionarily ancient system of the host defense mechanisms. The same molecular modules were found in both plants and animals, indicating that it arose before the split of these two kingdoms [3].

Skin and the epithelia that line our internal organs are performing the first line of innate immune defense against attacking organisms (pathogens and commensal). The second line of defense is the innate immune cells, namely natural killer cells (NK cells); macrophages; dendritic cells (DCs); mast cells; neutrophils and eosinophils. These cells are able to recognize pathogens by their innate immune receptors and become active [2]. The adaptive immunity adds to the innate immune system a specific recognition of proteins, carbohydrates, lipids, nucleic acids, and pathogens [2].

1.1.2 Pattern-Recognition Receptors

The protection from infections needs complex immune responses involving the innate and the adaptive immune systems. The innate immune system has the key role in starting and arranging of host defenses by regulating the production of interferons, proinflammatory cytokines and antimicrobial effector molecules from the innate immune cells, which detect the pathogens by their innate immune receptors (pattern-recognition receptors (PRRs)).

Many different types of PRRs have been discovered and their functions in the sensing of pathogens and pathogen molecules have been exposed. These include the Toll-like receptors (TLRs), the C-type lectin receptors, the RIG-like helicases, the NOD-like receptors (NLRs), the cytosolic DNA sensors DAI6, RNA polymerase III and AIM2.

PRRs are expressed as transmembrane proteins or soluble in the cytosol. These receptors sense microbial pattern from bacteria, fungi, viruses and parasites. Activation of these receptors leads to trigger signaling pathways that regulate transcription of genes involved in the immune response, including nuclear factor (NF)-kappa B; mitogen-activated protein kinases (MAPKs); and the type I interferon (IFN) response [4], [5], [6], [7], [8], [9], [10], [11], [12]; [13].

Understanding of the innate immune response has been significantly improved after identification of many families of PRRs. The Toll receptors are the first identified family of PRRs. Toll receptors were discovered in the fruit fly and are located either at the cell surface or within endosomes [5], [14]. The human homologs are the Toll like receptors (TLRs). These innate immune proteins establish a family of transmembrane receptors, which detect microbial associated molecular patterns (MAMPs) and danger associated molecular patterns (DAMPs), like lipopolysaccharides (LPS), DNA, RNA, ATP and uric acid [15].

1.1.3 Nucleotide-Binding Oligomerization Domain Like Receptors (NLRs)

The NLRs are a cytosolic family of MAMP and DAMP sensors. NLRs composed of a leucine rich repeat domain (LRR) for MAMPs and DAMPs detecting, a central nucleotide

binding and oligomerization domain (NOD=NACHT) for nucleotide triphosphate (NTP) binding and oligomerization, and an N-terminal domain for signal induction; like caspase recruitment domain (CARD) or a Pyrin domain (PYD) [16], [15].

The human genome contains twenty-two *NLRs* genes. The NOD domain is the only common domain to all NLR family members [17]. The NLR family comprises three different subfamilies; the CARD-containing subfamily (NLRCs); like (NOD1-2), the Pyrin containing (NLRPs); such as (NLRP1-2) and the IPAF; like (NAIP), (figure 1.1) [17].

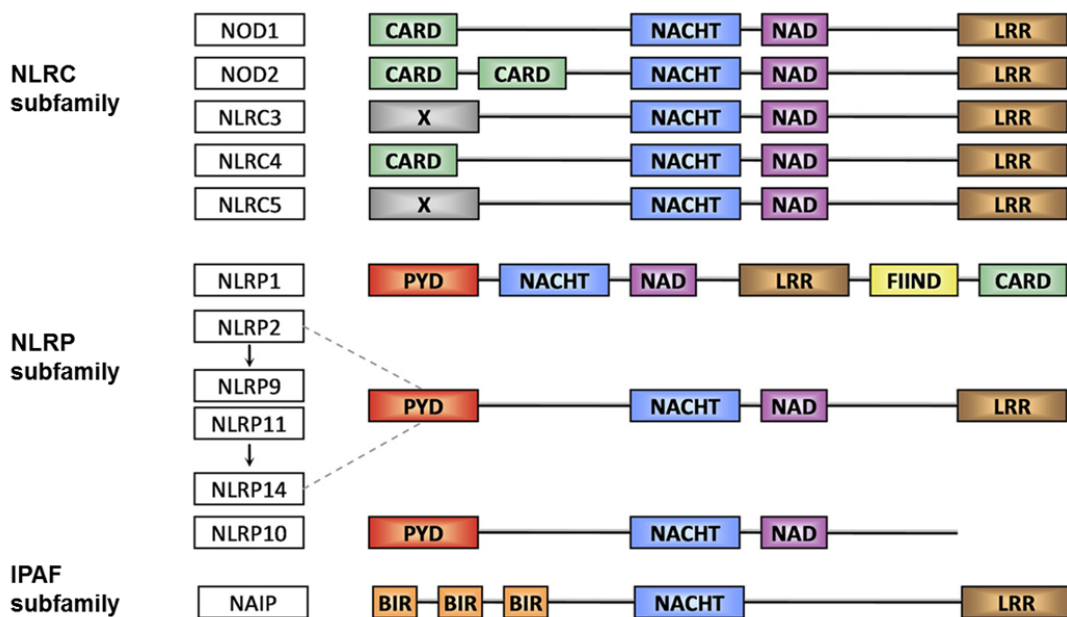


Figure 1.1: Domains arrangement of the NLR family. In human there are 22 members of NLR. The members have been categorized into different subfamilies NLRC, NLRP and IPAF. The NLR member consists of a variable N-terminal effector domain, a central domain NOD=NACHT, and an C-terminal LRR. NAD: NACHT=NOD-associated domain; X: Undefined domain; FIIND: Function-to-find domain; CIITA: MHC class II transactivator; AD: Acid transactivation domain; NAIP: Neuronal apoptosis inhibitor protein and BIR: Baculoviral inhibitory repeat [15].

1.1.4 Nucleotide-Binding Oligomerization Domain-Containing Protein 2

Nucleotide-binding oligomerization domain containing protein 2 (NOD2) is a member of NLRs family and belongs to NLRC superfamily. It functions as an intracellular receptor for the bacterial cell wall component muramyl dipeptide (MDP). NOD2 is also known as

caspace recruitment domain-containing protein 15 (CARD15) and inflammatory bowel disease protein 1 (IBD1). NOD2 was discovered twelve years ago [18] and is one of the most well studied members of the NLR family.

Of interest, polymorphisms of the *CARD15* gene, which encodes NOD2, are associated, among other diseases, with Crohn's disease [19]. NOD2 is expressed mainly in immune cells and in endothelial [20], [21].

Biochemical characterization of NOD2 indicates that it induces activation of NF-kappa B after stimulation in a TLR-independent manner [22], [23]. Further investigations revealed that NOD2 is the receptor for MDP. It is a molecule that originates from bacterial cell wall during synthesis and/or degradation of bacterial peptidoglycan (PGN) of the bacterial cell wall. MDP molecules are present in all Gram-positive and Gram-negative bacteria [24] [25].

According to the studies on other NLRs, it is widely believed that NOD2 undergoes a conformational change during activation, resulting in self-oligomerization, followed by recruitment and activation of the serine threonine kinase RICK, which is essential for activation of the NF-kappa B and MAPK signaling pathways [26]. It has been documented that *Rick* null cells and *Rick* knockout mice cannot activate NF-kappa B signaling downstream of NOD2, indicating that RICK is a crucial player for the induction of inflammatory responses [22], [27].

Mo *et al.* in 2012, could demonstrate using purified recombinant NOD2 that NOD2 binds directly to muramyl dipeptide and hydrolyzes ATP *in vitro* [28].

NOD2 possesses, additional to detecting bacterial pathogens, other vital functions. Recently, some studies have suggested that NOD2 signaling is required for the regulation of commensal microbiota [29], [30], induction of autophagy [31] and detection of single-stranded RNA (ssRNA) viruses. Activation of NOD2 by ssRNA leads to interferon regulatory factor 3 (IRF3)-dependent type I IFN secretion and antiviral immunity (figure 1.2) [32].

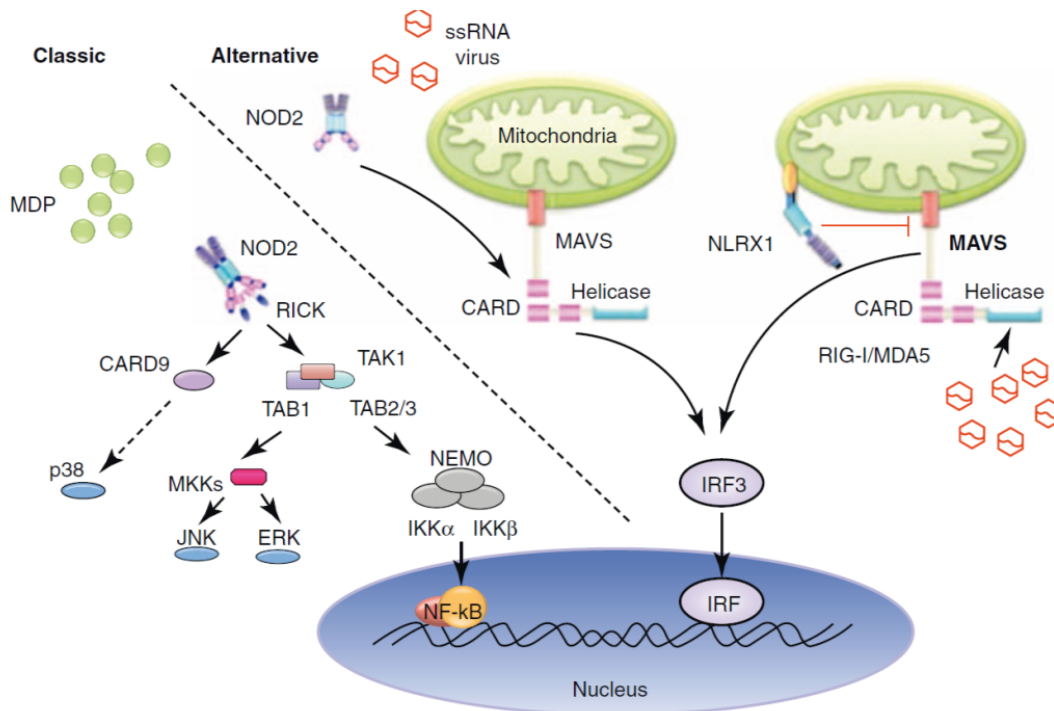


Figure 1.2: According to stimuli NOD2 signaling goes either classical or alternative pathway. Detection of MDP by NOD2 forces the signaling toward the classical pathway, which includes recruitment of the kinase RICK then followed by the activation of NF-kappa B, which leads to expression of inflammatory cytokines and antimicrobial peptides (AMPs). The alternative pathway contains ssRNA-viruses detection by NOD2. The ssRNA-NOD2 complex is translocated to mitochondria and interacts with mitochondrial antiviral-signaling protein (MAVS), resulted in activation of interferon regulatory factor 3 (IRF3), which leads to gene expression of IFN. The alternative pathway is RICK-independent [33].

Further studies showed that NOD2 plays a role in adaptive immune responses, in which MDP can induce the production of IL-17 from human memory CD4⁺ T cells, but not naive CD4⁺ T cells, in a NOD2-dependent manner. [34].

NOD2 comprises 1040 amino-acid residues. It possesses two N-terminal CARD domains (CARD1 and CARD2) for protein-protein interaction, one NOD=NACHT domain for NTP binding and oligomerization and one C-terminal LRR for detection of pathogens, (figure 1.3).

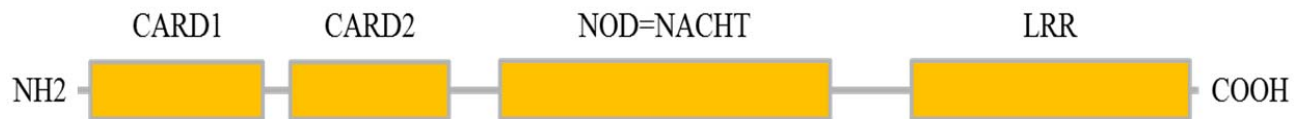


Figure 1.3: Schematic representation of NOD2 protein. NOD2 comprises two CARDs domain, for protein-protein interaction, NOD=NACHT domain for NTP-binding and oligomerization and LRR domain for MDP binding.

1.1.5 The Caspase-Activating and Recruitment Domain (CARD)

Hofmann and Bucher in 1997 denoted the name CARD for proteins, which is involved in the recruitment of caspases (a family of cysteine proteases that play essential roles in apoptosis, necrosis, and inflammation) to the receptor complexes signaling apoptosis [35]. CARD proteins are identified as a subfamily of Death Domain (DD) superfamily. DD superfamily members play an important role in the intracellular signaling of apoptosis and in inflammation.

DD superfamily covers four subfamilies, Caspase Recruitment Domain (CARD), Death Domain (DD), Death Effector Domain (DED) and Pyrin Domain (PYD). The DD superfamily is one of the biggest and most studied protein–protein interaction modules. The members of this superfamily play an essential role in inflammation, apoptosis, immune cell signaling pathways and necrosis [36].

The functional and structural similarities are the main character for specifying new members of DD superfamily. All of the DD superfamily members hold a typical six antiparallel alpha-helical bundle, which is named death fold. Members of DD superfamily can interact homotypic (within the same subclass to form dimer or trimer) or heterotypic (with other members of the superfamily) [37].

CARDs are involved in many signaling pathway; like regulation of caspase activity, activation of NF-Kappa B during the immune responses or function as intracellular caspase inhibitors [38],[39], [40].

According to associated domains and functional similarities, CARDs have been subdivided into four different subfamilies: (a) the NBD-CARDs; (b) the coiled-coil CARDs; (c) the bipartite CARDs; (d) and the CARD-only proteins.

CARDs are small protein of about 10 kDa. The RAIDD CARD was the first CARD structure that has been solved. The solution structure of RAIDD CARD consists of six-helix bundle with three helices vertically stacked on one side and the other three helices stacked to form the other side of the molecule. The six antiparallel amphipathic alpha helices are arranged firmly around the hydrophobic core of the RAIDD CARD protein [38].

NLR CARDs (like in NOD2) are involved in the apoptosis, NF-kappa B activation and formation of inflammasome [41], [39]. Zhou *et al.* determined the first NLR CARD solution structure (Apaf-I CARD). The solution structure of NOD1 CARD was solved in 2007 by Manon *et al.* Both structures (NOD1 CARD and Apaf-I CARD) contain six helices and they are similar to other CARDs of known structure (figure 1.4) [42], [43].

The CARD domains of NOD2 facilitated not only the interactions between activated NOD2 and other adaptor proteins but also possibly the homomerization of NOD2 [28].

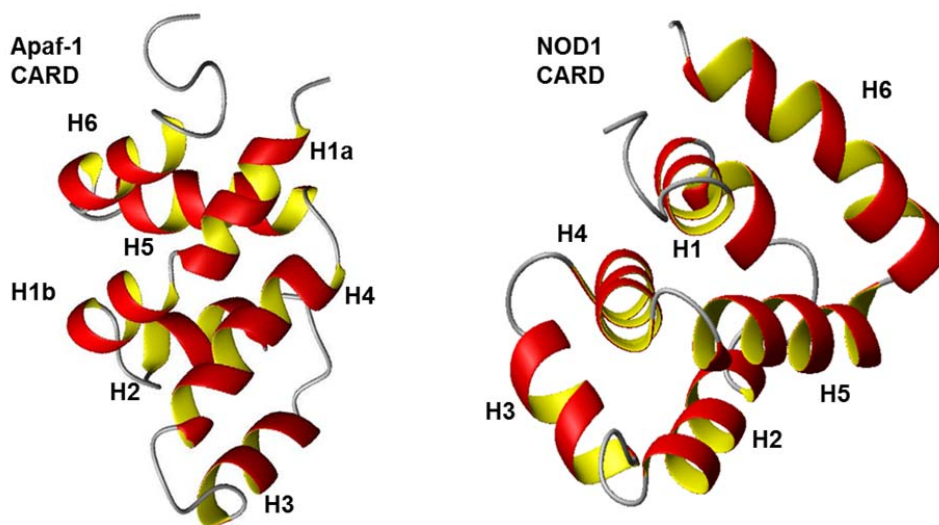


Figure 1.4: Solution structures of Apaf-1 CARD and NOD1 CARD presented in ribbon diagram. Both structures show the conserved six helices and they have the same orientation. The helices are numbered H1 to H6 accordingly. Apaf-1 CARD PDB ID code is 1C15 and NOD1 CARD PDB ID code is 2B1W.

Of particular interest, truncated NOD2, short isoform of NOD2 (NOD2-S), consisting of the first 126 amino acids of NOD2, is a key regulator of NOD2 activation in the colon. NOD2-S is specifically expressed in the human colon and its expression is up-regulated

by the expression of cytokine IL-10. Overexpression of NOD2-S down-regulates NOD2-induced NF-kappa B activation and IL-8 release. Furthermore, NOD2-S also affects the maturation and release of pro-IL-1 beta. This cytokine is a crucial player in inflammation, angiogenesis and tumors metastasis [44].

Therefore, it is of interest to set up a protocol for recombinant expression and purification of CARD2 to be the basis for functional investigations and structure determination. Investigation of this domain *in vitro* will help us better understanding the molecular mechanisms of NOD2.

1.2 Effector Substances of the Innate Immune System: Antimicrobial Peptides

The Antimicrobial peptides (AMPs) are small molecules, consist of 10 to 50 amino acids and are ancient weapons against pathogens. AMPs are a kind of innate immune responses against pathogens. They are largely dispersed in nature (in both animal and plant kingdom) and they form a distinctive amphipathic shape carrying positive charge [45]. Some of AMPs take the amphipathic shape after entering the membrane, like cecropin and magainin [46], [47].

According to their structure, AMPs are subdivided into three families: 1) linear alpha-helical peptides (cathelicidins), 2) beta-strand peptides connected by disulfide bonds (defensins), and 3) loop peptides (bactenecins) (figure 1.6) [48], [49], [50], [51]

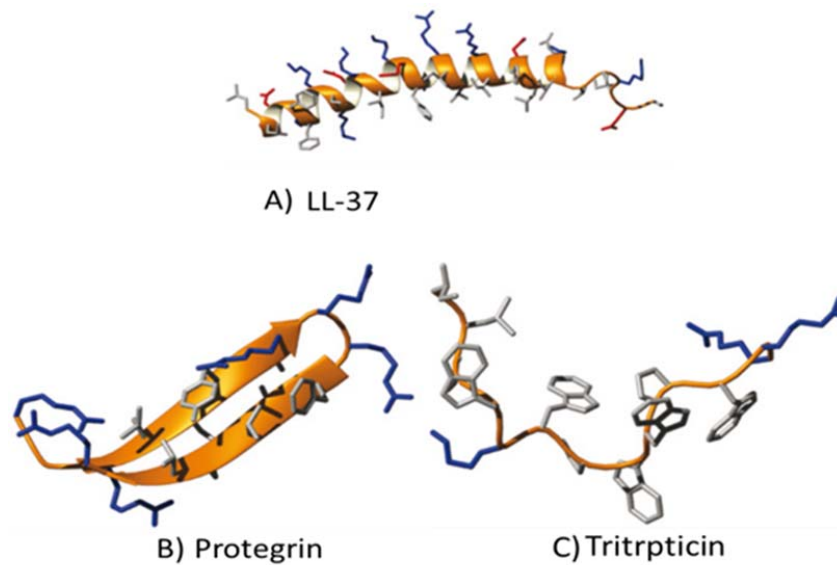


Figure 1.5: A summary of the structural based families of antimicrobial peptides: A) Alpha-Helical peptides, B) Beta-sheet peptides and C) Loop peptides. LL-37 and tritrpticin solution structures were solved in the presence of micelles, Protegrin structure was solved in aqueous solution. Blue is for positive charged side chain, red is for negative charged side chains and grey is for the remaining side chains [51].

In addition to killing pathogens, AMPs perform several other functions, such as endotoxin neutralizer, chemotaxis factors, induction of reactive oxygen species (ROS) formation, induction of wound healing, degranulation of mast cell, help in the opsonization process, complement inhibitor and as a transcriptional factor [52], [53], [54]. Therefore, AMPs also called host defense peptides (HDP) [55].

The major class of AMPs is the defensin family. Defensins are cationic, cysteine rich small molecules, which are 3 to 5 kDa and they are expressed in all multicellular organisms [56], [57]. The defensins are divided in 3 subfamilies, alpha-defensins, beta-defensins and theta-defensins. They have some common characters including small polypeptide sequences (from 18 to 45 amino acids), formation of 3 intramolecular disulfides bonds, lack of posttranslational modifications and turn-linked beta-strands as the most dominated features of their tertiary structures [58 440].

The first human alpha-defensin peptides were isolated and characterized by Ganz *et al.* (1985). They isolated three small peptides (molecular weight < 3,500) from human neutrophils and they were denoted as human neutrophil peptide (HNP) because of their

expression origin, HNP1-3. Of note, Ganz introduced the name defensins for such peptides. They exhibited antimicrobial activities against different strains of bacteria (*Staphylococcus aureus*, *Pseudomonas aeruginosa*, and *Escherichia coli*) [59].

To date, six alpha-defensins in human were identified HNP1-4 in neutrophil [60] and defensin 5 and 6 (HD-5 and HD-6) in Paneth cells of the small intestine [61]. Alpha-defensins possess six cysteine residues, which form three disulfide bonds. The disulfide bond pattern (Cys1–Cys6, Cys2–Cys4 and Cys3–Cys5) is the characteristic topology in alpha-defensin [62–64]. The overall charge ranges between +2 to +9 [63].

The beta-defensins are the second subfamily. In human, four beta-defensin peptides have been identified, termed human beta-defensins 1-4 (HBD1-4). Their expression, in contrast to alpha-defensin, is not limited to neutrophils and Paneth cells. HBD1-4 are broadly expressed in epithelial tissues, including skin, lung, urinary, oral epithelium and in neutrophils. Expression of beta-defensins is inducible and is usually up-regulated in response to activation of TLRs or in response to production of proinflammatory cytokines [64]. HDBs form 3 intramolecular disulfide bonds between Cys1–Cys5, Cys2–Cys4, and Cys3–Cys6 [65].

The third subfamily are the theta-defensins. Theta-defensins were first found in monocytes and neutrophils of the rhesus monkey [66]. In human, theta-defensin genes were identified; however, the genes contain premature stop codons that terminate their translation [67]. Theta-defensins have distinguished features from other types of defensin, they form cyclic polypeptide motif [68], and they are microbicidal in the occurrence of divalent cations, physiological concentrations of salt and serum [69], [70].

In addition to the antimicrobial properties, defensins play a role in immune modulation, wound healing and cell migration [71], [55].

Various models have been elaborated to explain how AMPs kill bacteria by rupturing bacterial membrane (figure 1.6). There are 3 proposed models suggesting that AMPs either form ion channels, pores or extensive disruption of the bacterial membrane: The first is the barrel-stave, the second is the toroidal (or worm-hole) and the third is the carpet model. Each model describes the permeabilization mechanisms of some of AMPs [72], [73], [74], [75].

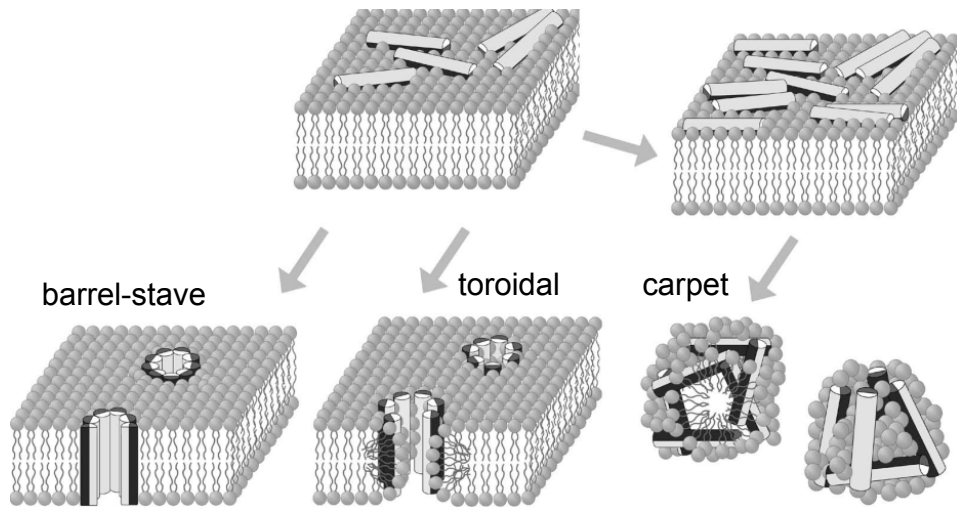


Figure 1.6: Schematic demonstration of the three major models elucidating the mechanisms of how AMPs (cationic amphipathic) interact with lipid bilayers and insert into it and result in rupturing the membrane. Hydrophilic and hydrophobic are represented in light grey and black respectively [76].

1.2.1 Antimicrobial Peptides of the Horse

Several antimicrobial peptides (AMPs) of equine have been identified either on mRNA and/or on protein level in many tissues of the horse [77]. In equine seven different antimicrobial peptide families have been identified and they are 1) Lysozyme [78], 2) Cathelicidin [79], 3) Hecpudin [80], 4) Neutrophil antimicrobial peptides [81], 5) NK-lysin [82], 6) Psoriasin [83] and 7) Defensin [83].

1.2.1.1 Equine Beta-Defensins

The first equine defensin (DEFB1) has been characterized by Davis *et al* [84]. The DEFB1 sequence is similar to the human HBD-2. DEFB1 shows the typical beta-defensin arrangement of disulfide bonds [84]. Many organs express DEFB1 (lung, spleen, kidney, liver, small intestine and heart) [84].

A transcriptional analysis with equine beta-defensin *DEFB1* revealed that *DEFB2* and *DEFB3* are copies of *DEFB1* [85]. The remaining beta defensins genes (*DEFL1*, *DEFL2*, *DEFL3* and *DEFB103*) were investigated by Bruhn (Ph.D. thesis) in 2008.

1.2.1.1 Equine Alpha-Defensins

Based on the sequence information for the equine BAC clone CHORI 241-245H5 (GenBank® Nucleotide Sequence Database accession number AY170305), Bruhn *et al.* (2007) showed using transcriptional analysis, that an equine small intestine transcript might be a potential equine alpha-defensin (*DEFA1*). The sequence of *DEFA1* is homologous to Paneth-cell alpha-defensins (*HD5*) from primates and rodents.

The peptide of *DEFA1* was expressed in *E.coli* and its biological activity was determined against different microorganisms [86]. The mechanism of action of *DEFA1* was investigated by studying the membrane-permeabilizing activity using viable bacteria and membrane models [86].

The predicted coding region of *DEFA1* is 297 nucleotides long. *DEFA1* peptide has 98 amino-acid residues, including the signal peptide and a prodomain. The mature peptide consists of 34 amino-acid residues (figure 1.7). *DEFA1* is the first equine alpha-defensin, which has been characterized in the *Laurasiatheria* [86].

**MRTLALLAAL LLLALQVQTQ SLEETADQVP AQDQPGAEAQ DITISFAGDE
RSAREASKSLIGTASCTCRR AWICRWGERH SGKCIDQKGS TYRLCCRR**

Figure 1.7: Primary structure of *DEFA1*. Blue is for the signal sequence, black is for peptide prodomain and red is for the mature *DEFA1*. The active peptide is thirty-four amino-acid residues. It is rich with arginine and contains six cysteine residues.

Further investigations of the repertoire of equine intestinal alpha-defensins using known alpha-defensin sequences as matrices revealed that 38 alpha-defensin transcripts are present in the equine intestine and at least twenty of them could code functional peptides [87]. The biological importance of expressing such a high number of different alpha-defensins in the horse intestine is still unclear. The authors claimed that the peptides may display various specificities against microorganisms or the intestinal tract needs different requirements for antimicrobial peptides through it and this may cause spatial expression patterns and sequential expression differences are also possible [87].

Schlüsselhuber *et al.* (2012) have evaluated the antibiotic activity of *DEFA1* peptide *in vitro* against *R. equi* and its associated pathogens. They found that *DEFA1* inhibits the

growth of *R. equi* and *S. zooepidemicus* and leads to their death by using low micromolar concentration. Of note, the bacteria needed much more generations to be less sensitive to DEFA1 compared to conventional antibiotics [88].

DEFA1, as mentioned above, is an equine alpha-defensin. The mature form of DEFA1 consists of 34 residues, which has a large repertoire and is a promising antibiotic peptide against resistant bacteria especially *R. equi* and *S. zooepidemicus*.

Therefore, the determination of DEFA1-structure will help to expose the mechanisms of action of this peptide and its structure will be a representative structure for other intestinal equine alpha-defensin.

1.3 Nuclear Magnetic Resonance Spectroscopy

The nuclear magnetic resonance (NMR) spectroscopy was first described in 1946 by Bloch and Purcell independently [89], [90]. NMR is a phenomenon of atoms that absorb radio-frequency electromagnetic radiation (RF) under the influence of a magnetic field. Years later, NMR was introduced as a second method for protein structure determination at atomic resolution beside crystallography [91].

1.3.1 Theory of NMR Spectroscopy

The idea of the NMR-spectroscopy technique is the usage of the magnetic properties of atomic nuclei to get chemical information of the respective nuclei. Only active nuclei are interesting from the NMR point of view. The active nuclei are defined as nuclei that need to have a property called spin.

The spin is a quantum mechanical character of atomic nuclei, like electrical charge or mass. Spin comes in multiples of 1/2 and can be + or -. From the nuclear spin of an atom, the magnetic moment (μ) can be calculated [92].

Nucleus with spin $I=1/2$ can have two nuclear spin states of different energy in the presence of an applied external magnetic field (two different μ states). Under the

influence of a static magnetic field B_0 , the spin takes two opposite arrangements according to the magnetic field axis and processes with respect to that axis. The state can be antiparallel to the magnetic field with low energy (α spin state) or parallel with high energy (β spin state). The energy difference (ΔE) between the spin states is proportional to the strength of B_0 (figure 1.8).

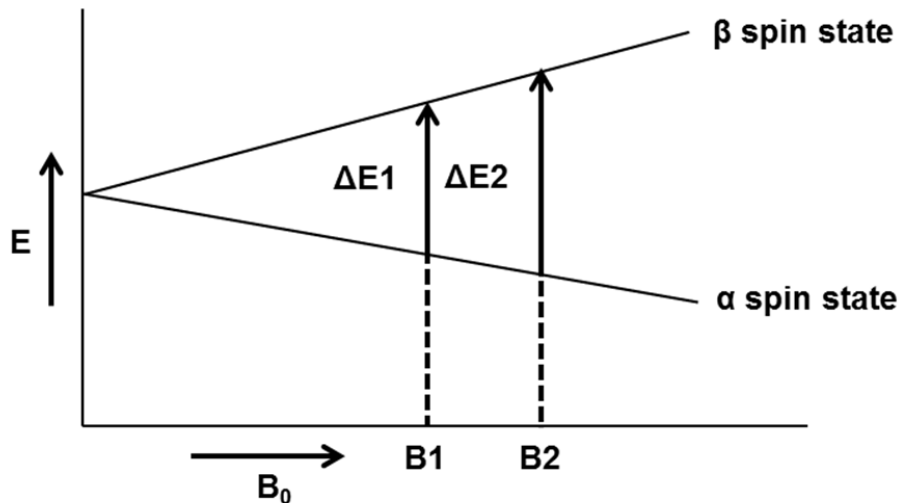


Figure 1.8: The figure shows the effect of the external magnetic field on nucleus spin states. In the presence of an external magnetic field the spins split into high energy state (β spin state) and low energy state (α state). The energy difference (ΔE) depends on the strength of the magnetic field (B_0) (modified figure, Lottspeich 1998).

The circulation of electrons, as a response to B_0 , produces an induced magnetic field (B_e) opposing the B_0 field. Therefore, the nucleus is slightly shielded by B_e field from the applied magnetic field B_0 and the difference between both magnetic fields ($B_0 - B_e$) represents the actual magnetic field experienced at the nucleus. The mathematical relationship between field and frequency is shown by equation 1.

$$\Delta E = h\nu = h(B_0 - B_e)\gamma$$

Equation 1

where: ΔE : Energy difference between spin states, h : Planck's constant, ν : The frequency of the applied magnetic field, B_e : The strength of the induced magnetic field, B_0 : The strength of the external magnetic field and γ : Gyromagnetic constant.

The precession frequency (ν) can be calculated by dividing equation 1 by h .

$$\nu = (B_0 - B_e)\gamma$$

Equation 2

The frequency of the precession is also called Larmor frequency, which is proportional to the strength of the external magnetic field and the gyromagnetic constant of the nucleus.

In NMR spectroscopy, chemical shifts for nuclei of interest are detected. The chemical shift is the frequency of absorption for a nucleus relative to the frequency of absorption of a molecular standard like tetramethylsilane (TMS). The chemical shifts of the same atoms in one molecule vary due to differences of the chemical environment of the atoms in the molecule. Therefore, many shifts appear on the spectrum for atoms of the same type. The chemical shift, abbreviated by δ , is expressed in parts per million (ppm) and it is calculated from:

$$\delta = (\nu - \nu_{\text{TMS}}) / \nu_0$$

Equation 3

- $(\nu - \nu_{\text{TMS}})$ is the difference between resonance frequency and that of the reference.
- ν_0 is the operating frequency of the spectrometer.

The chemical shifts are the main source of information in NMR-spectra [93].

Structuring of the amino acid chain by formation of secondary and tertiary structure in peptides and proteins is the main factors for occurrence of chemical shifts.

If a NMR-sample is placed in a homogenous magnetic field, the spins of the atoms split according to the occupancy of the energy level of the atoms. The low energy alpha-state is favored here. The energy states of the spins can be changed by irradiation of the sample using radio frequency-pulses.

In NMR spectroscopy, sample of condensed matter are investigated (not a free spin with a magnetic moment). The sample (like ^1H with $I=1/2$) includes a very large number of nuclei with magnetic moments. Therefore, the magnetic moments of the individual nuclear spins of a sample can be added up to a total magnetization M_0 , which can be graphically represented as a vector model. In thermodynamic equilibrium, the macroscopic M_0 is present parallel to the external magnetic field (B_0), figure 1.9 left.

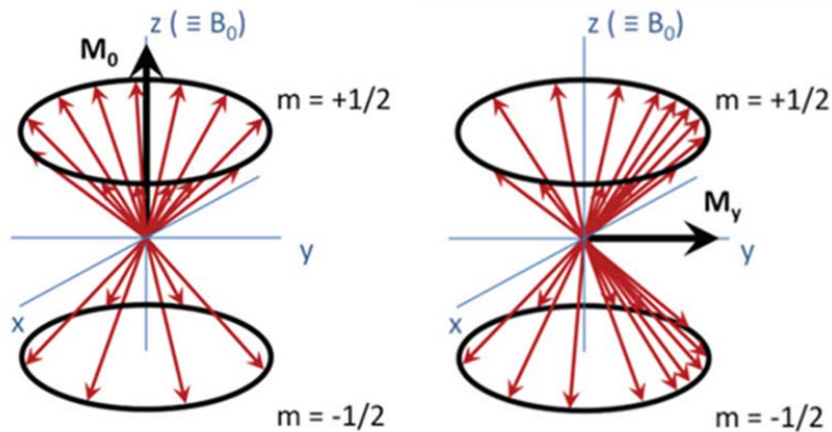


Figure 1.9: The magnetization can be changed from M_0 to M_y by irradiation the nuclei with RF 90° -pulses. Left: In the thermodynamic equilibrium, the M_0 is parallel to B_0 . Right: RF with 90° -pulse changes the direction from M_0 to M_y (modified figure, Lottspeich 1998).

If the nuclei are irradiated with radio frequency (RF) pulses along the x-axis, this would induce a transverse magnetic field B_1 in the xy-plane. If the used RF corresponds to the resonance frequency of the nuclei, it will follow a rotation of the magnetization M_0 to the radiation axis in the xy plane. The M_0 magnetization can be completely changed to M_y magnetization by using corresponding RF-pulses, (figure 1.9 right). Such pulse is called 90° -pulse. The change in the total magnetization (from M_0 to M_y) as a result of the irradiation by RF leads to the induction of an electric current, which can be detected by the inductor of the NMR spectrometer.

The change to M_y magnetization is a temporary state. The system attempts to return to its initial thermodynamic equilibrium state (M_0). This effect is called relaxation, which is identified by the longitudinal relaxation time (T_1) and the transverse relaxation time (T_2). The T_1 relaxation involves redistributing the spins to reach the thermodynamic equilibrium and depends on the external field strength (B_0). The transverse relaxation time T_2 corresponds to decoherence of the transverse spins magnetization (i.e. loss of the spin-spin interactions) and be influenced by the molecular weight of the sample. For large molecules T_2 -relaxation is much smaller than T_1 -relaxation and therefore, T_2 -relaxation has a limiting effect on the life time of the NMR-signals. Due to T_2 -relaxation, the NMR-signal is measured as a damped oscillation, which is called free induction decay (FID) [92].

Nowadays all modern NMR spectrometers are using the pulse technique. In which, a single radio frequency pulse (RF-pulse) or a sequence of RF pulses is sent to a sample that is located in a strong magnetic field. The FID signal following a pulse sequence is registered as a function of time. By Fourier-transformation, the time signal is transformed into a frequency domain signal on the spectrum.

The simplest and the most common used NMR-experiment is the one-dimensional NMR spectroscopy (1D-NMR), figure 1.10.

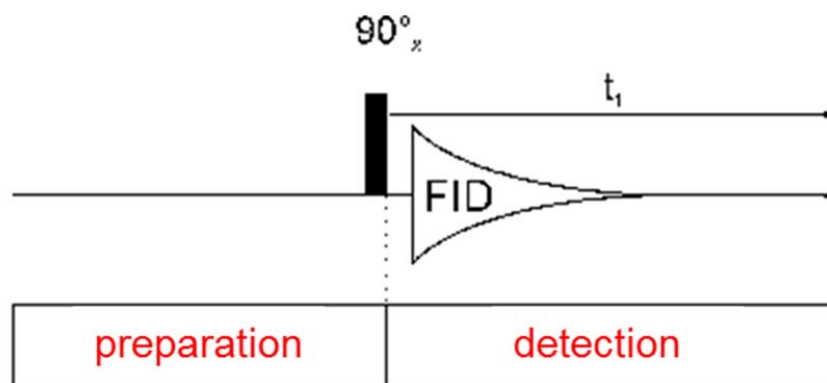


Figure 1.10: Scheme of a 1D-NMR experiment. The experiment consists of preparation and detection phase, which are separated by 90° -pulse. The FID is detected during t_1 and transformed to frequency domain spectrum (modified figure, Lottspeich 1998).

The 1D-Fourier-transformation-spectroscopy experiment consists of two phases, the preparation and the detection. The simplest of such experiment is when the preparation phase is comprised of a single 90° -pulse, which turns the total magnetization from M_0 to M_y . In the detection phase, due to T_2 relaxation time an electric current is induced and detected as FID, which is transformed to frequency domain by Fourier-transformation [91].

1.3.2 Protein NMR Spectroscopy

NMR spectroscopy (beside crystallography) is a widely used method for three-dimensional structure determination of proteins. Wüthrich introduced this method to study the protein structures in solution [94].

To determine a protein structure by NMR spectroscopy, very complex NMR-experiments are needed. 1D-NMR spectroscopy provides only general information about the quality of the sample. Therefore, 2D and 3D-NMR-experiments are used. The protein size determines if the NMR-experiments have to be homonuclear or heteronuclear (i.e. labeling the protein sample with C and/or N isotopes) [94].

1.3.3 Homonuclear Two Dimensional NMR Spectroscopy

2-dimensional ($2D-^1H$) homonuclear NMR-experiments are used to determine the structure of small proteins (<10 kDa). Homonuclear means that magnetization transfer occurs between nuclei of the same type. 2D-experiment involves applying a sequence of RF-pulses with delay periods in between them. The intensities, frequencies, and timing of these pulses distinguish 2D-NMR-experiments from each other.

Almost all 2D-experiments consist of 4 periods: the preparation period, where a magnetization coherence is produced by applying of a set of RF pulses; the evolution period, where a determined length of time during which no pulses are applied and the spins are allowed to rotate; the mixing period, where the coherence is manipulated by another series of pulses into a state which will give an observable signal; and the last period is the detection, in which the FID signal is detected and recorded as a function of time [92], figure 1.11. The recorded FID is translated to frequency domain, which can be seen on the NMR-spectrum.

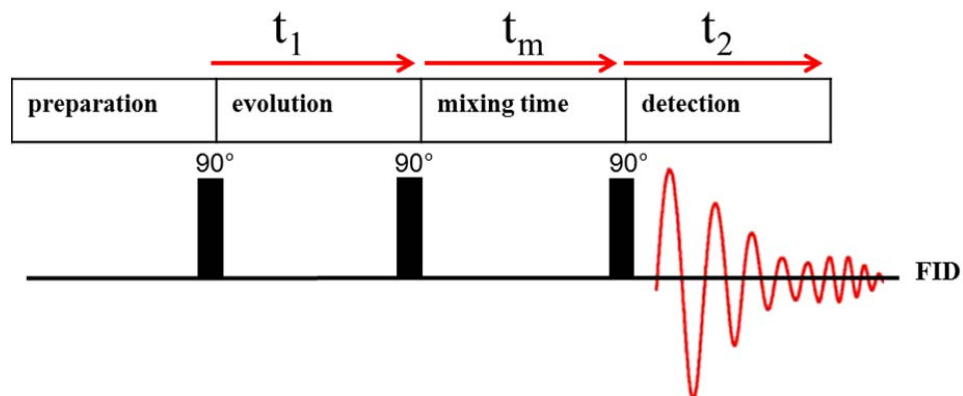


Figure 1.11: 2D-NMR-experiment schemes. On the top is the general schematic of a 2D-NMR-experiment, it consists of four blocks. Bottom: Schematic representation of the 2D-NOESY-experiment in which a total of three 90° pulses are irradiated. During the detection phase the FID is recorded as a function of time (modified figure, Lottspeich 1998).

Through repetitions of the experiment, each new repeated experiment will have specific evolution time. In these successive experiments, we obtain a series of 1D-spectra, which are gradually changing the magnetization that is detected during the evolution phase. A further FID-signal appears as a result of increasing the evolution time. The new FID-signal is translated to frequency domain and the final 2D-spectrum is finished.

Homonuclear TOCSY (Total Correlation Spectroscopy) and NOESY (Nuclear Overhauser Effect Spectroscopy) are the essential 2D-NMR-experiments, which are used for homonuclear structure determination.

In the homonuclear 2D-TOCSY-experiment, the protons are coupled with each other over scalar coupling. If magnetization occurs between protons, it appears as a cross-peak signal.

The TOCSY-spectrum facilitates the identification of a present amino-acid residue. The magnetization goes gradually from a start proton and due to scalar coupling over all the protons in this amino-acid residue. Thus, the correlation between the start proton and the sequence of all up to three atomic bonds of one amino-acid residue can be observed. The correlation of all protons of a residue is defined as the spin system. The spin system is a total chemical shift of all protons existing in an amino acid (alpha, beta and side chain), figure 1.12.

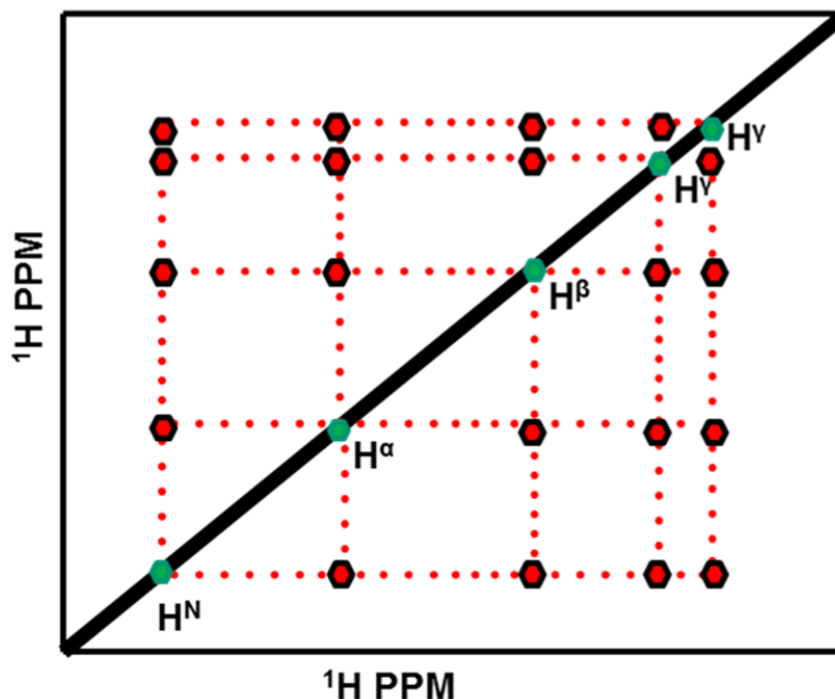


Figure 1.12: Illustration of diagonal signals and cross peaks for a spin system in a TOCSY experiment. When nuclei coupled with each other in 2D-NMR experiment, cross-peak signals will be detected (red point with black line). Green points represent the resonance of protons on the diagonal in the NMR-spectrum.

In NOESY-experiment, the magnetization transfer bases on the nuclear overhauser effect (NOE). The magnetization is transferred over space due to dipolar interaction of spins and this is dipolar coupling. This coupling can be detected if the nuclei are closed to each other in the space (the distance has to be smaller than 5 Å). The intensity of the cross-peak signals is proportional to distance between the protons in the space. The relation between intensity of the cross-peak signal and the distance is shown in equation 4.

$$v(\text{intensity}) = 1/r^6$$

Equation 4

where r is the distance between two nuclei undergoing cross-relaxation.

The most important information obtained from NOESY-experiment for determination of protein structures are depicted in figure 1.13. In NOESY-experiment, the correlation of different groups of protons can be detected. On the upper left side of the figure the

correlation between amide, aliphatic and alpha-protons can be detected, while at the bottom, the correlation between amide protons is observed.

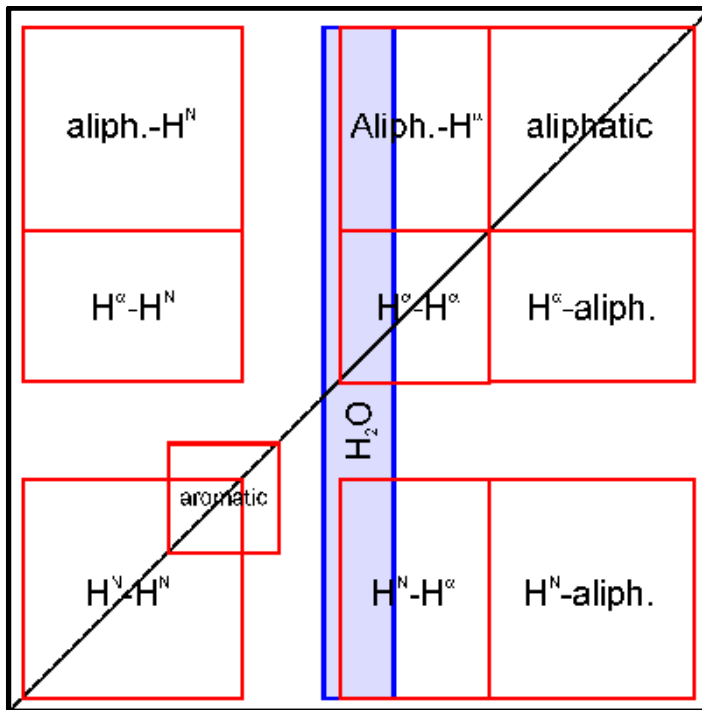


Figure 1.13: Arrangement of magnetization transfer for a 2D- ^1H -NOESY-experiment in H_2O . It shows the correlating chemical shift coordinates to proton-proton magnetization transfer [93].

1.4 Aim of the Thesis

Nucleotide-binding oligomerization domain-containing protein 2 (NOD2) is one of the best studied nucleotide-binding oligomerization domain like receptors (NLRs). NOD2 is important for innate immune response, autophagy, regulation of commensal microbiota and viral immunity [33].

Furthermore, the short isoform of NOD2 (NOD2-S) plays an important role in the regulation of NOD2 activity in the intestine [44]. NOD2 protein contains CARDs domains that are predicted to have a role in protein-protein interaction. However homotypic and heterotypic interactions of NOD2 CARDs domains are yet to be identified *in vitro*.

DEFA1 is a thirty-four amino acids long equine intestinal alpha-defensin, which has a large repertoire in equine intestine and display a broad spectrum against Gram-positive, Gram-negative bacteria and against yeast [87].

DEFA1 becomes interesting after discovery of its potential as a promising antibiotic peptide drug especially against *R. equi* and *S. zooepidemicus*. Determination of the three dimensional structure of DEFA1 peptide will help in illustrating the mechanism of action of this peptide and its structure will be the representative structure for other equine intestinal alpha-defensins. Of particular interest, DEFA1 will be the first equine alpha-defensin structure, which to be determined.

The specific aims of this thesis are:

- 1** To establish a protocol for expression, renaturation and purification of NOD2 CARD2. Such protocol will enable the production of sufficient amount of a purified protein for tertiary structure determination and will also facilitate investigation of the homotypic and heterotypic interactions of NOD2 CARD2.
- 2** To determine the solution structure of the equine alpha-defensin (DEFA1) and compare its structure to structures of other AMPs to better understand its mode of action.

2 Materials and Methods

2.1 Cloning of the Human NOD2 CARD2 into pET-32a(+) Expression Vector

2.1.1 Restriction Digest

In order to clone the human NOD2 CARD2 as a thioredoxin fusion protein into the pET-32a(+) bacterial expression vector (Novagen, Merck KGaA, Darmstadt, Germany), the human NOD2 CARD2 cDNA (codon-optimized for bacterial expression) was ordered from GeneArt (Regensburg, Germany). The cDNA was flanked with *KpnI* and *XhoI* restriction sites at N- and C-terminus respectively. The human NOD2 CARD2 cDNA comprised the His-tag and the enterokinase cleavage site to simplify further working steps.

The size of the cDNA was 369 base pairs (bp) long. Figure 2.1 shows the amino-acid sequence of the ordered cDNA. The red letters represent His-tag, green letters represent enterokinase cleavage site, blue letters represent amino acid residues derived from the expression vector and black letters represent the sequence of human NOD2 CARD2

MGSSHHHHHSSGDDDKHPARDLQSHRPAIVRRLHSHVENMLDLAWERG
FVSQYECDEIRLPIFTSPQRARLLDLATVKANGLAAFLQHVQELPVPL
ALPLEAATCKKYMAKLR

Figure 2.1: The amino acid sequence of the human NOD2 CARD2. Blue letters represent the amino acid residues derived from pET-32a(+), red is for His-tag, green letters represent the enterokinase cleavage site, black letters represent the human NOD2 CARD2.

To clone the human NOD2 CARD2 cDNA into the bacterial expression vector pET-32a(+), the vector and human NOD2 CARD2 cDNA were digested using *KpnI* and *XhoI* restriction enzymes (Fermentas GmbH, Leon-Rot). For restriction digestion 1.5 µg human NOD2 CARD2 cDNA and 1.0 µg vector were used and the reaction was done using 2X Tango buffer (Fermentas GmbH, Leon-Rot, Germany).

The followings were placed in a clean 1.5 ml tubes:

	Human NOD2 CARD2	pET-32a(+)
DNA	15 μ l (0.1 μ g/ μ l)	2 μ l (0.5 μ g/ μ l)
Buffer (10X Tango)	5 μ l	5 μ l
<i>Kpn</i> I	2 μ l	2 μ l
<i>Xho</i> I	2 μ l	2 μ l
Water	26 μ l	39 μ l
Total	50 μ l	50 μ l

The reaction mixtures were mixed by tapping, centrifuged in a Eppendorf bench-top centrifuge (Eppendorf AG, Hamburg, Germany) and incubated at 37 °C overnight in a thermomixer compact (Eppendorf AG, Hamburg, Germany). The mixtures were separated on 1% agarose gel (Carl Roth GmbH, Karlsruhe, Germany) in 1X TBE buffer for 30 min at 100 V. The electrophoresis was applied using Sub-Cell[®] GT systems (Bio-Rad Laboratories, Inc, USA). The agarose gel was stained in 1% ethidium bromide (EtBr) bath (Carl Roth GmbH, Karlsruhe, Germany) and the fragments were detected under ultraviolet light at 230 nm. The fragments with the corresponding sizes were cut and isolated from the agarose gel using gel extraction kit (Nucleo Spin Extract II, Macherey-Nagel, Dueren, Germany). The image of the agarose gel was documented using gel documentation system (Bio-Rad Laboratories, Inc, USA).

1% agarose gel

1g agarose

100 ml 1x TBA

1xTris-borate-EDTA (TBE) buffer

10 g TRIS

5.5 g boric acid

4 ml 0.5 M EDTA

Top up the solution to a final volume of 1000 ml with distilled water (dH₂O).

2.1.2 Ligation

Ligation is the process of the formation of phosphodiester bonds in the presence of ATP between double- stranded DNAs with 3'-hydroxyl and 5'-phosphate termini [95].

The digested vector and cDNA were both resuspended in an appropriate volume of clean water. The followings were added in a 0.2 ml reaction tube:

Digested cDNA (insert fragment)	5 μ l
Digested vector (pET-32a(+))	1.5 μ l
T4 ligase (Fermentas GmbH, Leon-Rot, Gemany)	1 μ l 10 U/ μ l
T4 ligase buffer (Fermentas GmbH, Leon-Rot, Gemany)	2 μ l
Water	10.5 μ l
Total	20 μ l

The reaction mixture was mixed, quick centrifuge and incubated 16 hours at 17 °C.

2.1.3 Transformation of Chemically Competent *Escherichia coli* (*E.coli*) strain DH5-Alpha

To produce high amount of expression plasmid for further use, chemically competent *E.coli* strain DH5-alpha cells (Novagen [Merk KGaA], Darmstadt, Germany) were used, [96]. The cells were transformed using heat shock transformation method [97].

To transform the cells, 50 μ l of the chemically competent cells were mixed with 10 μ l of ligation mixture. The cells were incubated on ice for 10 min followed by exposing them to 42 °C for 2 min. Immediately after 2 min, the cells were incubated on ice for further 5 min, followed by addition of 1000 μ l of pre-wormed LB medium (without antibiotic) and incubated at 37 °C for 1 hour. 100 μ l of the culture was plated on ampicillin (Carl Roth GmbH, Karlsruhe, Germany) (100 μ g/ml) containing agar plate. The colonies were scored and 2 colonies were selected and further propagated.

The plasmid DNA was purified using plasmid isolation kit (Nucleo Spin, Plasmid Quick Pure, Macherey-Nagel, Dueren, Germany) and sequenced using T7-promoter and T7-terminator primers by GATC company (GATC, Konstanz , Germany). The two clones

showed no mutation. One of these clones was further propagated to produce large amount of plasmid. The plasmid was purified using the kit Nucleobond PC 500 (Nucleobond PC 500, Macherey-Nagel, Dueren, Germany).

2.1.4 PCR Cloning of TEV Protease Cleavage Site

TEV cleavage site was cloned into the pET-32a(+)-NOD2-CARD2 using Polymerase Chain Reaction (PCR) technique [98]. PCR reaction was performed using a site-specific forward primer containing the nucleotide sequence of the TEV protease cleavage site and a *HindIII* restriction site as well as a specific reverse primer containing *XhoI* and a stop codon.

In a PCR tube (0.2 ml) the followings were added:

DNA template (pET-32(+a)-NOD2-CARD2)	3 μ l (10ng/ml)
Forward primer	1.5 μ l (10 pmol/ μ l)
Reverse primer	1.5 μ l (10 pmol/ μ l)
dNTPs (Fermentas GmbH, Leon-Rot, Gemany)	1 μ l (10 mmol/ μ l)
PCR buffer (Fermentas GmbH, Leon-Rot, Gemany)	5 μ l
<i>pfu</i> -Polymerase (Fermentas GmbH, Leon-Rot, Gemany)	1 μ l
Clean water	37. μ l
Total	50 μ l

The reaction was then cycled in a Biometra personal cyler (Biometra biomedizinische Analytik GmbH Goettingen, Germany) using the following parameters:

95 °C	120 sec	1x
95 °C	30 sec	4x
54 °C	40 sec	4x
72 °C	60 sec	4x
95 °C	30 sec	30x
66 °C	40 sec	30x
72 °C	60 sec	30x
72 °C	600 sec	1x

Next, the PCR mixture was separated on a 1% agarose gel, purified from the gel and digested using *Hind*III and *Xho*I in Red reaction buffer (Fermentas GmbH, Leon-Rot, Germany). The expression plasmid pET-32a(+) was digested using the same restriction enzymes. The digested PCR fragment and the digested vector were isolated from the agarose gel and ligated with each other.

The ligation mixture contained:

Digested PCR fragment	10 µl
Digested pET-32a(+)	2 µl
Buffer (T4 ligase buffer)	2 µl
T4 ligase	1 µl
Water	5 µl
Total	20 µl

The reaction was performed for 16 hours at 17 °C. Chemically competent *E. coli* (DH5-alpha) cells were transformed with 10 µl of ligation mixture and 100 µl of the culture was plated on ampicillin containing agar plate. Plasmid DNA was propagated, purified and sequenced. One clone, which has the correct sequence were used for protein expression.

Figure 2.2 shows the construct that was generated for expression of the fusion protein.

MSDKIIHLTD DSFDTDVLKA DGAILVDFWA EWCGPCKMIA PILDEIADEY QGKLTVAKLN
 IDQNPGTAPK YGIRGIPTLL LFKNGEVAAT KVGALSKGQL KEFLDANLAG SGSGMHHHH
 HHSSGLVPRG SGMKETAAAK FERQHMDSPD LGTDDDDKAM ADIGSEFELR RQASENLYFQ
GHPARDLQSH RPAIVRRLHS HVENMLDLAW ERGFVSQYEC DEIRLPIFTP SQRARLLDL
ATVKANGLAA FLLQHVQELP VPLALPLEAA TCKKYMAKLR

Figure 2.2: Protein sequence of TEV-NOD2 CARD2 as a thioredoxin fusion protein (Trx-TEV-NOD2-CARD2). Red dark colored letters represent the thioredoxin, blue colored letters represent the enterokinase cleavage site, green colored letters represent the His-Tag, red colored letters represent TEV cleavage site, black bold colored letters represent the human NOD2 CARD2 and black colored letters represent the amino acids derived from the expression vector.

2.2 Recombinant Protein Expression

2.2.1 Protein Expression of Trx-TEV-NOD2 CARD2 Fusion Protein in *E. coli* Strain BL21 (DE3)

For over-night cultures, 4 ml LB-medium supplemented with 100 µg/ml ampicillin was inoculated with a single colony containing the expression plasmid (pET-TEV-NOD2-CARD2) and incubated at 37 °C with shaking at 220 rpm for 10 hours followed by transfer of the starter culture into 50 ml LB-medium supplemented with 100 µg/ml ampicillin and incubated at 37 °C with shaking at 220 rpm overnight.

The overnight culture was diluted 1:200 in 1000 ml fresh LB-medium containing antibiotics (100 µg/ml) and was further incubated at 37 °C. The protein expression was induced by addition of 1 mM isopropyl-β-D-thiogalactopyranosid [IPTG] (Carl Roth GmbH, Karlsruhe, Germany) final concentration, when the OD₆₀₀ reached 0.7. The cells were harvested two hours later by centrifugation using Sorvall RC-5B RSC (Thermo Fisher Scientific Inc., MA, USA) at 4°C, 8000 g for 20 min. The Pellets were stored at -20°C until further use.

2.2.2 Isolation of Inclusion Bodies

The fusion protein (Trx-His-EV-NOD2-CARD2) was expressed in inclusion bodies, so the next step was to isolate the inclusion bodies. The pellet gained from the culture was thawed and resuspended in 50 mM Tris (Carl Roth GmbH, Karlsruhe, Germany) containing 0.1% Tween 20 (Carl Roth GmbH, Karlsruhe, Germany) at pH 8.0. The cells were ruptured under cooling using sonication (1 min, power 40% and cycle 60%) Sonotrode SH213G (Bandelin GmbH & Co. KG, Berlin). The sonication process was repeated three times. Next, the suspension was centrifuged at 4 °C, 40000 g for 30 min. The washing steps were repeated three times with washing buffer (50 mM Tris, pH 8.0) containing 0.1% tween-20 and three times with washing buffer without tween-20. In each washing step the pellet was resuspended in the corresponding washing buffer, sonicated three times on ice and centrifuged to remove the supernatant.

2.2.3 Purification and Renaturation of the Fusion Protein

The inclusion bodies were dissolved in 50 mM Tris-HCl, 6 M guanidine hydrochloride (GuHCl) (Roche, Mannheim, Germany), pH 8.0 and incubated for three hours at room temperature under rotation. The sample was centrifuged at 40000 g for 30 min to remove the non-dissolved parts. The supernatant was incubated with pre-equilibrated (with 50 mM Tris-HCl, 6 M GuHCl, pH 8.0) Ni²⁺-agarose matrix (Qiagen, Hillen, Germany) for three hours at room temperature under rotation. Next, Ni²⁺-agarose with the adsorbed protein was sediment by centrifugation (Sigma 4-16K, SIGMA Laborzentrifugen GmbH, Osterode am Harz, Germany), 500 g, 2 min, at room temperature. The sediment was washed four times with 50 mM Tris-HCl, 6 M GuHCl, pH 8.0 to remove all non-adsorbed proteins. Afterward the protein, which adsorbed to Ni²⁺-agarose, was eluted by incubation of the agarose with with 50 mM Tris-HCl, 6 M GuHCl, 250 mM imidazole (Carl Roth GmbH, Karlsruhe Germany), pH 8.0.

The Renaturation of the fusion protein was done using dialysis. The fusion protein was dialyzed three times, each four hours against 50 mM CAPS (Carl Roth GmbH, Karlsruhe, Germany), pH 12 using dialysis membrane ZelluTrans, MWCO: 4000-6000 Da (Carl Roth GmbH, Karlsruhe, Germany) and the volume ratio of the renaturing buffer

to the sample was 1:100. The dialyzed sample was collected and centrifuged to remove the precipitated protein and concentrated using Vivaspin 20 concentrators (Sartorius Stedim Biotech GmbH, Goettingen, Germany). The renaturing buffer was exchanged to 50 mM Tris pH 8.0 using NAP columns (GE Healthcare Europe GmbH, Freiburg, Germany).

2.2.4 Determination of Protein Concentration

The simplest way to determine the concentration of a protein is the usage of UV-spectrophotometry. To use this method, a protein has to contain amino-acid residues with aromatic side chain, like phenolic or/and indolic group, which absorb UV-light at 280 nm. To calculate the concentration of the protein the following equation was used:

$$c = A_{280} / (\epsilon_{280} d)$$

c: Protein concentration (mol/l), A_{280} : The absorption at 280 nm, ϵ_{280} : the absorption coefficient ($M^{-1}cm^{-1}$) and d: The path length of the cuvette (cm).

The protein concentration of the fusion protein as well as the cleaved form was determined using NanoDrop NP-1000 UV-spectrophotometer (PEQLAB Biotechnologie GmbH, Erlangen, Germany). The reference was always the protein buffer. For the fusion protein the ϵ_{280} was $23710 M^{-1}cm^{-1}$ and for the cleaved form was $9650 M^{-1}cm^{-1}$. The extinction coefficient was estimated by the method of Gill and von Hippel [99].

2.2.5 Discontinuous SDS Polyacrylamide Gel Electrophoresis (SDS-PAGE)

SDS-PAGE is used to separate protein mixture according to protein size and to display the purity of a protein sample. The proteins were separated using stacking and separating gel according to Laemmli [100]. The gel electrophoresis was applied using Mini-PROTEAN[®] 3 electrophoresis system from Bio-Rad (Bio-rad Laboratories GmbH, München, Germany) and run at 200 V. The protein samples were dissolved in a Laemmli loading buffer, boiled for 5 min by 95 °C and loaded onto a gel. The size of protein was estimated by comparing the protein band with the band of unstained protein

standard (Fermentas GmbH, St. Leon-Rot, Germany). Next, the gels were stained with Coomassie staining solution for 1 h and destained for 1 h.

Stacking gel (7.5%):

H ₂ O	2.45 ml
30% Acrylamide, 0.8% Bisacrylamid (37.5:1)	1.25 ml
0.5 M Tris-HCl, pH 6.8	1.25 ml
10% SDS solution	50 µl
10% Ammonium Peroxydisulphate solution (APS)	50 µl
N, N, N', N'- tetramethylethylenediamine (TEMED)	5 µl

Separating gel (15%):

H ₂ O	2.75 ml
30% Acrylamide, 0.8% Bisacrylamid (37.5:1)	6 ml
1.5 M Tris-HCl, pH 8.8	3 ml
10% SDS solution	120 µl
10% APS	120 µl
TEMED	6 µl

All the chemicals were obtained from Carl Roth (Carl Roth GmbH, Karlsruhe, Germany)

Coomassie stain solution

- 10% Methanol
- 10% Acetic acid
- 0.1% Brilliant Blue G 250 (Carl Roth, Karlsruhe, Germany)

Destaining solution:

- 10% Methanol
- 10% Acetic acid

2x Laemmli Loading buffer

Glycerin	2 ml
10% (w/v) SDS	4 ml
0.5 M TRIS-HCl, pH 6,8	2.5 ml
2.5 ml beta-Mercaptoethanol for the reducing buffer/2.5 ml water for non-reducing buffer	
ddH ₂ O	0.5 ml
Bromphenolblau	0.002 mg

2.2.6 Proteolytic Cleavage of Fusion Protein

After successful renaturation of the fusion protein, the fusion protein could be cleaved by enterokinase (Invitrogen GmbH, Karlsruhe, Germany). 1 U enterokinase was used to cleave 300 µg fusion protein. The reaction was performed in 50 mM Tris-HCl, pH 8.0, for two hours at room temperature under slight rotation.

2.2.7 Gradient Reverse Phase-High Performance Liquid Chromatography (RP-HPLC) and Lyophilization

After cleavage, the protein mixture was separated by RP-HPLC method (880-PU, Jasco GmbH, Groß-Umstadt, Germany). The preparative column C₁₈ (VP250/10, Macherey-Nagel, Düren, Germany) was equilibrated with 100% of HPLC solvent A for 5 min, the flow rate was 3.33 ml/min. 1.5 ml (1 mg) of the cleaved fusion protein was acidified using 6 µl trifluoroacetic acid (TFA) (Sigma Aldrich Chemie GmbH, Steinheim, Germany) then centrifuged for 5 min at 20000 g. Afterwards, the supernatant was applied onto the column. The gradient elution was performed by increasing the concentration of RP-HPLC solvent B from 0 to 100% and decreasing solvent A from 100 to 0% within 30 min. At the end the column was washed with solvent B for 5 min. The detection was performed using a Jasco 875-UV detector (Jasco Labor- und Datentechnik GmbH, Gross-Umstadt, Germany) at 280 nm. The fractions of interest were collected and lyophilized using Alpha 2-4 LSC Lyophilizer (Christ GmbH, Osterode, Germany). The

lyophilized samples were analyzed by mass spectrometry (MS) to verify their molecular weights.

Solvent A (5% acetonitrile/0.1% (v/v) TFA)

20 ml acetonitril/0.1% (v/v) TFA (LC-MS Grade, Carl Roth GmbH, Karlsruhe, Germany)

Top up the to 1000 ml with 0.1% TFA (v/v) water (LC-MS Grade, Carl Roth GmbH, Karlsruhe, Germany)

Solvent B (95% acetonitrile/0.1% (v/v) TFA)

950 ml acetonitril/0.1% (v/v) TFA

Add 50 ml 0.1% TFA water (v/v)

2.2.8 Circular Dichroism (CD) Spectroscopy

CD spectroscopy has a wide range of applications in many different fields. Most notably, UV CD spectroscopy is used to investigate the secondary structure of proteins. In the far-UV range, the absorption is principally due to the peptide bond, so the different types of regular secondary structures found in proteins give rise to characteristic CD-spectra. The circular dichroism originates from the differential absorption of right- and left-handed circularly polarized components of plane polarized light [101]. The resulting light is elliptically polarized, therefore circular dichroism spectra are presented in terms of the mean residue ellipticity θ at wavelength λ defined by:

$$\Theta_{\lambda}^{\text{MRW}} = \text{MRW} \times \theta_{\lambda} / (10 \times d \times c)$$

MRW: The mean residue weight (g mol^{-1}), **θ :** The observed ellipticity at wavelength λ (mgrad), **d:** The path length (cm) and last **c:** The protein concentration (g cm^{-3}).

In addition, the thermal stability of the protein was investigated by keeping the wavelength at 222 nm during increasing the temperature gradually ($1 \text{ }^{\circ}\text{C}/\text{min}$) from $20 \text{ }^{\circ}\text{C}$ to $90 \text{ }^{\circ}\text{C}$. The measurements were done using J-720 spectropolarimeter (Jasco GmbH Deutschland, Groß-Umstadt, Germany) and quartz cuvettes (Helma GmbH & Co. KG, Müllheim, Gemany). The calibration of the CD-spectropolarimeter was carried out according to Chen und Yang [102].

2.2.9 Dynamic Light Scattering

Dynamic Light Scattering (DLS) is a rapid, non-invasive technique for determination of the protein size. In DLS, the scattering intensity fluctuations are monitored and then correlated, followed by calculation the size of the particles using the Stokes-Einstein equation:

$$R_H = k_B T / 6\pi\eta D_0$$

R_H : The particles hydrodynamic radius, k_B : Boltzmann's constant, T : Temperature, η : The solvent viscosity, D_0 : Self-diffusion coefficient [103].

The protein sample (1 mg/ml) was centrifuged at 20000 g. Sample of 40 μ l of the protein was transferred into a washed and dried quartz cuvette. The experiment consists of 10 measurements each with 13 second duration time using Lase-Spectroscatter 201 (RiNA GmbH, Berlin, Germany).

2.3 NMR Spectroscopy

2.3.1 Preparation of Equine Alpha-Defensin (DEFA1) Sample for NMR Spectroscopy

All the experiments, which were necessary to prepare the peptide sample for two-dimensional NMR experiments (2D- 1 H-NMR), were done by Dr. Sascha Jung (Group of Prof. Dr. Grötzinger, Institute of Biochemistry, University of Kiel). This included, order of the synthetic peptide, renaturation, purification using RP-HPLC and characterization of the peptide (Ellmann's test, mass spectrometry and CD-spectroscopy). The NMR experiments were done by Prof. Dr. Sönnichsen (Department of Organic Chemistry, University of Kiel).

2.3.2 Performance of 2D- 1 H Homonuclear TOCSY and NOESY

To determine the three-dimensional structure of the DEFA1 peptide, two TOCSY and four NOESY experiments by different temperatures and mixing times were recorded using NMR spectrometer Bruker Avance 600 MHz (Bruker Corp., MA, USA) equipped with active shielded Z-gradient triple resonance cryoprobe.

The data sets were processed using the program NMRPipe [104] and NMRView software was used for the analysis of the spectra [105].

2.3.3 Sequence-Specific Assignment

Sequence-specific assignments are the basis for three-dimensional structure determination and other comprehensive studies on dynamics, conformation and function by NMR spectroscopy [94.] To perform a sequence-specific assignment of a protein, the spin systems for all amino-acid residues of a protein in TOCSY spectrum have to be identified based on their specific spin system patterns. The sequence-specific assignment of a protein bases on the fact that the distance of the amide proton (H^N) of one amino acid (i) is shorter than 5 Å to H^α , H^β and H^γ protons of the precursor amino-acid residue (i-1). NOESY spectrum contains intraresidual and interresidual signals. By comparison of both spectra (TOCSY and NOESY) the interresidual signals can be identified.

From the interresidual signals of NOESY spectrum it is possible to identify the neighboring amino acid in the protein. On the resonance frequency of one amide proton (H^N) the interresidual cross signals from the side chain of the neighboring amino acid (i-1) should be visible.

Using this principle, the amino acid chains of neighboring amino acids for equine defensin (DEFA1) were determined. The TOCSY and NOESY spectra (experiment [13], experiment [14]) were used to identify the amino acids spin systems and to perform sequential assignment. The other spectra were used to verify the results.

2.3.4 Structure Calculation

The assigned resonance signals from the 2-D homonuclear NOESY spectrum were converted in proton-proton distances using NMRViewJ. The distances between the protons were calculated using the cross-peak signal intensities. The smallest distance was set to 1.8 Å and the biggest to 5 Å. The determined distances were calibrated

using the r^6 function; r refers to the distance between two protons. The average intensities of all the NOEs were equated to a distance of 2.8 Å and the tolerance was 0.125 times to the respective distance square. The intensity of the methyl group was halved. The distances information's were used for structure calculation using the program CYANA 2.1 [106]. The disulfide bonds were set between C1-C6, C2-C4 and C3-C5 and 18 additional distances have been added to the calculation to define the three disulfide bonds of the peptide. For the S-S bound, the following was applied $2.0 \leq d(S_i^Y, S_j^Y) \leq 2.1 \text{ \AA}$; $3.0 \leq d(C_i^\beta, S_j^Y) \leq 3.1 \text{ \AA}$; $3.0 \leq d(S_i^Y, C_j^\beta) \leq 3.1 \text{ \AA}$.

The structures were represented using MOLMOL [107] and GRASP2 programs [108]. The analysis of the dihedral angles and the Ramachandran plot were done using CYANA 2.1 program. The electrostatic surface potential was represented using GRASP2 program.

100 structures were calculated using CYANA program. From the 100 calculated structures, 10 structures with the lowest target functions were selected.

3 Results

3.1 NOD2 CARD2

In the present work, a protocol for NOD2 CARD2 expression, renaturation and purification was established.

3.1.1 Protein Expression

Expression of TEV-NOD2 CARD2 fusion protein in the chemically competent *E.coli* strain BL21 (DE3), using the expression vector pET-32a(+) containing N-terminal thioredoxin (Trx)-, His-tag and enterokinase cleavage site, was induced by 1 mM IPTG (final concentration and OD₆₀₀ reaching 0.7) in LB medium. SDS-PAGE analysis detected a band with a molecular weight between 25 and 35 kDa (figure 3.1 (A)), which corresponds to the expected molecular weight of the fusion protein (31 kDa). Various expression times were tested in order to maximize the expression of the fusion protein. The data showed equal amount of protein after 2 and 16 hours of expression, indicating that the amount of protein does not increase with longer expression time (figure 3.1(A)).

To characterize the solubility of the expressed fusion protein, the bacterial cells were disrupted in 50 mM Tris, pH 8.0 by sonication. Then soluble and insoluble materials were separated by centrifugation and analyzed by SDS-PAGE. The data demonstrated that the fusion protein was expressed as unfolded aggregates in inclusion bodies rather than as a soluble protein (figure 3.1(B)).

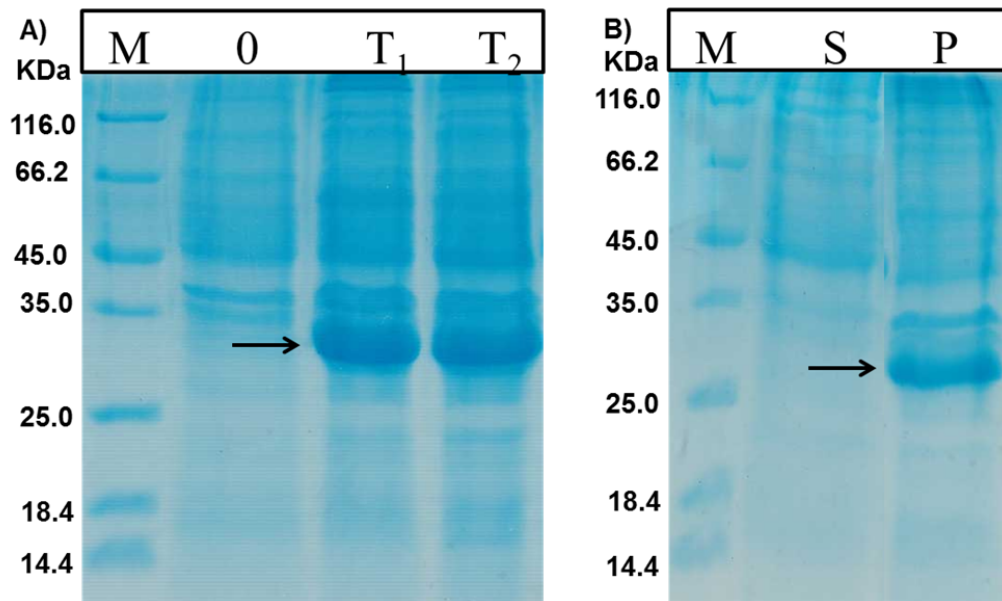


Figure 3.1: SDS-PAGE analysis of the expressed fusion protein in *E.coli* strain BL 21 (DE3). A) The SDS-gel electrophoresis separation of the expressed fusion protein in bacteria before induction (0), 2 hours (T₁) and 16 hours after induction (T₂), showing that longer expression time does not increase the amount of the expressed fusion protein. B) SDS-gel shows that the fusion protein is expressed as aggregated unfolded protein in inclusion bodies, but not in a soluble form. S: Cell supernatant, P: Cell debris, M indicates the protein molecular weight standard (kDa). Black arrows indicate the expressed fusion protein.

3.1.3 Purification of the Trx-TEV-NOD2 CARD2 Using Ni²⁺-NTA Agarose Beads under Denaturing Condition.

In order to purify the expressed fusion protein, bacterial cells were collected after 2 hours of induction, centrifuged and disrupted by sonication in an ice bath. Then, inclusion bodies (IBs) were isolated by centrifugation and washed six times with the corresponding washing buffers under sonication. The washed IBs were dissolved in a denaturing buffer (50 mM Tris, 6 M GuHCl, pH 8.0), followed by incubation with pre-equilibrated Ni²⁺-NTA agarose beads at RT for three hours. The beads were washed four times with the denaturing buffer, followed by an elution buffer (50 mM Tris, 6 M GuHCl, 250 mM imidazole, pH 8.0). Samples of the IBs were collected at each step during this purification process, including before loading (B); flow through (FT); washing

supernatants (W_1 and W_4); and elution fractions (E_1 and E_2). The collected samples were then analyzed by SDS-PAGE (figure 3.2 (A)), which demonstrated that the fusion protein is present in significantly larger quantities in E_1 and E_2 than in the original sample (B) before purification as shown in figure 3.2 (A). To ensure the sensitivity and the specificity of the purification process, E_1 and E_2 fractions were combined, diluted 10 times and reexamined on an SDS-PAGE. As shown in figure 3.2 (B), the combined diluted E_1 and E_2 fractions (E_{1+2}) shows only one band corresponding with the predicted size of the fusion protein, indicating an overloading of the purified protein in E_1 and E_2 fractions (figure 3.2 (A)), beyond the capacity of the SDS-PAGE gel, rather than the presence of impure proteins. Therefore, the presence of a significant amount of the fusion protein in the flow through (FT) sample as well as some traces in the supernatant of W_1 and W_4 samples (Figure 3.2 (A)) suggested that the quantity of the fusion protein is exceeding the binding capacity of the beads. Thus, the data suggest that the fusion protein is almost pure.

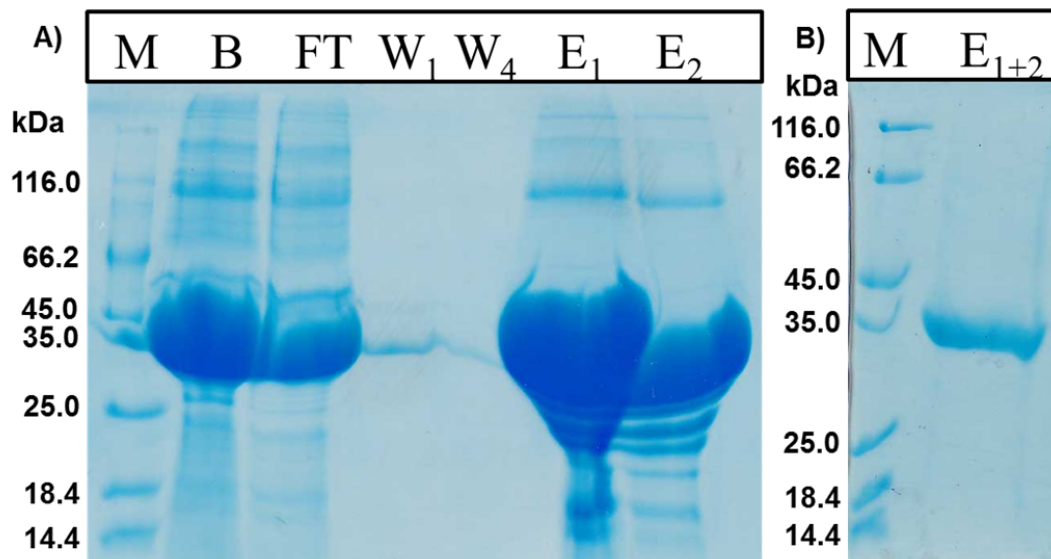


Figure 3.2: SDS-PAGE analysis of the purified Trx-TEV-NOD2 CARD2 fusion protein. A) Samples of solubilized IBs before loading (B), flow through (FT), washing steps (W) and elution steps (E) were analyzed. The SDS-gel capacity was overloaded in E_1 and E_2 (elution lines). B). the elution fractions (E_{1+2}) were combined together, diluted 10 times and reanalyzed. The E_{1+2} fraction showed that the fusion protein is almost pure.

3.1.5 Renaturation of the Trx-TEV-NOD2 CARD2 Fusion Protein

The purified fusion protein was renatured by dialysis, followed by a rapid buffer exchange. In particular, the fusion protein was dialyzed against 50 mM CAPS, pH 12, three times, four hours each and concentrated, followed by changing the dialysis buffer to 50 mM Tris, pH 8. The purity of the fusion protein (FP) was assessed on SDS-PAGE under reducing (FP_R) and non-reducing conditions (FP_{nonR}). The size of the fusion protein was not affected by the non-reducing Laemmli buffer treatment (figure 3.3 the lines (FP_{nonR})). As shown in figure 3.3, the data suggest that the fusion protein is almost pure and did not form oligomers through disulfide bond formation.

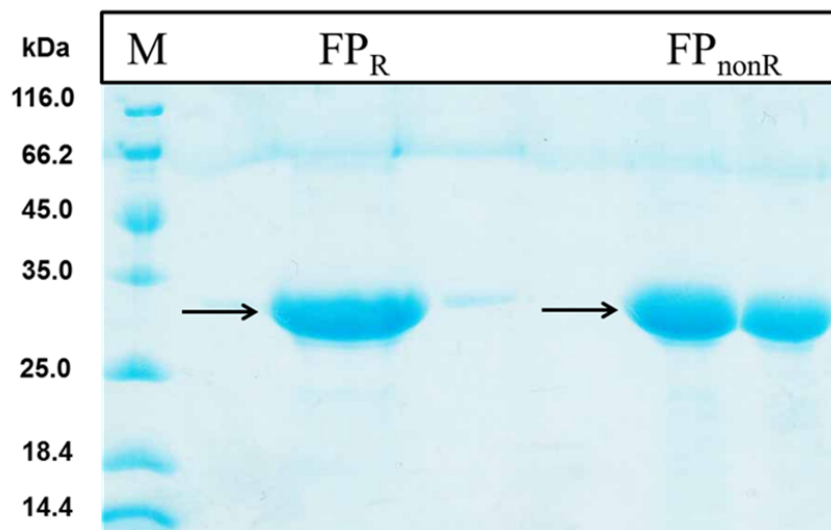


Figure 3.3: SDS-PAGE analysis of the fusion protein after renaturation. The Fusion protein was next refolded by dialysis, followed by rapid buffer exchange. The fusion protein (FP) was analyzed on SDS-PAGE under reducing (FP_R) and under non-reducing conditions (FP_{nonR}), M: Protein standard, black arrows indicate the fusion protein.

3.1.6 Dynamic Light Scattering (DLS) of Fusion Protein

DLS was used to precisely determine the size of the renatured fusion protein, where 40 μ l of the renatured fusion protein (1 mg/ml) was measured 10 times, 13 seconds each at room temperature. As shown in figure 3.4, the blue dots represent the radius of the protein in relation to a particular measurement time. The number of dots in each measurement represents the number of the present species in the protein solution. The

data demonstrated that the radius of the fusion protein was 12 nm and the fusion protein is present in a monodisperse form. The size of the radius (12 nm) is larger than the expected size for a 31 kDa protein according to the control experiment (albumin 1 mg/ml, 66 kDa). The radius of albumin under the same experiment conditions was 5 nm (data not shown). The data suggest that the renatured fusion protein is present in the buffer system as small monodisperse soluble oligomers. Unfortunately, the size of the renatured protein could not be confirmed using size-exclusion chromatography (SEC) due to a high hydrophobic affinity of the fusion protein to the SEC matrix (data not shown).

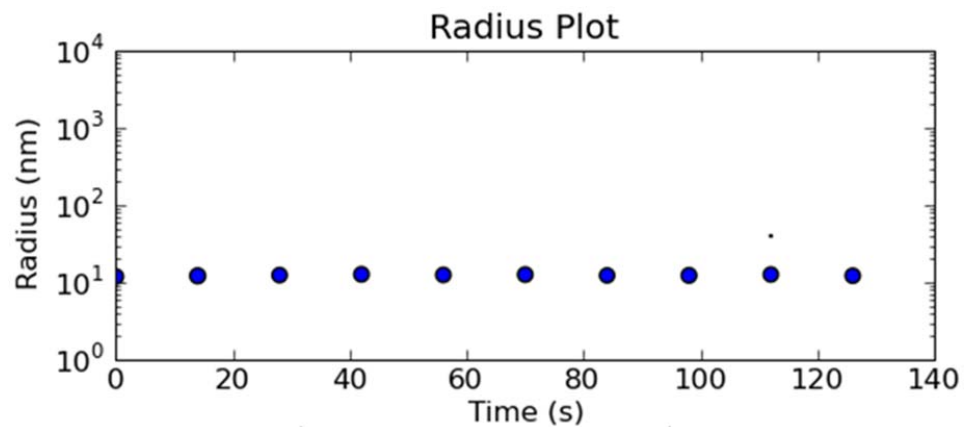


Figure 3.4: The radius of the renatured fusion protein was determined using dynamic light scattering (DLS). Sample of 40 μ l fusion protein (1 mg/ml) was measured in DLS. The radius (Y-axis) was plotted against the time (X-axis). The plot demonstrates the radius and the monodispersity of the fusion protein.

3.1.7 Cleavage of the Fusion Protein

After purifying and determining the size of the fusion protein, we set out to purify the protein of interest (NOD2 CARD2). The fusion protein has two cleavage sites, a TEV and enterokinase (figure 2.2). The fusion protein in its native form was cleaved by the TEV protease. Aliquots of the cleavage mixtures, after 2 hours of incubation time, were centrifuged to separate soluble and non-soluble materials, followed by analyzing the fractions by SDS-PAGE under non-reducing conditions. The untreated fusion protein was used as a reference to estimate the cleavage efficiency. The TEV protease cleaved

the fusion protein into a 20 kDa fusion tag and 11.4 kDa NOD2 CARD2. SDS-gel analysis of the soluble fraction detected two bands (figure 3.5 (A)). The lower band, according to the protein standard, is about 20 kDa and the upper band about 31 kDa. The 20 kDa and 31 kDa bands contain the fusion tag and the uncleaved fusion protein, respectively. NOD2 CARD2 protein (11.4 kDa) was not detected.

An SDS-PAGE analysis of the insoluble fraction of the cleavage mixture is shown in figure 3.5 (B). The gel electrophoresis separation of the sample resulted in three protein bands. The lowest band is about 12 kDa, which probably contains NOD2 CARD2 protein. The upper two bands contain the fusion tag and the fusion protein. The upper band (31 kDa), which represents the uncleaved fusion protein in figure 3.5 B, is very small compared to the fusion protein before cleavage, while the lowest band (12 kDa), which contains NOD2 CARD2 protein, appears large and intense. The 20 kDa band in figure 3.5 B, which contains the fusion tag, is very weak compared to the fusion tag band in figure 3.5 A. This data suggest that the cleavage of the fusion tag by TEV protease induces instability in NOD2 CARD2 and led to precipitation of the protein, which is present in the insoluble fraction. Thus, the data demonstrate that almost all of the fusion protein was cleaved by TEV protease and NOD2 CARD2 is stable in the buffer system as a fusion protein.

Many experiments have been attempted to increase the stability of the cleaved NOD2 CARD2 by changing the cleavage reaction conditions, however; NOD2 CARD2 remains unstable after cleavage of the fusion tag (data not shown).

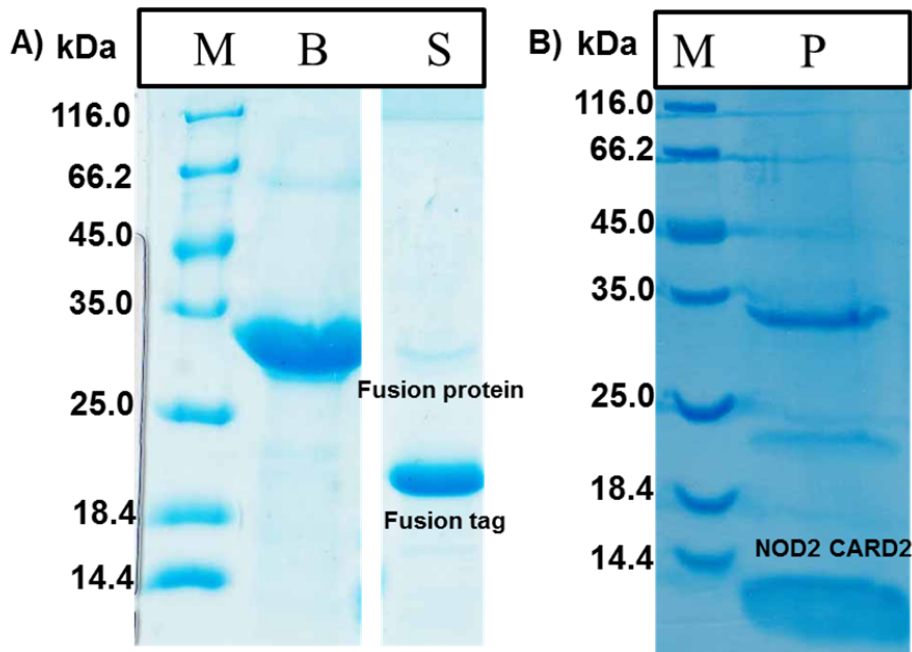


Figure 3.5: SDS-PAGE analysis of proteolytic cleavage of the fusion protein (31 kDa) by the TEV protease. Sample of 300 μ g of fusion protein was used. The sample was incubated with 9 μ g TEV protease for 2 hours at room temperature. Sample of 20 μ l was taken from the reaction mixture, centrifuged and the soluble fraction was analyzed by SDS-PAGE under non-reducing condition (A) and the insoluble fraction as well (B). M: Protein marker, B: The fusion protein before cleavage, S: The soluble material, P: The insoluble material.

Therefore, the renatured fusion protein was cleaved by enterokinase. The cleavage mixture was centrifuged and the supernatant was analyzed by SDS-PAGE under non-reducing condition. The endoprotease cleaved the fusion protein into a 13.9 kDa NOD2 CARD2 and a 17.1 kDa fusion tag. Samples of fusion protein before cleavage (as a reference) and the cleavage mixture, 2 hours after of cleavage time, were analyzed by SDS-PAGE (figure 3.6). Gel electrophoresis of the cleavage mixture detected three protein bands (figure 3.2 lane S). The lowest protein band is about 14 kDa and it contains NOD2 CARD2. The remaining two upper bands contain the fusion tag (about 17 kDa) and the uncleaved fusion protein (31 kDa). After cleavage, NOD2 CARD2, non-cleaved fusion protein and fusion tag are present in the soluble fraction, indicating that cleavage of the fusion tag by the enterokinase does not alter the stability of NOD2 CARD2, in contrast to the cleavage of the fusion protein by TEV protease. However, NOD2 CARD2 fragment resulting from the endoprotease cleavage contains 23

additional amino-acid residues upstream of its N-terminus and therefore; was donated as 23aa-NOD2 CARD2. The data show that enterokinase cleavage of the fusion protein resulted in a stable 23aa-NOD2 CARD2. However; the cleavage efficiency of the enterokinase was not 100 %. Experiments to increase the efficiency of the enterokinase cleavage by changing the reaction conditions have been attempted but the cleavage efficiency did not change (data not shown).

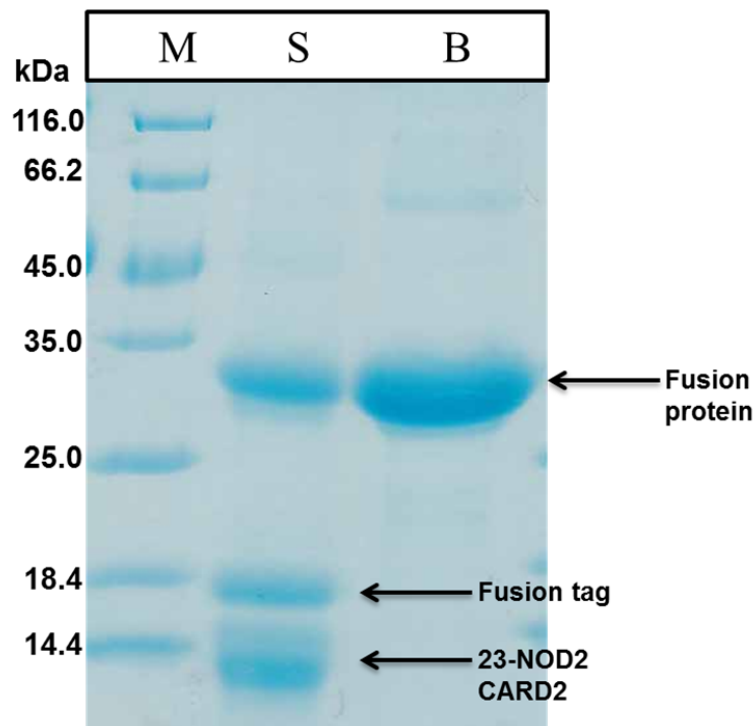


Figure 3.6: SDS-PAGE analysis of the proteolytic cleavage of the renatured fusion protein by the enterokinase. Sample of 300 μg fusion protein was incubated with 1 U of the enterokinase for 2 hours at room temperature. Sample of 20 μl of the reaction mixture was centrifuged and analyzed by SDS-PAGE under non-reducing condition. B: The fusion protein before cleavage, S: Sample of cleavage mixture, M: protein standard.

3.1.8 Purification of the 23aa-NOD2 CARD2

In order to purify the 23aa-NOD2 CARD2, the fusion protein solution after proteolytic cleavage was fractionated using reversed phase high performance liquid chromatography (RP-HPLC) (figure 3.7). RP-HPLC chromatogram showed two

interesting fractions (fraction 1 and 2). These two fractions were collected, lyophilized and characterized by mass spectrometry.

Mass spectrometry analysis of fraction 1, eluted at 21.8 min, detected a protein with a mass of 13965 Da, which corresponds to the expected molecular weight of the 23aa-NOD2 CARD2 (figure 3.8).

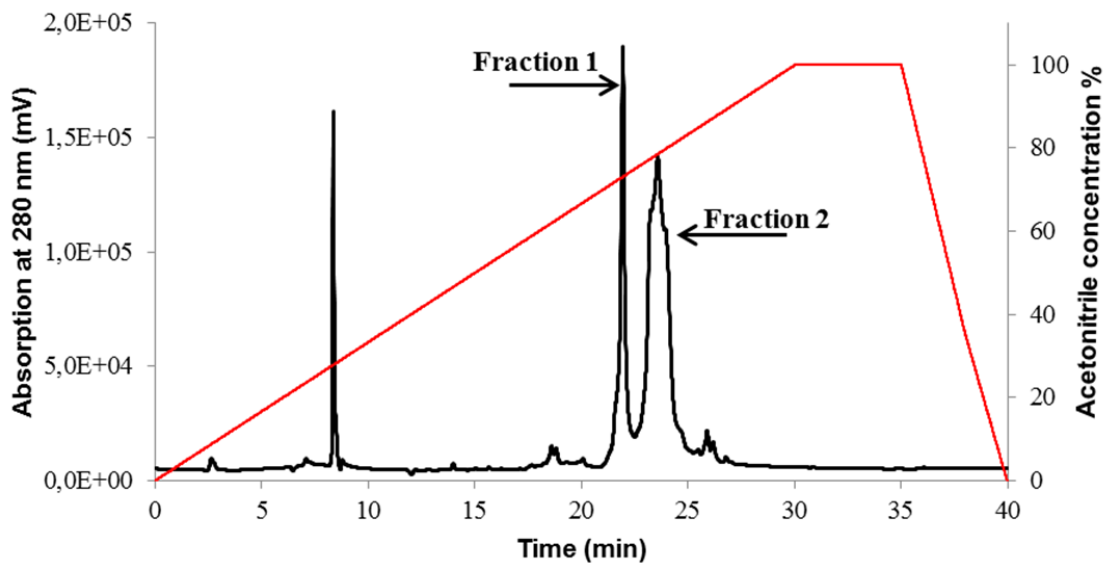


Figure 3.7: Reversed phase high performance liquid chromatography (RP-HPLC) purification chromatogram of the 23aa-NOD2 CARD2. The cleavage reaction mixture was purified by RP-HPLC. Black line: Elution run, red line: Acetonitrile gradient. Both fractions were lyophilized and analyzed by mass spectrometry.

The purity of the purified lyophilized 23aa-NOD2 CRAD2 was analyzed by SDS-PAGE under non-reducing conditions (figure 3.9). Gel electrophoresis detected only one 14 kDa protein band, which did not form oligomers through formation of disulfide bridges. The data demonstrate that the 23aa-NOD2 CARD2 could be purified using RP-HPLC and the protein is pure.

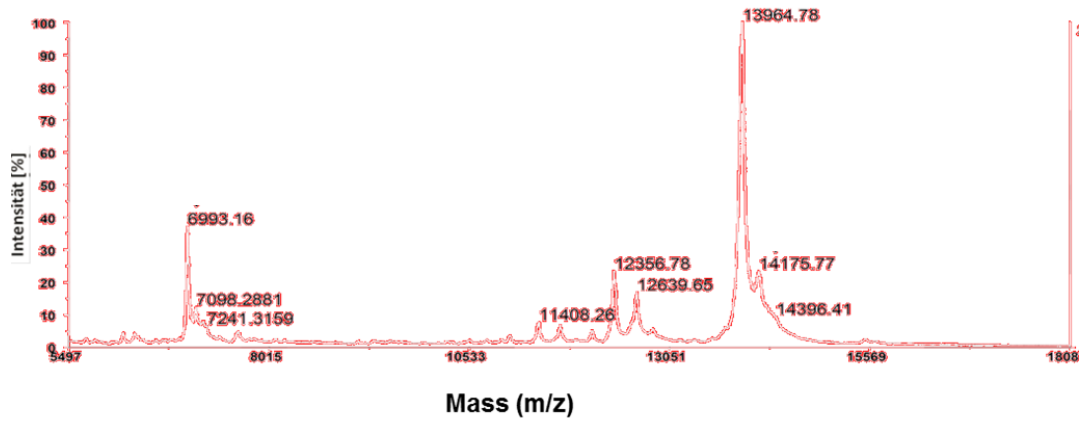


Figure 3.8: Mass spectrometry analysis of the fraction 1 eluted at 21.8 min. The mass of 23aa-NOD2 CARD2 was determined by MALDI-TOF mass spectrometry. Fraction 1 contains the 23aa-NOD2 CARD2 protein. The mass to charge was represented as m/z.

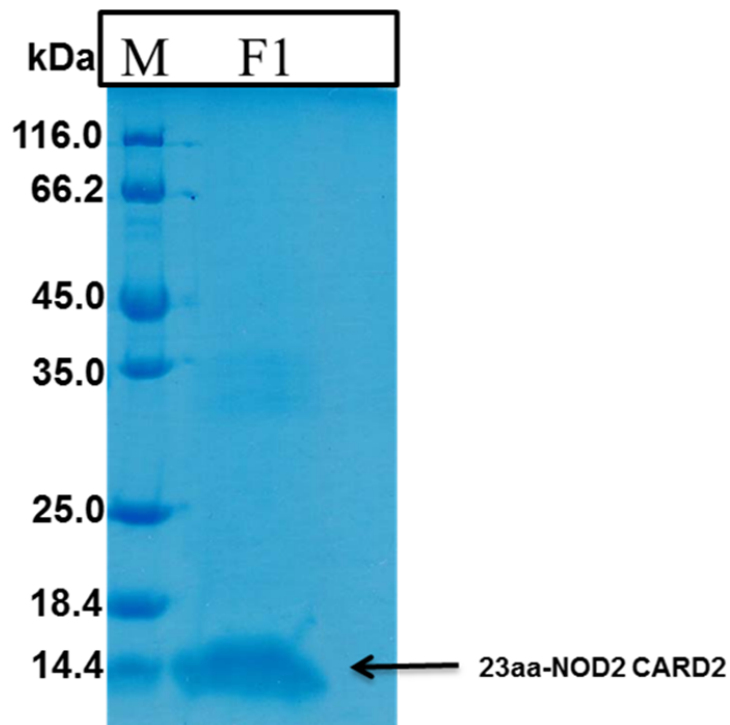


Figure 3.9: SDS-PAGE analysis of the 23aa-NOD2 CARD2 from fraction 1. The SDS-gel was performed under non-reducing condition. The arrow indicates the 23aa-NOD2 CARD2 protein. M: Protein marker, F1: RP-HPLC fraction 1 at 21.8 min.

3.1.9 Determination of the Secondary Structure of the 23-NOD2 CARD2 Using CD-spectroscopy

To further characterize the 23aa-NOD2 CARD2, its secondary structure was investigated by far-UV CD-spectroscopy.

The lyophilized 23aa-NOD2 CARD2 was reconstituted in 50 mM phosphate, pH 4.6 and its secondary structure and thermal stability were studied. Figure 3.10 demonstrated the CD-spectrum of the 23aa-NOD2 CARD2 protein at room temperature. The curve shape is similar to a CD-spectrum of alpha-helical proteins, which are characterized by two minima, at 208 and 222 nm, followed by an increase of the ellipticity at 205 nm.

In addition, the thermal stability of the 23aa-NOD2 CARD2 was studied. The alteration of the signal intensity at 222 nm was observed at increasing temperatures. The signal intensity (Y-axis) was plotted against the temperature (X-axis). The curve, shown in figure 3.11, displays the heat stability spectrum of the 23aa-NOD2 CARD2. The intensity of the signal remains constant until the temperature reaches 55 °C and then the intensity starts to decrease until the temperature reaches 80 °C. The alteration of the CD-signal at 222 nm indicates that the secondary structure elements, alpha-helices in the case of 23aa-NOD2 CARD2, are lost under the influence of increasing temperature.

To investigate the reversibility of the denaturing process, the protein was gradually heated and cooled. The CD-spectra, which were recorded during heating and cooling phases, indicate that the heat denaturing process is not reversible; because the signal at 222 nm did not increase during the cooling phase (data not shown).

To further investigate the heating effect on the 23aa-NOD2 CARD2, two different CD-spectra were recorded, the first one at 20 °C and second at 90 °C. In comparison to the spectrum at 20 °C, the spectrum at 90 °C showed less intensity and lost the minima. The data show that the purified 23aa-NOD2 CARD2 is refolded, forms alpha-helices as the main secondary structures, heat sensitive and the thermal unfolding process is not reversible.

Effect of heat on the protein was further investigated by DLS. The protein was heated for a short time and measured (see section 3.1.10).

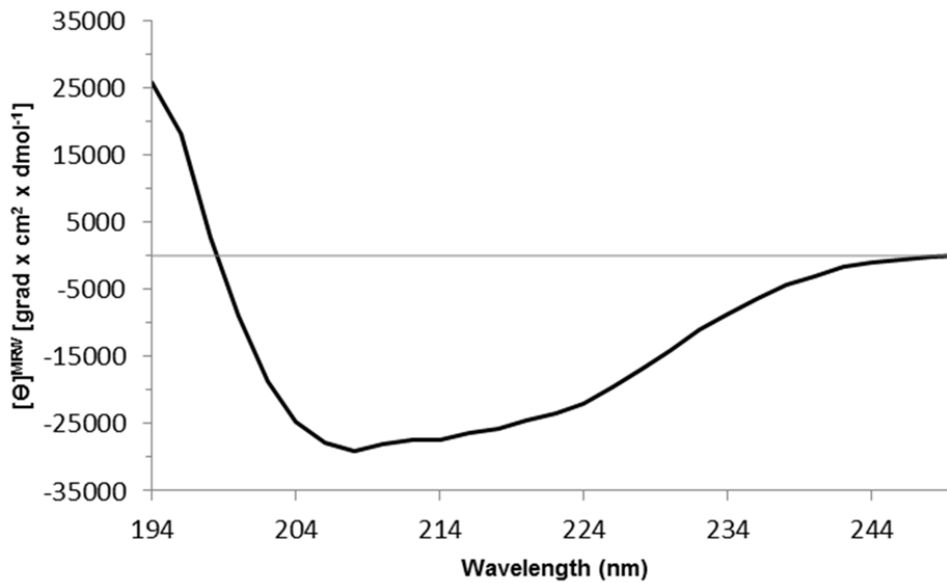


Figure 3.10: CD-spectrum of the 23aa-NOD2 CARD2, reconstituted in 50 mM sodium phosphate, pH 4.6, at room temperature. The spectrum shows a typical alpha-helical structure. The spectrum shows two minima at 222 and 208 nm respectively and increasing of the intensity at 205 nm.

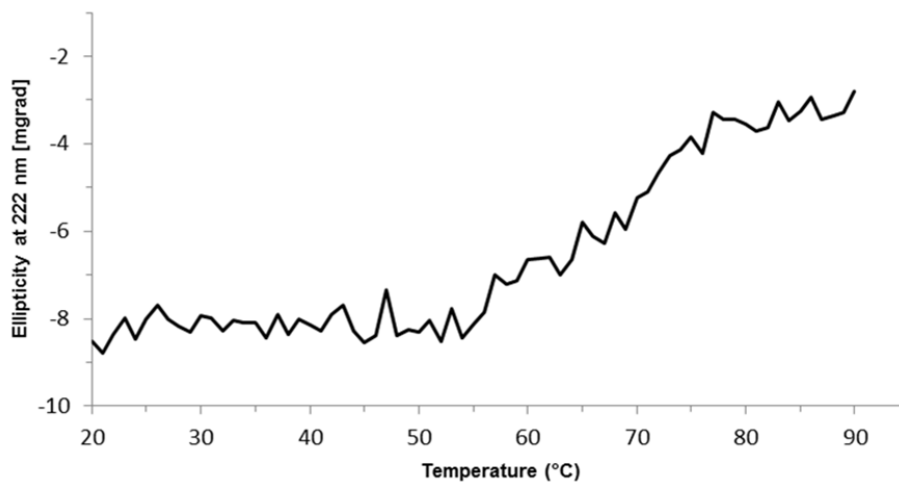


Figure 3.11: Investigation of thermal stability of 23aa-NOD2 CARD2. The CD-spectrum shows the signal intensity of the protein at 222 nm in relation to temperature. The temperature was gradually increased (1 °C/min) from 20 °C to 90 °C.

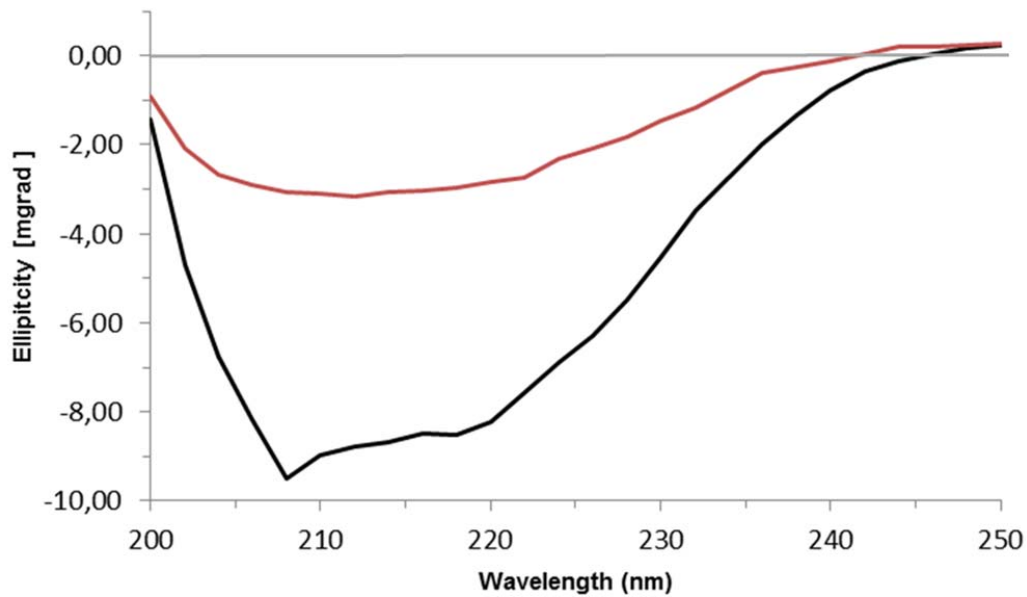


Figure 3.12: CD-spectra of the 23aa-NOD2 CARD2, reconstituted in in 50 mM phosphate, pH 4.6 before and after thermal treatment. Black line: CD-spectrum of the 23aa-NOD2 CARD2 at room temperature and red line is for the CD-spectrum at 90 °C.

3.1.10 Dynamic Light Scattering of 23aa-NOD2 CARD2

The 23aa-NOD2 CARD2 was further characterized by determining its size by DLS. The radius plot, shown in figure 3.13, represents the radius of the protein in 10 different measurements. The blue dots show the radius in relation to the time of measurement and the number of present species in the solution. The size of the dots represents the dominance of the recorded species to other species in a particular measurement; where large dots represent large amount of particular species and small dots represent small amount in the solution. The most dominant species is that with 17 nm radius. Of note, other species are present in small amounts. The data demonstrate that the radius of 23aa-NOD2 CARD2 is 17 nm and this species is mostly present in the solution.

The thermal effect on 23aa-NOD2 CARD2 was investigated. The protein was heated and measured in DLS under the same experimental conditions. Figure 3.14 shows that heating of the protein sample for a short time led to formation of big oligomers. The size of the protein after treatment increased dramatically from 17 nm to 90 nm. The same phenomenon was observed as 150 mM NaCl was added to 23aa-NOD2 CARD2 in

phosphate buffer (figure 3.15). Compared to heat treatment the monodispersity of 23aa-NOD2 CARD2 is almost lost. The data show that the protein is heat and salt sensitive. Interestingly, the protein remained almost monodisperse at least after heat treatment and soluble after both treatments.

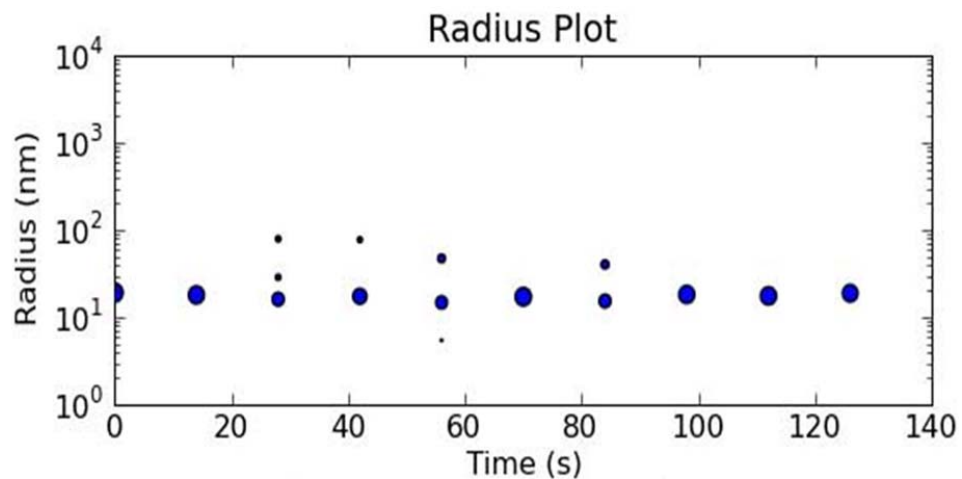


Figure 3.13: The hydrodynamic radius of the 23aa-NOD2 CARD2 was determined using dynamic light scattering (DLS). The Radius plot shows the dispersity and the size of the radius of 23aa-NOD2 CARD2.

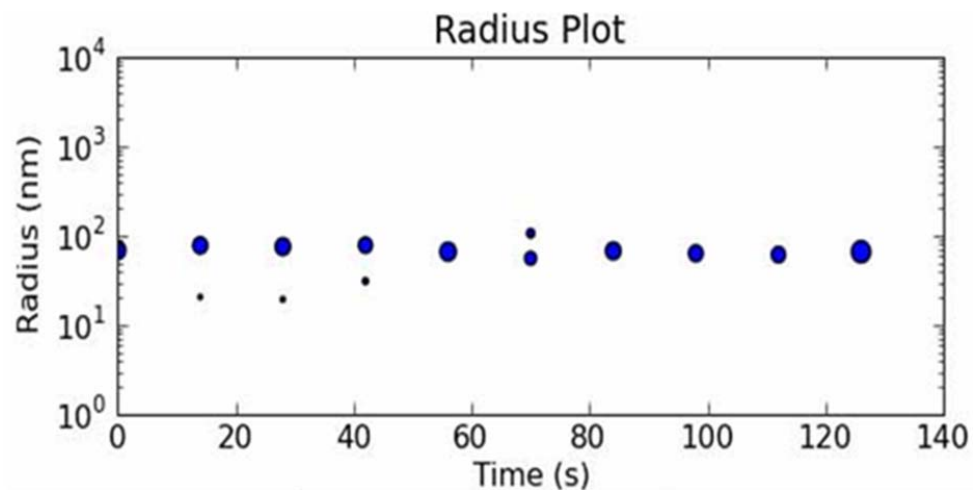


Figure 3.14: The effect of heat on 23aa-NOD2 CARD2 size. The protein was heated and measured in DLS. The radius plot displays the size and dispersity of the protein.

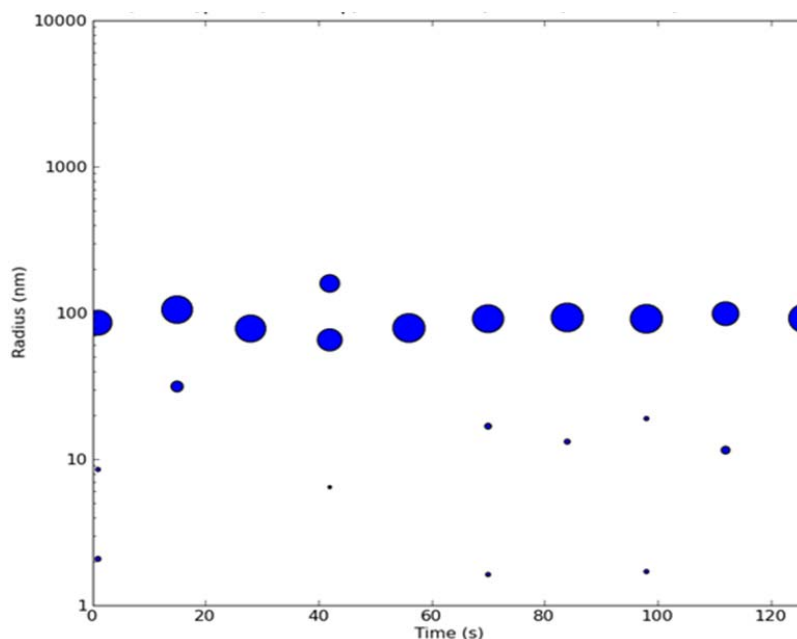


Figure 3.15: The effect of NaCl on 23aa-NOD2 CARD2 size. NaCl (150 mM) was added to protein in phosphate and measured in DLS. The radius plot displays the size and dispersity of the protein.

3.1.11 NMR-Spectroscopy of the 23aa-CARD2 NOD2

The goal was to prepare a NOD2 CARD2 protein sample, which is suitable for NMR experiments, in order to determine the 3D-structure. 1D-¹H-experiment gives information about the suitability of the sample for NMR-spectroscopy. The most important information obtained from a 1D-¹H-experiment is the shape and dispersion of the proton signals in the spectrum. The both parameters are determining the suitability of a given sample for NMR. The 1D-¹H-NMR spectrum, shown in figure 3.14, represents 1D-¹H-NMR experiment of 23aa-NOD2 CARD2. The spectrum shows that the dispersion of the backbone amide and aliphatic protons is very low and the sample in its actual status is not suitable for NMR experiments.

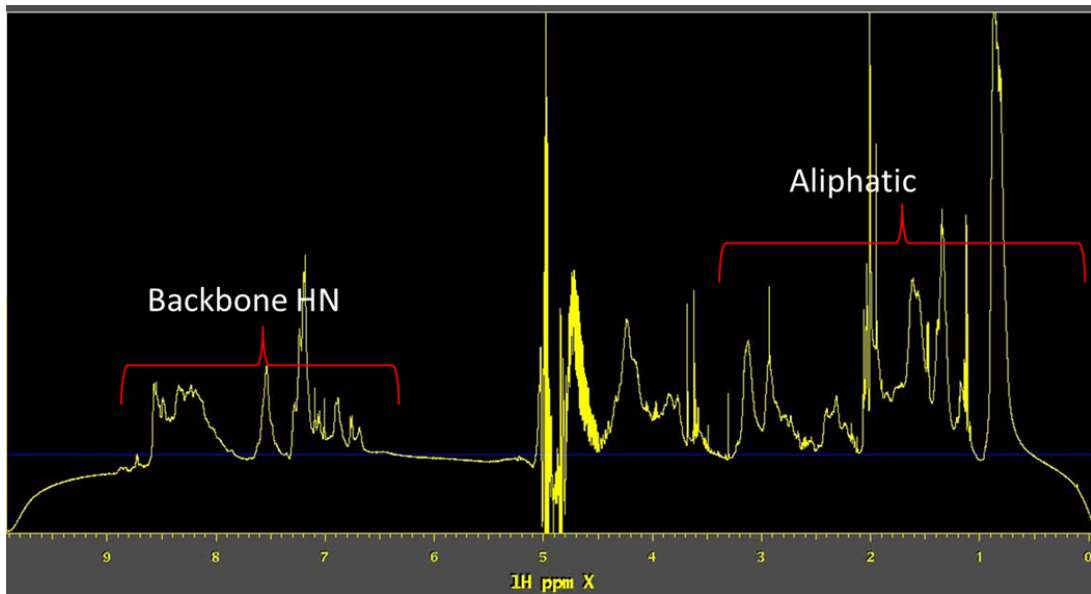


Figure 3.16: A 1D-¹H-NMR experiment of the 23aa-NOD2 CARD2. The spectrum shows the dispersion of the backbone H^N and the aliphatic protons.

3.2 Determination of the Three-Dimensional Structure of Equine DEFA1

DEFA1 was identified and characterized by Bruhn *et al* [86]. In the present work, the three dimensional structure of DEFA1 peptide will be determined using 2D-¹H-homonuclear NMR-spectroscopy.

The synthetic DEFA1 was refolded, purified and reconstituted in 20 mM phosphate at pH 5.7, the concentration of the peptide sample for NMR-spectroscopy was 0.3 mM.

Homonuclear TOCSY and NOSEY experiments were recorded at different temperatures and mixing times.

The structure was determined using spectra, which have low signal-to-noise ratio and a high number of signals. The TOCSY-spectrum was recorded at 278 K with a mixing time of 60 ms and the NOESY-spectrum at 278 K with 200 ms

3.2.1 Identification of the Spin Systems of DEFA1

The first step to determine the solution structure of a peptide is to identify the amino-acid spin systems. 2D-¹H homonuclear TOCSY experiments served to identify the amino-acid spin systems.

In a TOCSY experiment all protons of a spin system correlate via scalar couplings. Using characteristic spin system pattern it is possible to identify the related amino-acid residue. TOCSY-spectrum displays only the intraresidual signals; therefore it also serves to distinguish the interresidual from intraresidual resonance signals in 2D-¹H homonuclear NOESY-spectrum.

The TOCSY-spectrum of DEFA1 peptide at 278 K and 60 ms mixing time is shown in figure 3.17. The rectangles represent the type of protons that correlate with each other. The backbone amide proton of an amino-acid residue correlates with the present alpha-, beta-, gamma- or delta-protons of its own residue. According to the type of correlated protons the location of the cross peaks (resonance) on the spectrum will differ. Therefore, the correlation of aromatic protons can be seen between 6 and 7 ppm, while the amide with alpha-protons or the amide with aliphatic proton can be seen between 7

and 10 ppm. The parallel vertical signal rows on the upper left side of the figure 3.15 represent the correlated protons resonance signals of the amino-acid residues of DEFA1.

The TOCSY-spectrum also enables the identification of some of the amino-acid residues according to their characteristic spin system patterns, including leucine, isoleucine, glycine, threonine, lysine and alanine. The spin system patterns of the remaining amino-acid residues are similar and additional information is needed to identify them.

DEFA1 comprises 34 residues. Out of the 34 spin system 33 could be identified. Alanine 7 is the only residue that was identified from the TOCSY-spectrum due to its characteristic spin system pattern.

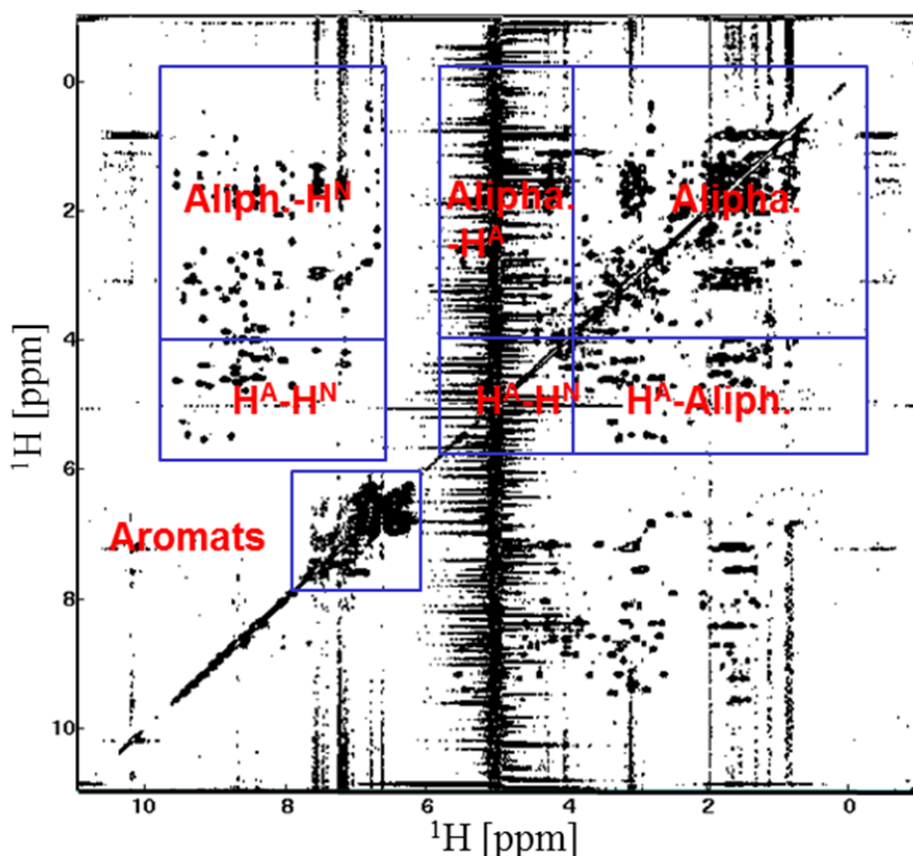


Figure 3.17: ^1H -Homonuclear 2D-TOCSY-spectrum of DEFA1. The resonance signals (black dots) are resulted from scalar coupling of the all amino-acid residues protons of DEFA1. The present spin systems (the upper left blue square) resulted from the correlation of the backbone amide protons with the side chain protons. This spectrum was recorded at 278 K and with 60 ms mixing time.

To illustrate the identification of the spin systems of DEFA1 amino-acid residues, glycine 13 spin system is shown in figure 3.18. The figure shows the unambiguous spin system pattern of glycine 13. It has only 2 alpha-protons and due to the strong coupling between them, both protons can be seen in TOCSY-spectrum. The resonance signals show the correlation between the amide proton and the alpha-protons of glycine, i.e., the correlation between $H^{\alpha 1}(i)-H^N(i)$ and $H^{\alpha 2}(i)-H^N(i)$.

The identification of a spin system is based on the difference in chemical shifts of its protons. DEFA1 peptide contains 34 amino-acid residues. Seven of its amino-acid residues are present only one time in the peptide, including alanine, glutamate, aspartate, glutamine, histidine, leucine and tyrosine. Otherwise the remaining residues appear at least two times. Alanine is the only residue, which could be unambiguously identified using the TOCSY-spectrum.

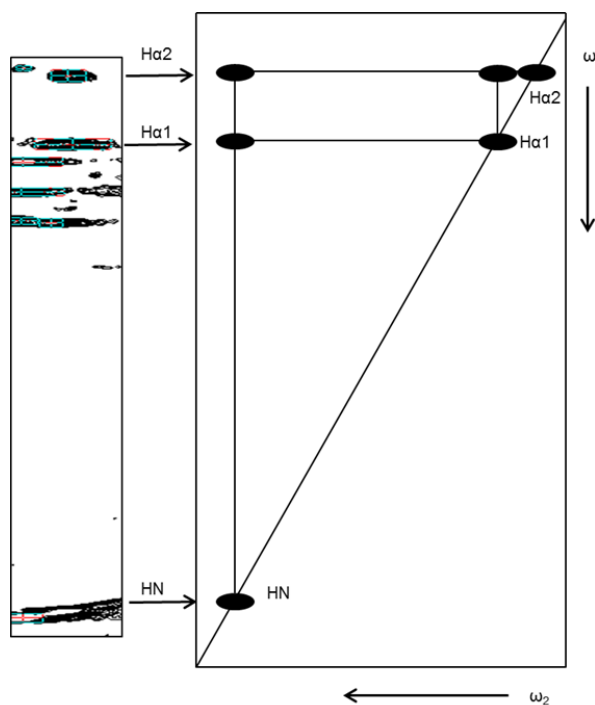


Figure 3.18: The spin system pattern of the L-glycine. On the left side is a section from 60 ms TOCSY spectrum of DEFA1. It shows the spin system pattern of the glycine 13. On the right side is the graphical presentation of a typical spin system pattern of L-glycine.

3.2.2 Homonuclear Sequential Assignment

The next step after identification of the spin systems of DEFA1 amino-acid residues is to determine their location in the sequence (sequential assignment). The 2D-NOESY-spectrum was used to do so, where all protons correlate via dipolar coupling, i.e. a NOESY-experiment detects the intraresidual signals of a residue (its own protons resonances) and interresidual (not own protons resonances). However, the interresidual signals can be only detected if the distances between the protons are $\leq 5 \text{ \AA}$. The interresidual signals can be seen because of the spatial proximity (due to direct neighboring of two amino acids and folding of the peptide).

A NOESY-spectrum with 200 ms mixing time was used to sequentially assign the amino-acid residues of DEFA1 and is shown in figure 3.19. The spectrum shows the proton resonances, which correlate via dipolar coupling. The overlay of both spectra (TOCSY and NOESY) (figure 3.20) illustrates the difference in the number of resonance signals. The black resonances are much more compared to red resonances due to interresidual resonance.

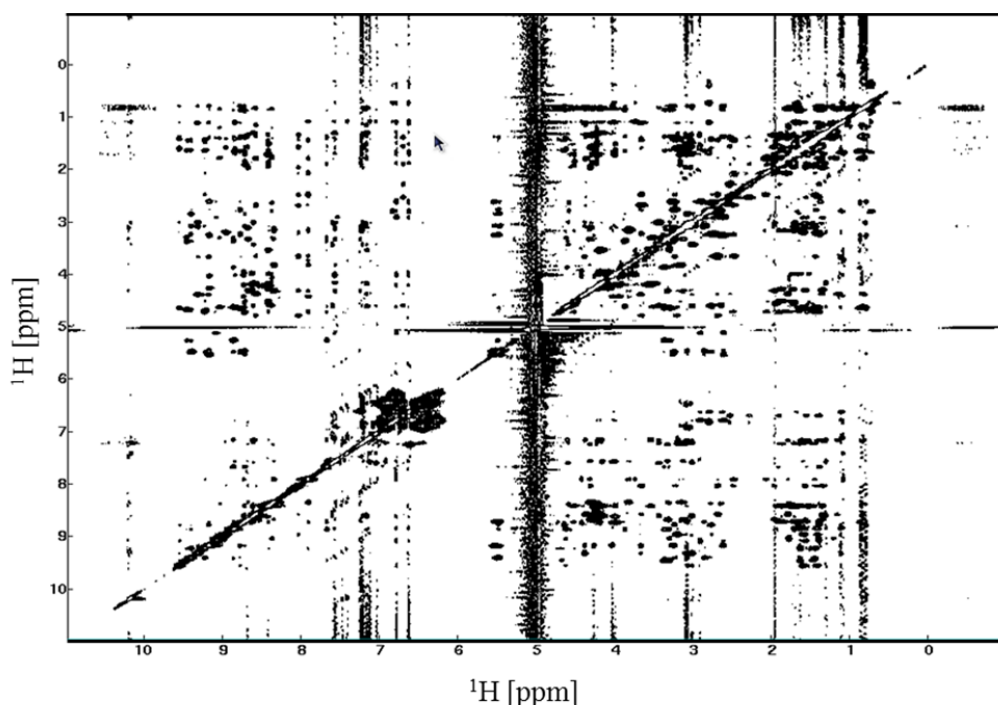


Figure 3.19: Homonuclear 2D-NOESY spectrum of DEFA1 with 200 ms mixing time. It shows the resonance signals due to dipolar interaction of protons, which are less than 5 Å apart.

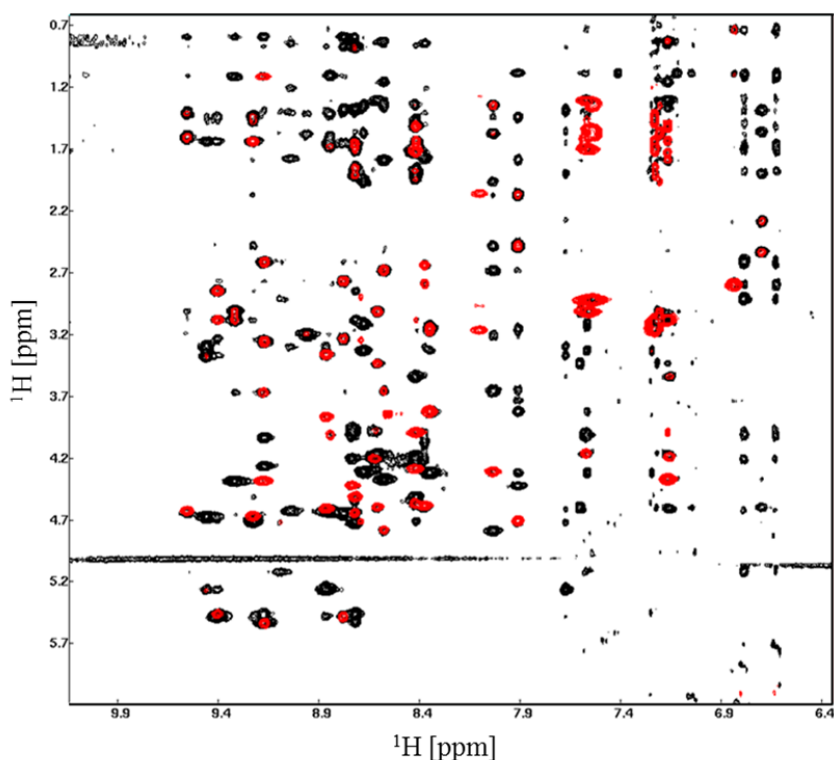


Figure 3.20: Overlay of a section from DEFA1 NOESY- and TOCSY-spectrum. The figure shows the overlay of NOESY (black dots) and TOCSY resonance signals (red dots). The red dots refer to intraresidual and black to interresidual signals. The NOESY- contains much more resonance signals than TOCSY-spectrum.

As was mentioned earlier, 33 out of 34 spin systems could be identified. The first step to make a sequential assignment is the identification of amino-acid residues, which have a unique spin system pattern. After the identification of the interresidual resonance signals on these spin systems, it will help in the identification of the neighboring amino-acid residues. Usually, the distance between the protons (H^{α} , H^{β} , H^N ,...) of an amino-acid residue (i) and the amide proton of the residue (i+1) is smaller than 5 Å, and due to dipolar coupling, interresidual resonance signals can be detected on the vertical frequency axis of the amide proton of the amino acid (i+1) beside its own intraresidual signals.

Figure 3.21 shows an example for the sequential assignment of the neighboring amino-acid residues through identification of the interresidual signals in NOESY-spectrum. The figure displays the sequential assignment of arginine 6 to isoleucine 9.

Alanine 7 and tryptophan 8 contain besides their intraresidual signals the interresidual H^α protons from each preceding amino acid. Isoleucine 9 contains only the H^β proton from the preceding tryptophan 8.

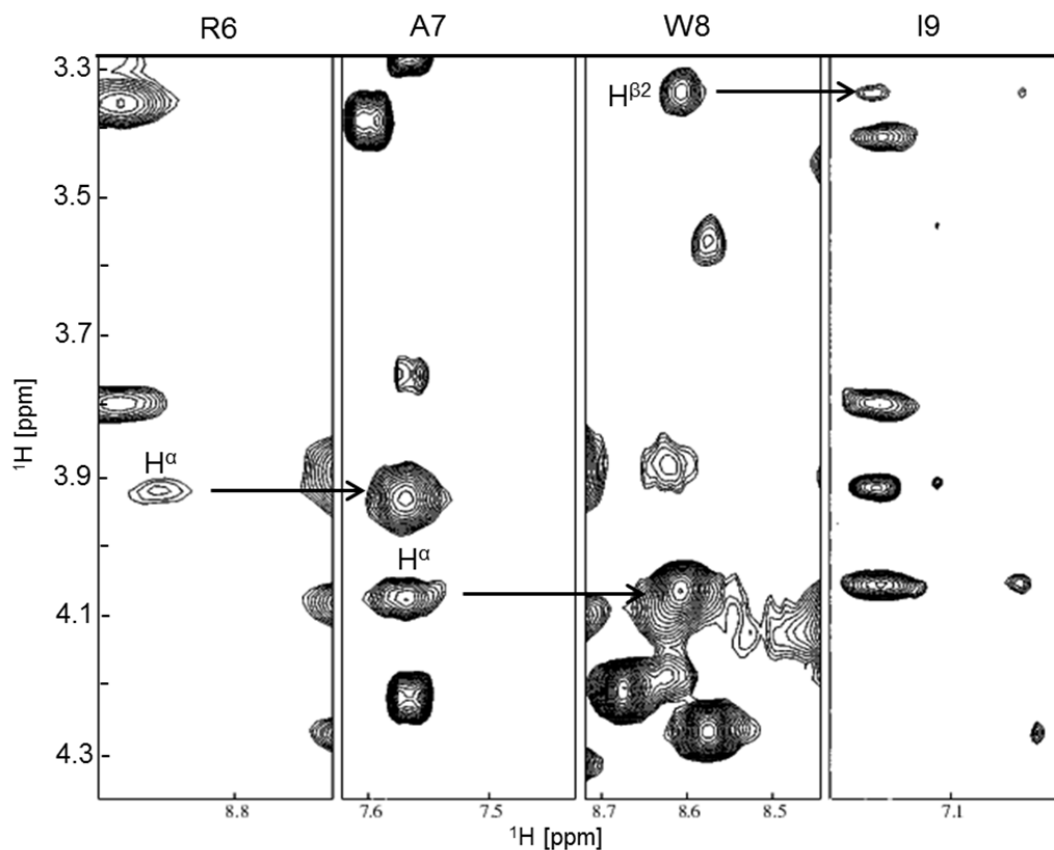


Figure 3.21: Homonuclear sequential assignment strategy of DEFA1 using NOESY-experiment. Four strips from NOESY-spectrum show the spin system of the amino-acid residues arginine 6 to isoleucine 9. The arrows point out the interresidual signals from the neighboring amino acids. Using this strategy almost all the amino acid spin systems of DEFA1 were identified. The strips were taken from the NOESY-spectrum with 200 ms mixing time.

Using this strategy, 30 out of 34 amino-acid residues were identified and sequential assigned. The residues are serine 1 to lysine 19, serine 25 to arginine 34 and glutamine 23. The remaining four amino acids (Cys20, Ile21, Asp22 and Lys24) could not be identified.

3.2.3 The Secondary Structure Elements of DEFA1

After sequential assignment of the spin systems and identification of the protons resonances in the NOESY-spectrum, the existing secondary structure elements in DEFA1 could be estimated.

The formation of secondary structural motives is depended on the existence of contacts between protons of neighboring amino acids or between amino acids, which are over an average distance of up to four amino acid residues, namely short range and medium range contacts, respectively.

A beta-sheet structure is characterized by the presence of a correlation between $H^N(i)$ - $H^N(i+1)$ and $H^\alpha(i)$ - $H^N(i+1)$ of the neighboring amino-acid residues in the NOESY-spectrum. Figure 3.22 shows the sequential and medium range contacts obtained from a 2D-homonuclear NOESY-spectrum. The bars represent the protons contacts and the thickness of the bars represents the correlation strength. Thick bars represent strong coupling while thin bars represent weak coupling. The sequential contacts between the protons $H^N(i)$ - $H^N(i+1)$ and $H^\alpha(i)$ - $H^N(i+1)$ show a typical beta-sheet signal pattern. Medium range contacts, which are typical for alpha-helical structure, were not detected.

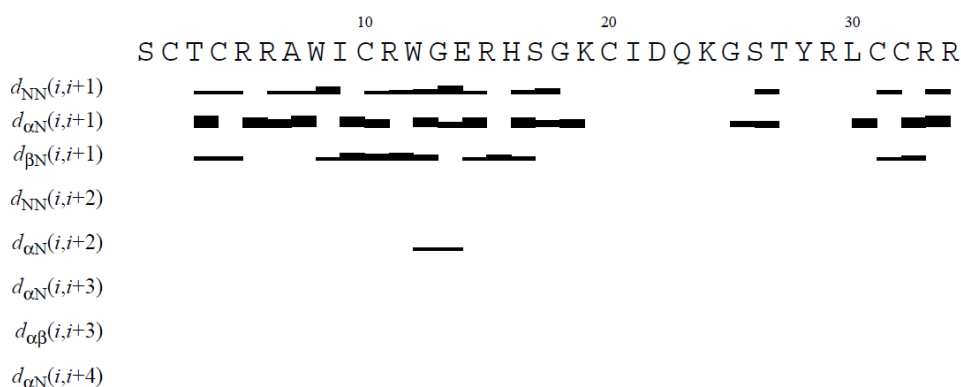


Figure 3.22: Sequential plot of the identified contacts. The figure shows the short and medium range contacts obtained from the homonuclear 2D-NOESY-spectrum of DEFA1. These contacts define the secondary structure of DEFA1. The amino acid sequence of DEFA1 is represented at the top. The bars represent the correlation between neighboring protons $H^N(i)$ - $H^N(i+1)$ and $H^\alpha(i)$ - $H^N(i+1)$. The thickness of the bars corresponds to the intensities of the detected resonance signals.

3.2.4 The Tertiary Structure of DEFA1

Secondary structural motives depends on the presence of sequential and medium range contacts, while the long range contacts are crucial for the tertiary structure.

The long range contacts of DEFA1 residues in the NOSEY-spectrum were assigned. An example of the correlation between protons over a long distance is shown in figure 3.23. The figure shows the coupling of alpha-protons and amide protons of 4 amino-acid residues of DEFA1. The amide proton (H^N) of arginine 15 correlates with the alpha-proton (H^α) of arginine 33 and the H^N of cysteine 32 correlates with the H^α of histidine 16 (represented by the dotted arrows and the circle, respectively).

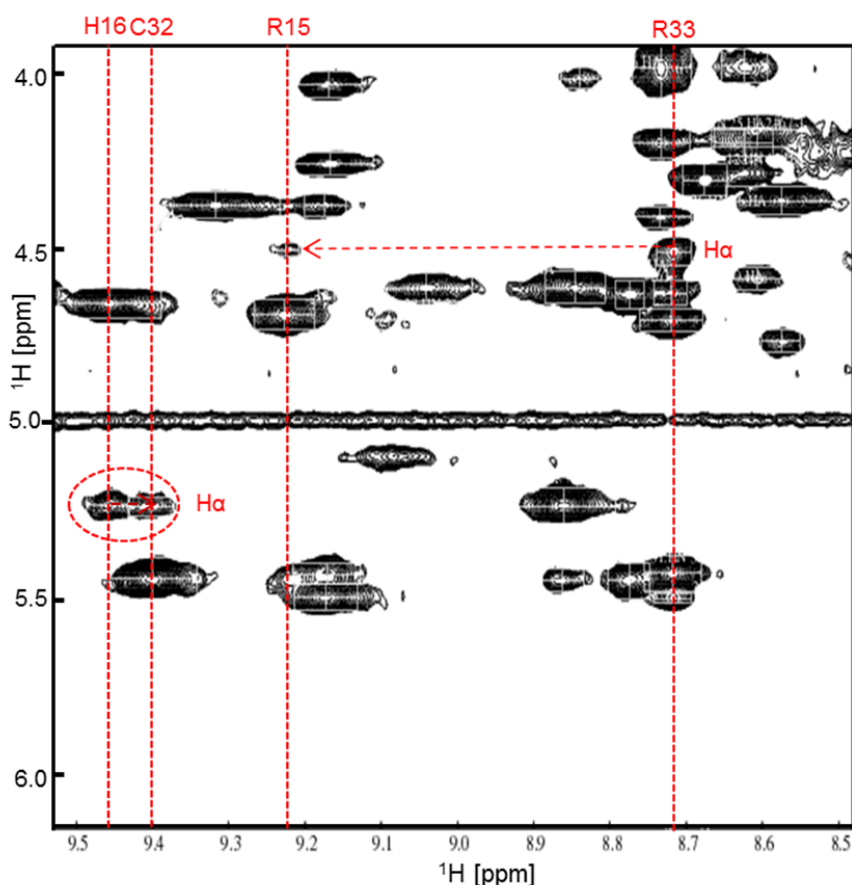


Figure 3.23: NOESY-spectrum for the long range contacts in DEFA1. The section shows the correlation between the amide proton of cysteine 32 (H^N) and the alpha-proton of histidine 16 (H^α) as well as the amide proton of the arginine 15 and the alpha-proton of arginine 33. The vertical dotted lines represents the spin systems of the corresponded amino acids and the dotted arrows and the circle represent the long range distance coupling.

Figure 3.24 represents the distance restraints, which were used for the calculation of DEFA1 structure. The distance restraints were divided into 4 groups and schematically shown as bar for each amino-acid residue. The division into groups was based on the distance of the respective contacts to each other. These groups included the intraresidual, sequential, medium and long range contacts.

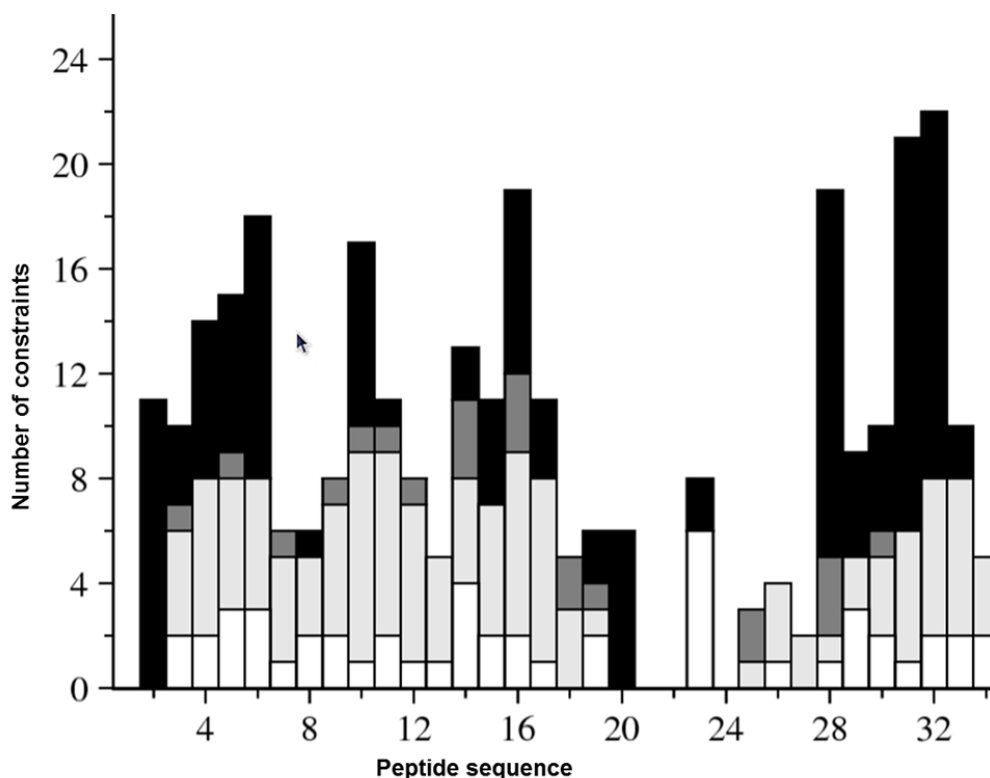


Figure 3.24: Distribution of the distance restraints over DEFA1 peptide sequence. The distance restraints for each amino-acid residue were divided into groups according to the contact type; the white bars represent the intraresidual contacts, light gray bars represent sequential contacts, gray bars represent medium range contacts and black bars represent long range contacts. Both termini of the peptide and the tyrosine 28 show the most long range contacts and the side chain of tyrosine 28 is oriented towards the core of the peptide.

The chart (figure 3.24) shows that the N- and C-termini of the peptide as well as the tyrosine side chain contain the most long range contacts (black bars). This indicates that both termini constitute the peptide core.

Analysis of the NOSEY-spectrum of DEFA1 showed that the amide proton of C31 is correlated with the beta-proton of the C10 and the alpha-proton of C2 is correlated with

beta-proton of C32. Therefore, the combination of the cysteine-residues is represented in the following pattern: C2-C32, C4-C20 and C10-C31. This topology matches the characteristic topology of disulfide bonds of all known alpha-defensins.

The final tertiary structure of DEFA1 was calculated using the simulated-annealing protocol of CYANA 2.1 program performed in dihedral angles space. The identified resonance signals in the NOSEY-spectrum were then converted to distance restraints. The converted 230 distance restraints were used for structure calculation.

Based on these data, 100 structures were calculated and 10 structures were selected according to the lowest target functions that represent the solution conformations of DEFA1. The table 3.1 represents the main parameters of CYANA structure calculation and the ϕ - and ψ -dihedral angles of the peptide backbones of the structures. A very important parameter of CYANA structure calculation is that the selected structures should not violate the distance restraints or the violated distance restraints have to be smaller than 0.5 Å. The selected structures of DEFA1 with the lowest target functions show no violation of distance restraints.

Table 3.1: Structural statistical data for the selected structures of DEFA1 with the lowest target functions. The structures showed no violated distance constraint, rmsd = root mean square deviation in Å.

Distance restraints	
Intraresidual ($i - j=0$)	87
Sequential ($ i - j =1$)	64
Medium range ($2 \leq i - j \leq 4$)	13
Long range ($ i - j \geq 5$)	48
Disulfide bonds	18
All distance restraints	230
Pairwise rmsd for residues 1–34 in Å	
Mean global backbone rmsd	1.13 +/- 0.19
Mean global heavy atom rmsd	1.87 +/- 0.23
Pairwise rmsd for residues 3-21 and 28-32 in Å	
Mean global backbone rmsd	0.63 +/- 0.11
Mean global heavy atom rmsd	1.43 +/- 0.21
Ramachandran plot (mean values for all 10 structures)	
Most favored regions (%)	42.4
Additional allowed regions (%)	52.4
Generously allowed regions (%)	4.8
Disallowed regions (%)	0.3

The Ramachandran plot is used to visualize the backbone dihedral angles ψ (ψ) against ϕ (ϕ) of all the amino-acid residues and to validate the selected structures [109].

The Ramachandran plot of the best 10 structures is shown in figure 3.25. The ψ (ψ) and ϕ (ϕ) of each amino-acid residue were represented as potential energy. The colors indicate the differences in energy level. The highest potential energy area (white) represents the disallowed regions. Only 0.3% of the dihedral angles are in the disallowed regions, which corresponds to amino-acid residue leucine 30. On the other hand, the generously allowed regions (grey) represent 4.8% , the additional allowed regions (light blue) represent 52% and the most favored regions (blue) with the lowest potential energy represent 42% of the dihedral angles. Nearly all the residues are located in the allowed regions (99.7%). Only Leu 30 is located in the disallowed regions.

The data show that most of the amino-acid residues dispose dihedral angles, for ψ the value is between 45° and 180° and for ϕ is from -180° to -45° . The corresponding conformation of the dihedral angles in these structures is characteristic for beta-sheet elements.

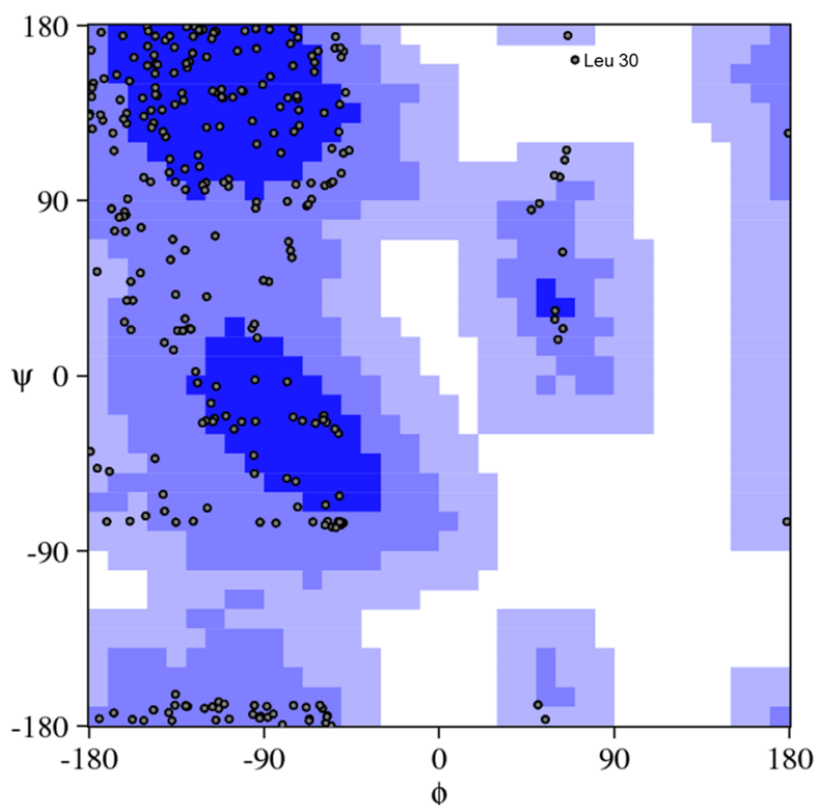


Figure 3.25: Ramachandran plot of the best 10 structures of DEFA1. Both dihedral angles (psi and phi) of all amino-acid residues are distributed in different regions according to their potential energy. Blue color refers to most favored regions, which represent the lowest potential energy, light blue represents additional allowed regions, grey denotes generously allowed regions and white regions represent the disallowed regions, which have the highest potential energy. 99.7% of the amino-acids residues are in the allowed regions. Only Leu 30 is located in the disallowed region.

Next, the best 10 structures were superimposed to represent the tertiary structure of DEFA1. Figure 3.25 (A) shows the structure ensemble based on a superposition onto the segments spanning residues 3–21 and 28–32, which make up 70% of the peptide. The structures differ at the N-, C-termini and in the segment spanning residues 20-24. This indicates a high flexibility of the molecule in these regions. The tertiary structure of one of the 10 structures (structure number 4), which has the lowest rmsd to the average structure, was selected and is shown in figure 3.26 (B).

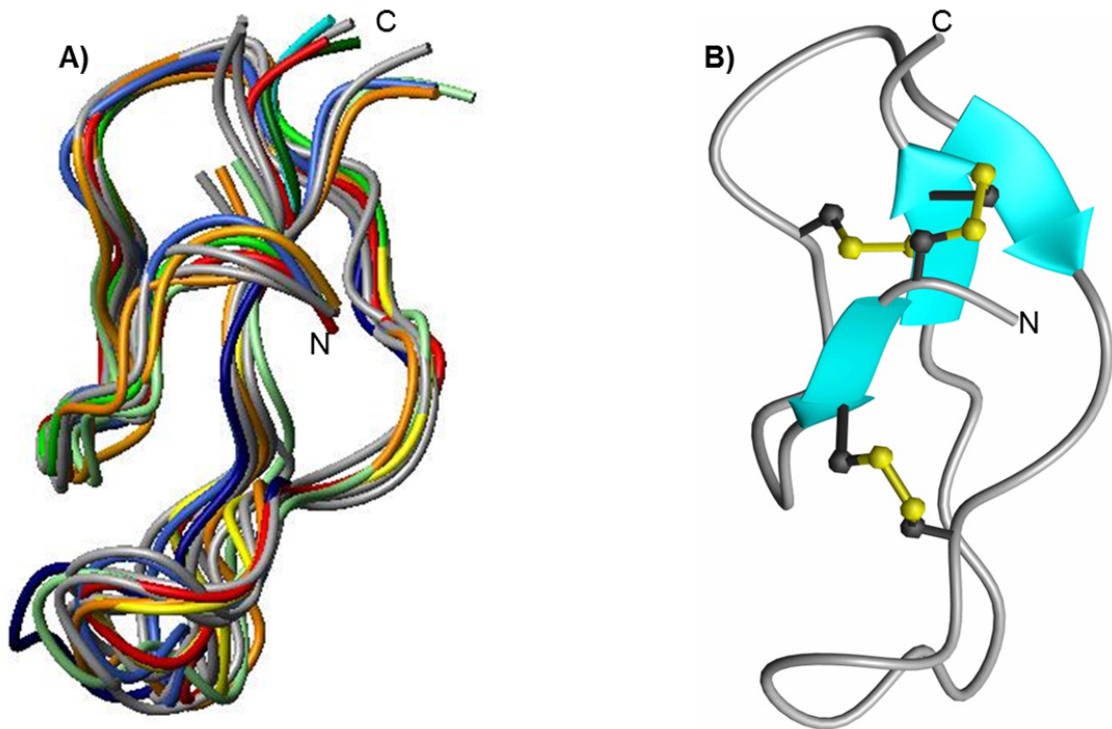


Figure 3.26: The tertiary structure of DEFA1. (A) Spaghetti representation of the ensemble of the best 10 calculated structures with the lowest target functions. (B) Ribbon diagram of structure number 4, which was selected to be representative for the average structure. N and C denote N and C-termini, respectively, DSB refers to disulfide bond. Figures (A and B) were illustrated using MOLMOL program.

The predominant secondary structure of DEFA1 is beta-strand as shown in the ribbon diagram in figure 3.26 (B). DEFA1 comprises three beta-strands ($\beta 1$, $\beta 2$ and $\beta 3$) arrange in an anti-parallel manner. The N-terminus of DEFA1 consists of a flexible and unstructured region of two amino acid residues, followed by a first beta-strand ($\beta 1$). The first disulfide bond, DSB1 (C2-C32) positions the $\beta 1$ closer to the core of the peptide. The $\beta 1$ is followed by the first long loop (loop1) and it connects the $\beta 1$ to the $\beta 2$. The second disulfide bond, DSB2 (C4-C20), stabilizes this loop. $\beta 2$ is followed by a the second loop (loop2), which connects $\beta 2$ to the C-terminal $\beta 3$, which is stabilized by the third disulfide bridge, DSB3 (C10-C31).

The electrostatic surface potential of DEFA1 was calculated (figure 3.27). The uncharged areas contain the hydrophobic amino-acid residues, represented in white color, while the colored areas represent hydrophilic amino-acid residues. The positive

charges are shown in blue and the negative in red (figure 3.27). DEFA1 molecule shows a globular protein shape with two almost hydrophobic faces that are separated from each other by a belt of positive charges.

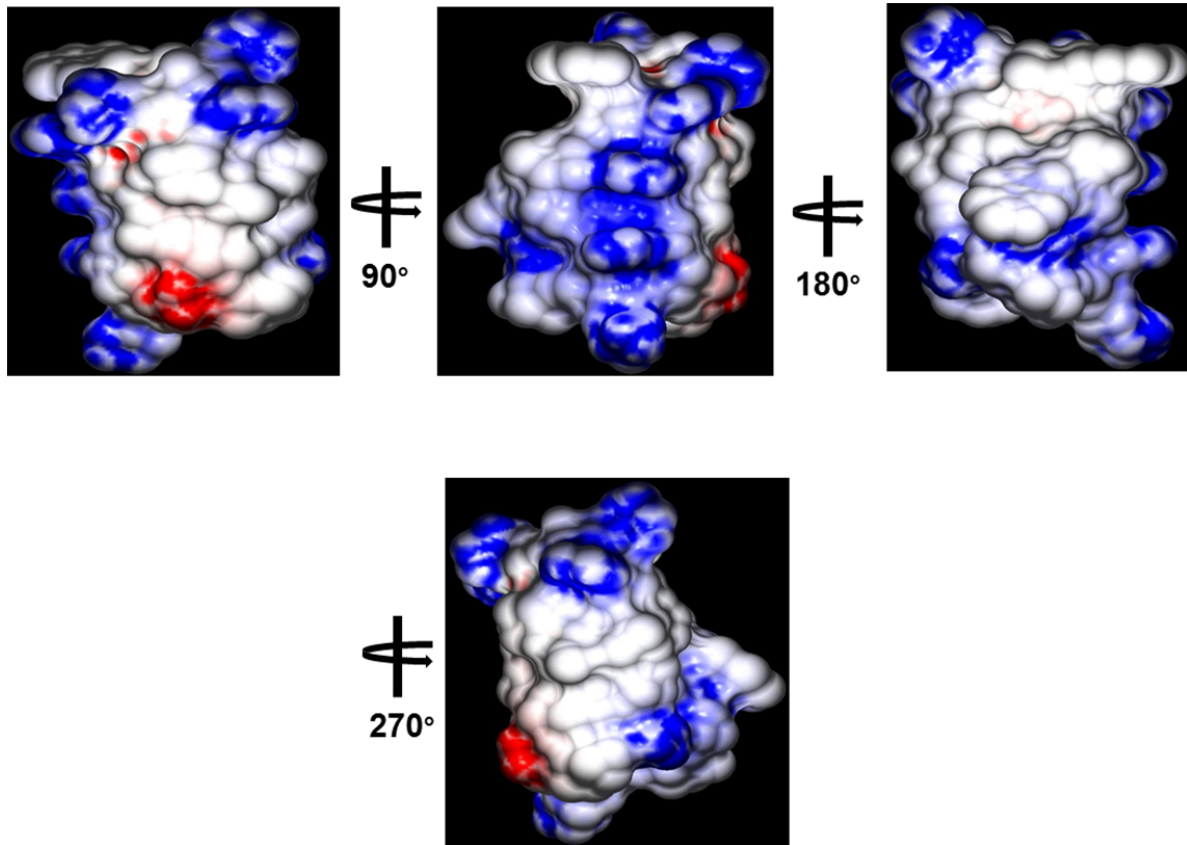


Figure 3.27: The electrostatic surface potential of DEFA1 from different views. Four faces are shown differing by a 90° each. The positive charged regions are colored in blue and negative charged regions in red. The distribution of hydrophobic amino-acid residues is represented in white.

3.2.5 Structural Comparison of DEFA1 with other Alpha-defensin Family Members

Sequence homology analysis of DEFA1 with other alpha-defensin family members revealed that DEFA1 is a homolog to Paneth-cell-specific human alpha-defensin 5 (HD5) [86]. As shown in figure 3.28 (A), DEFA1 structure adopts a typical alpha-defensin fold with a core structure consists of three antiparallel β -strands stabilized by three intramolecular disulfide bonds. The tertiary structure of DEFA1 shows a high similarity to

the tertiary structure of human neutrophil peptide 3 (HNP3) and alpha-defensin 5 (HD5) (figure 3.28 B, C).

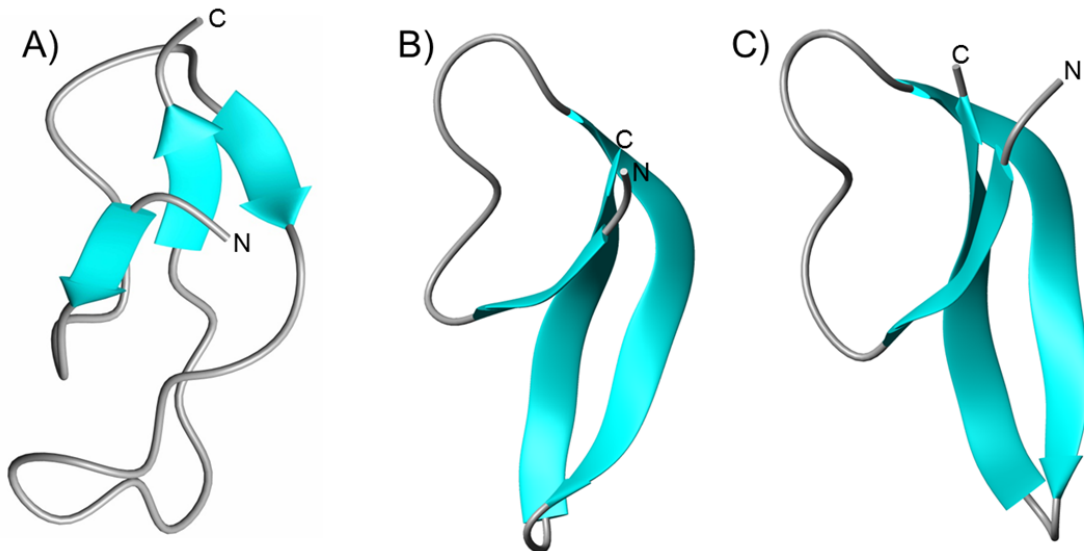


Figure 3.28: The tertiary structures of DEFA1, HNP3 and HD5. A) DEFA1. B) HNP3 (PDB ID: 1DFN. C) HD5 (PDB ID: 1ZMP). The three peptides comprise three antiparallel beta-strands. The beta-strands of all three peptides show the same orientation. N and C signify the N-and C-terminus, respectively.

Like HNP3 and HD5, DEFA1 has a small unstructured N-terminal region, followed by the first β 1. β 1 is followed by the first loop, which connects β 1 to β 2. β 2 is connected to β 3 by the second loop. The beta-strands in DEFA1 show the same orientation as in HNP3 and HD5. Compared to HD5 and HNP3 the second loop in DEFA1 is longer and beta-hairpin is not distinctive formed like in HD5 and HNP3. The termini of DEFA1 are apart in comparison to termini of HD5 and HNP3, which are much closer to each other.

Due to high identity between DEFA1 and HD5 surface potential of DEFA1 is compared with HD5. Figure 3.28 shows the electrostatic surface potential of DEFA1 and HD5. HD5, in contrast to DEFA1, forms dimers in solution. In addition, HD5 peptide (monomer) forms a globular shape with an extension at the N-terminus (figure 3.28 (A)). The positive charges of the HD5 are located on one region, while the only one negative charge is located on the other side (rotation 180°). These charged areas of HD5 are separated by a narrow uncharged section (figure 3.28 (A)).

Whereas high identity between the peptides and the number of arginine residues almost equal (HD5 6 and DEFA1 7 residues) the distribution of charges on the surface of HD5 and DEFA1 is completely different (figure 3.29). DEFA1 displayed an amphipathic structure with hydrophobic residues forming two hydrophobic areas and positively charged residues forming a hydrophilic ring, as shown in figure 3.27. While in DEFA1 positive charges appear to be dispersed about the perimeter, the hydrophobic regions appear to join around one side of the molecule. This charges distribution of DEFA1 results in one region of positive residues, one of charged-uncharged residues and one of hydrophobic residues, which contains two negative charges of E14 and D22 (figure 3.27).

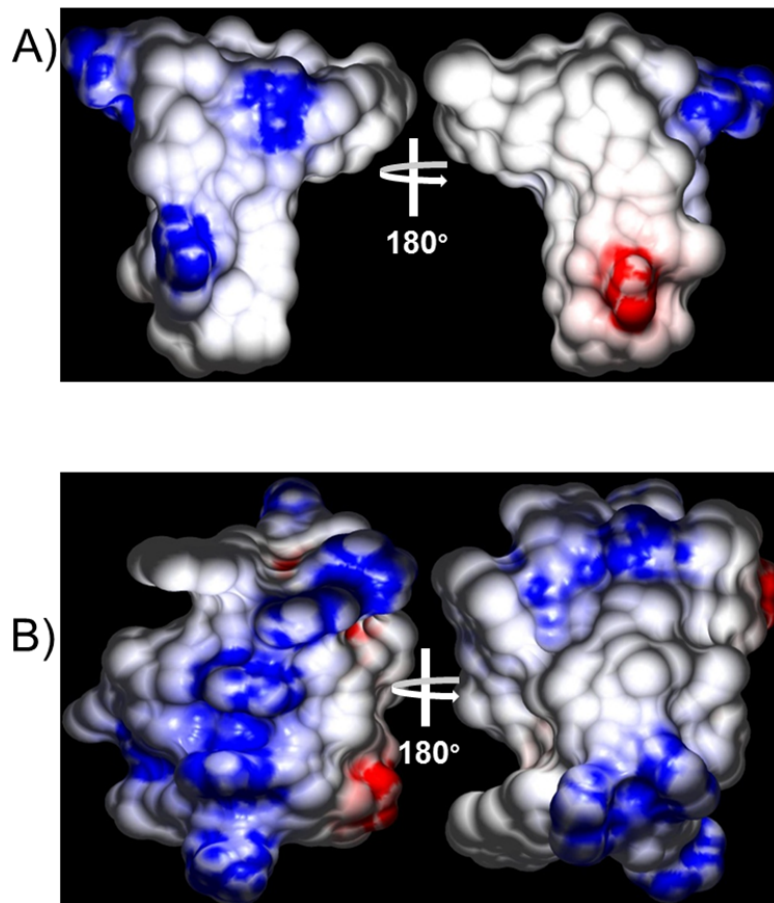


Figure 3.29: The electrostatic surface potential of DEFA1 and HD5. The figure shows the distribution of the positive and negative charges on the surface of HD5 as monomer (A) and DEFA1 (B). Positively and negatively charged regions are represented in blue and red, respectively, white color represents the hydrophobic residues.

4 Discussion

4.1 NOD2 CARD2

The Nucleotide binding and oligomerization domain containing protein 2 (NOD2) is an intracellular pattern recognition receptor that regulates nuclear factor Kappa B (NF-Kappa B) activation and mutations in *NOD2* were linked to Crohn's disease [19]. NOD2 contains two CARDs domain (CARD1 and CARD2), one NOD domain and one LRR domain [18].

CARDs are protein-protein interaction domains, which belong to the death domain (DD) superfamily. They facilitate homo- or / and hetero-oligomerization of proteins and play a key role in many cellular processes, like apoptosis, cancer, inflammation and development of auto-inflammatory diseases by activating caspase-1, caspase-8 or NF-kappa B [35]. Investigations of the interaction between the CARD domains of Apaf1 and caspase-9 ([110]) as well as between the CARDs of RAIDD and caspase-2 [38] revealed that interactions between these domains are primarily electrostatic.

NOD2 CARD2 is involved in signaling of NOD2 and of note, a NOD2-short isoform (NOD2-S) (the first 126 amino acid residues of NOD2) acts as a regulatory inhibitor of NOD2 in the colon [44]. Recently, it was shown that both CARD domains of NOD2 are involved in oligomerization of NOD2 after stimulation with MDP in the presence of ATP and magnesium-ions [28].

In the present work, a protocol for the expression and purification of NOD2 CARD2 was established to facilitate the investigation of NOD2 CARD2 function *in vitro* and provide the basis for structure determination.

The borders of the NOD2 CARD2 domain were set according to the sequence of other known CARD domains. NOD2 CARD2 has a predicted molecular weight of 11.35 kDa and an pI of 9.41.

A TEV cleave site was cloned by PCR directly at the N-terminus of NOD2 CARD2. The construct was cloned into the two different bacterial expression vectors. To verify expression and solubility of His-TEV-NOD2 CARD2 and Trx-TEV-NOD2 CARD2 fusion

proteins, an expression test was performed using various bacterial expression strains. Both fusion proteins were expressed in inclusion bodies.

The fusion proteins were isolated from inclusion bodies and renatured by dialysis; Trx-TEV-NOD2 CARD2 fusion protein was stable in Tris buffer pH 8, whereas His-TEV-NOD2 CARD2 was stable only in buffer systems (acetate pH 5 and CAPS pH 12). In such buffer systems with low or high pH the fusion protein is not cleavable neither using TEV nor thrombin proteases.

Therefore, the work was continued with the Trx-TEV-NOD2 CARD2 fusion protein. The DLS analysis showed that the solution of fusion protein was monodisperse. However, its hydrodynamic radius was larger than its expected size, indicating that it may be present in small soluble oligomers. The CD-spectroscopy experiments and Ellman's test showed that the protein was refolded and all four cysteine residues are involved in disulfide bonds.

The fusion protein contains both protease cleavage sites (TEV and enterokinase) (figure 2.2) and was proteolytically cleaved. Cleavage of the fusion protein by the TEV protease induced instability in the cleaved NOD2 CARD2 fragment that led to precipitation. In contrast, cleavage of the fusion protein by the enterokinase resulted in a stable NOD2 CARD2 fragment, which was isolated using RP-HPLC. The NOD2 CARD2 fragment containing additional 23 amino-acid residues was named as 23aa-NOD2 CARD2.

The additional 23 residues gave somehow stability to NOD2 CARD2. These amino-acid residues are (AMADIGSEFELRRQASENLYFQG). Analysis of the secondary structure using secondary structure prediction programs showed that these residues have the ability to build an alpha-helix. The peptide was investigated on its potential to form secondary structure three times by using three different secondary structure prediction programs. The results of all three predictions showed that the peptide displays an alpha-helical structure. The additional alpha-helix reduces oligomerization and prevents the precipitation of NOD2 CARD2 after cleavage.

CARD domains have 6 to 7 antiparallel alpha-helices and they are heat sensitive [35]. CD spectroscopy of 23aa-NOD2 CARD2 (figure 3.10) demonstrated that the protein contains only alpha-helices.

Analysis of the heat stability of 23aa-NOD2 CARD2 showed that the protein non-reversibly unfolds at $T_m=55$ °C (figure 3.11). A comparison of the melting temperatures of 23aa-NOD2 CARD2 to NOD2 CARD2, which unfolds at $T_m=38.0$ [111] highlights that 23aa-NOD2 CARD2 unfolds at higher temperature. Compared to the melting temperatures of other known CARD domains such Apaf-1 CARD ($T_m=59.7$ °C), procaspase-9 CARD ($T_m=53.4$ °C) and NOD1 CARD ($T_m=78.0$ °C) [111], 23aa-NOD2 CARD2 unfolds at similar temperature. Heating of 23aa-NOD2 CARD2 at 40 °C for short time led to formation of large oligomers (figure 3.14), however the protein did not unfold, suggesting that the covalent link of the additional 23 residues might enhance the thermal stability of the whole molecule.

Friedh *et al* reported that NOD2 CARD1 and NOD2 CARD2 were expressed as one construct to overcome the expression problems. To isolate single domains, a thrombin cleavage site was cloned between the CARDs domains. Using this strategy they were able to produce single CARD domains of NOD2 [111].

Compared to NOD2 CARD2 [111], 23aa-NOD2 CARD2 is salt sensitive. Addition of 150 mM NaCl to the protein in phosphate buffer (figure 3.15) led to formation of high order oligomers.

The additional peptide on one hand might enhance the thermal stability and on other hand worsens salt stability of 23aa-NOD2 CARD2.

NOD2 is the only member of the NOD-like receptor that contains two N-terminal CARD domains (CARD1 and CARD2) and the presence of both CARDs is vital for NOD2 functionality. On one hand, the NOD2 CARDs (1 and 2) have to be expressed as one construct due to stabilization effect of the both CARDs domain on each other as reported by Friedh *et al*. On the other hand, NOD2 CARD2 might need only the last helix (number 6) of NOD2 CARD1 but not the whole domain to be stable. It is possible that both domains (CARD1 and CARD2) share this helix.

4.2 Equine Alpha-Defensin (DEFA1)

DEFA1 is an equine alpha-defensin, which was identified and characterized by Bruhn *et al.* The peptide displayed antimicrobial activity against Gram positive, Gram negative bacteria and fungus. DEFA1 is only expressed in the small intestine of equine.

The synthetic DEFA1 peptide was refolded and purified using RP-HPLC and its activity was tested against pathogens [88]. Schlüsselhuber *et al.* suggested that DEFA1 could be a potential therapeutic antibiotic peptide against *R. equi* and *S. zooepidemicus*. Therefore, determination of the tertiary structure of DEFA1 helps in defining its mechanism of action.

The observed activity of DEFA1 against *R. equi* and *S. zooepidemicus* confirms that the peptide is present in a folded form and CD-spectroscopy of DEFA1 showed that the peptide contains beta-strands.

Determination of the solution structure of DEFA1 was reached by means of homonuclear ¹H-2D-NMR spectroscopy. DEFA1 is composed of 34 amino-acid residues. In ideal case, all 34 amino acid residues should be identified. In the TOCSY-experiment, all the residue's spin systems could be detected. However, the sequential assignment of DEFA1 showed that only 30 residues could be assigned using ¹H-2D-homonuclear TOCSY and NOESY spectra. The amino-acid residues Cys20, Ileu2, Asp22 and Lys24 could not be assigned.

The results of the Ellman's test and mass spectrometry of purified DEFA1 indicated that all six cysteine residues in the molecule are oxidized and they form three disulfide bridges. According to the conserved disulfide bridge pattern of alpha-defensins [55], the disulfide bonds should be formed in DEFA1 between Cys2 and Cys32, Cys4 and Cys20 and Cys10 and Cys31.

Analysis of NOEs derived from the NOESY-spectrum displayed that Cys2 correlated with Cys32 and Cys10 with Cys3. However, no correlations were found between the protons of Cys4 and Cys20 side chains. Despite of that, the third disulfide bond is predicted to be between Cys4 and Cys20 because there is no other possibility to form a third bond. In addition, structure calculations using CYANA program with different

combination of paired cysteine residues were done to ascertain the results. The calculations showed that the most favourable combination of disulfide bridges pattern, according to the target function values, was the conserved alpha-defensins disulfide bridges pattern.

The results conclusively illustrate the 3D-structure of equine DEFA1 (figure 3.26). The tertiary structure of equine DEFA1 is similar to other known alpha-defensins (figure 3.28). The 3D-structure of DEFA1 shows that it consists of three beta-strands, including a loop, which align to form antiparallel beta-strands.

DEFA1 contains three antiparallel beta-strands. The beta-strands are short in compared to HD5 and HNP3. However, the orientation of all beta-strands of DEFA1 corresponds to the beta-strands orientation of the alpha-defensin fold, which is characterized by formation of 3 antiparallel beta-strands, which are stabilized by 3 intramolecular disulfide bonds [112]. The beta-strands of DEFA1 are short compared to beta-strands of HNP3 and HD5, it might due to missing medium range contacts between DEFA1 residues.

The NMR-data showed that in contrast to all human alpha-defensins [113], [112], DEFA1 is monomeric in solution like cryptdin-4 [114], a mouse Paneth cell alpha-defensin.

Electrostatic surface potential analysis helped to understand the structure-function relationship of DEFA1 (figure 3.27). The surface potential analysis displays a unique charges distribution on DEFA1 surface, compared to the surface potential distribution of human alpha-defensins. The common character of surface potentials of all human alpha-defensins is that the charged residues are located on one side of molecules and uncharged residues on the opposite side to form an amphipathic character [112]. The results of DEFA1 showed that the positive charges are located about the perimeter and the hydrophobic regions are located on the two areas of the molecule.

Bruhn *et al* investigated the interaction between DEFA1 and different liposomes using CD-spectroscopy and tryptophan fluorescence-emission spectroscopy [86]. They showed that DEFA1 interacted with negative charged liposomes (phosphatidylglycerol liposomes [PG-liposomes]) and the fluorescence emission of tryptophan changed after incubation of the PG-liposomes with the peptides. It means that DEFA1 translocates

through the lipid layer. These effects were not observed, as the uncharged liposomes were incubated with DEFA1. Incubation of the PG-liposomes with DEFA1 led to a reduction of the intensity of the CD-ellipticity signal. Schlüsselhuber *et al* have confirmed these results [88]. The authors showed that incubation of DEFA1 with PG-liposomes led to formation of precipitates. Dr. Sascha Jung investigated the effect of DEFA1 on negative and neutral liposomes using DLS (personal communication). He showed that incubation of DEFA1 with PG-liposomes led to the formation of large aggregates, while no effect was monitored, when uncharged liposomes were used.

DEFA1 is homolog to human alpha-defensin 5 (HD5) [86]. The precise mechanism of antimicrobial action of human enteric alpha-defensin is unclear [115]. HD5 performs different mechanisms of action against Gram-positive and Gram-negative bacteria [115]. The mechanism of action of DEFA1 is not intensively investigated. Bruhn *et al* described the mechanism of action of DEFA1 using a minimalistic system (depolarization of liposomes as a measurement of pore-forming activity) [86]. He proposed that the peptide has a moderate pore-forming activity. Schlüsselhuber *et al* showed that anionic vesicles, as substrates for DEFA1, had revealed an aggregation pattern for the effects of DEFA1 on the anionic vesicles [88]. Scanning electron microscopy of *R. equi* treated with DEFA1 showed that incubation of DEFA1 with bacteria leads to clustering of bacteria. However, Schlüsselhuber did not discuss this phenomenon.

Interestingly, the charge distribution on the surface of DEFA1 is very similar to Hydramacin-1, a *Hydra* antimicrobial peptide, which was characterized by Jung *et al* [116] and cryptdin-4 (Crp4), a mouse intestinal Paneth cells alpha-defensin [114]. The peptides exhibited an amphipathic structure and the hydrophobic residues are located on two areas, while the positive charge residues form a hydrophilic ring. The initial step of the bactericidal mechanism of hydramacin-1 is aggregation of treated bacteria before the extensive killing effect. The aggregation phenomenon was also observed once negative liposomes were used as substrate for hydramacin-1 [116]. In contrast to hydramacin-1, Crp4 interacts with the bacterial membrane and directly permeabilizes them without formation of initial bacterial aggregation step [117], [114].

Taken together, these observations indicate that DEFA1 is similar to hydramacin-1 in the charges distribution on the surface and at least in the initial step of the killing

mechanism. It is tempting to speculate that mode of action of DEFA1 is similar to the mode of action of hydramacin-1 and the killing mechanism of DEFA1 can be describe using the proposed model of mode of action of hydramacin-1. The both hydrophobic areas of DEFA1 submerge into the outer membrane of two neighboring bacterial cells. Thus, negative charges of the phospholipids of the membrane surfaces are compensated by the set of positive charges around the perimeter of the molecule. This electrostatic interaction could enhance the aggregation of bacterial cells at the point of immersion. Hydrophobic and electrostatic interaction stabilizes the peptide-lipid complex. However, this statement is speculative and the exact bactericidal mechanism of action of DEFA1 on various Gram-negative, Gram-positive bacterial and fungus has to be identified. Elucidating the detailed mechanism of action will require further investigations of structure-functions and structure-actions using putative physiological targets.

4.3 Prospective

4.3.1 NOD2 CARD2

Activated NOD2 binds to the protein kinase RICK to direct NF-kappa B-mediated cytokine responses and the interaction between the both proteins is mediated *via* CARD domains [18]. To understand the interaction, *in vitro* functional studies and structural information are needed. The established protocol for expression and purification of NOD2 CARD2 in the present thesis is the basis for future investigations of NOD2 CARD2 interaction with other domains of NOD2 and with other CARD containing proteins. Future experiments including, determination of structures of NOD2 CARD2 and NOD2 NOD1 might help in a development of strategies for therapies of people with NOD2-hyperactivation state [118].

Moreover, define NOD2 mechanism of activation by NOD2 LRR-ligands complex and how this activation is regulated will help in understanding how the mutations in *NOD2* link to Crohn's disease and it might be the first step for development a therapy [119],[120].

4.3.2 DEFA1

The theatrical increase in resistance to antibiotics by pathogens has made a major medical need for new anti-infective products. For example, more than 25% of *K. pneumoniae* isolates found in 11 countries of EU, are resistant to third-generation cephalosporin. Only in EU, it was estimated that in 2007 about 25 000 people died from an infection due to multidrug-resistant bacteria. It might be the situations in other many countries even worse [121]. Therefore, it is important to develop new drugs to treatment people most affected. One promising potential is utilizing of AMPs due to development of resistance by bacteria is very rare and AMPs have a board spectrum of antimicrobial activity [51]. Therefore, optimization of mode of action, as example, by design chimeric peptide [122], and definition of their mode of action will accelerate their medical application. Determination of the tertiary structure of DEFA1 provided a better understanding of the mode of action of this defensin.

5 Summary

Nucleotide-binding oligomerization domain-containing protein 2 (NOD2) is a cytosolic pattern recognition receptor (PRR). It binds muramyl dipeptide and consists of two N-terminal caspase-activating and recruitment domains (CARD) (CARD1 and CARD2), one central nucleotide-binding oligomerization domain (NOD) and C-terminal leucine rich repeats (LRR). The CARD2 domain of NOD2 (NOD2 CARD2) is a member of death domain superfamily, which is characterized by holding six antiparallel α -helices. NOD2 CARD2 is involved in signaling of NOD2. Recently it was shown that NOD2 CARDs (CARD1 and CARD2) are involved in the oligomerization of NOD2 *in vitro*, however the precise function of CARD2 domain in NOD2 is still unclear.

In the first part of this thesis a protocol for expression, purification and refolding was established to be the basis for tertiary structure determination and *in vitro* functional investigations.

The second part of the thesis deals with determination of tertiary structure of equine α -defensin 1. The peptide shows high killing activity against Gram-positive, Gram-negative bacteria and fungus and it is a potential antibiotic peptide against *R. equi* and *S. zooepidemicus*.

To elucidate the mechanism of action of equine α -defensin 1 the solution structure was determined by two-dimensional homonuclear NMR-spectroscopy. The synthetic peptide was refolded, purified and NMR spectra of the purified peptide were recorded. The tertiary structure contains a cysteine-stabilized β -strands motif and shows a high structural homology to other α -defensins. Compared to the surface potential of human defensins, DEFA1 displays an unusual distribution of the charges. The similarity between DEFA1 and hydramacin-1 in charges distribution and inducement of aggregation in treated bacterial cells and liposomes supports the hypothesis that the mode of action of DEFA1 is similar to the mode of action of hydramacin-1.

6 Zusammenfassung

Nucleotide-binding oligomerization domain-containing protein 2 (NOD2) ist ein intrazellulärer PRR (*pattern recognition receptor*). Dieser Rezeptor bindet Muramyl-dipeptid und besteht aus zwei N-terminalen *caspase-activating and recruitment domains* (CARD1 und CARD2), einer zentralen *nucleotide-binding oligomerization domain* (NOD) und einer C-terminalen *leucin rich repeats* (LRR). Die CARD2 Domäne von NOD2 (NOD2-CARD2) ist ein Mitglied der Todesdomäne Superfamilie (*death domain superfamily*), die durch sechs antiparallele alpha-Helices gekennzeichnet ist. Die NOD2-CARD2 ist an der Weiterleitung der Signal von NOD2 beteiligt. Kürzlich wurde gezeigt, dass die CARD-Domänen von NOD2 (CARD1 und CARD2) auch an der Oligomerisierung von NOD2 *in vitro* beteiligt sind, die genaue Funktion der CARD2-Domäne in NOD2 ist jedoch bis jetzt unklar.

Im ersten Teil dieser vorliegenden Arbeit wurde ein Protokoll für die Expression, Reinigung und Rückfaltung etabliert, um die Basis für Tertiärstrukturaufklärung und *in vitro* funktionelle Untersuchungen von der NOD2-CARD2 Domäne zu schaffen.

Der zweite Teil der vorliegenden Arbeit behandelt die Tertiärstruktur des Equine Alpha-Defensins 1 (DEFA1). Das Peptid verfügt über eine hohe antimikrobielle Aktivität gegen Gram-positiven und Gram-negativen Bakterien sowie gegen Pilze. Um den Wirkmechanismus des Peptids näher zu bestimmen, sollte die Tertiärstruktur des DEFA1-Peptides mittels zweidimensionaler homonuklearer (2D-¹H) NMR-Spektroskopie aufgeklärt werden.

Zu diesem Zweck wurde ein Renaturierungs- und Reinigungsprotokoll für DEFA1 etabliert. Von dem gereinigten und renaturierten Peptid wurden 2D-¹H-NMR-Spektren aufgenommen. Die aufgeklärte Tertiärstruktur des DEFA1 entspricht einem durch Disulfidbrücken stabilisierten β -Faltblattmotiv und weist eine hohe strukturelle Verwandtschaft zu den Alpha-Defensinen auf. Im Vergleich zu Oberflächenpotentialen von humanen Alpha-Defensinen zeichnet sich die Oberflächenpotential des DEFA1 durch eine ungewöhnlich Verteilung der Ladungen aus. Die Ähnlichkeit zwischen

DEFA1 und Hydamycin-1 bezüglich der Oberflächenverteilung von Ladungen und Veranlassung der Aggregation in behandelten Bakterienzellen und Liposomen unterstützt die Hypothese, dass die Wirkungsweise der DEFA1 der Wirkungsweise von Hydamacin-1 ähnelt.

7 References

1. Klein, J., *Immunology*. 1991, Boston; Oxford; London: Blackwell Scientific Publication.
2. Janeway, C.A., Jr. and R. Medzhitov, *Innate immune recognition*. *Annu Rev Immunol*, 2002. **20**: p. 197-216.
3. Ausubel, F.M., *Are innate immune signaling pathways in plants and animals conserved?* *Nat Immunol*, 2005. **6**(10): p. 973-9.
4. Kawai, T. and S. Akira, *Toll-like receptor and RIG-I-like receptor signaling*. *Ann N Y Acad Sci*, 2008. **1143**: p. 1-20.
5. Takeda, K. and S. Akira, *Toll-like receptors in innate immunity*. *Int Immunol*, 2005. **17**(1): p. 1-14.
6. Huysamen, C. and G.D. Brown, *The fungal pattern recognition receptor, Dectin-1, and the associated cluster of C-type lectin-like receptors*. *FEMS Microbiol Lett*, 2009. **290**(2): p. 121-8.
7. Yoneyama, M. and T. Fujita, *RIG-I family RNA helicases: cytoplasmic sensor for antiviral innate immunity*. *Cytokine Growth Factor Rev*, 2007. **18**(5-6): p. 545-51.
8. Takaoka, A., et al., *DAI (DLM-1/ZBP1) is a cytosolic DNA sensor and an activator of innate immune response*. *Nature*, 2007. **448**(7152): p. 501-5.
9. Chiu, Y.H., J.B. Macmillan, and Z.J. Chen, *RNA polymerase III detects cytosolic DNA and induces type I interferons through the RIG-I pathway*. *Cell*, 2009. **138**(3): p. 576-91.
10. Hornung, V., et al., *AIM2 recognizes cytosolic dsDNA and forms a caspase-1-activating inflammasome with ASC*. *Nature*, 2009. **458**(7237): p. 514-8.
11. Martinon, F., A. Mayor, and J. Tschopp, *The inflammasomes: guardians of the body*. *Annu Rev Immunol*, 2009. **27**: p. 229-65.
12. Franchi, L., et al., *Function of Nod-like receptors in microbial recognition and host defense*. *Immunol Rev*, 2009. **227**(1): p. 106-28.
13. Kawai, T. and S. Akira, *TLR signaling*. *Cell Death Differ*, 2006. **13**(5): p. 816-25.
14. Uematsu, S. and S. Akira, *Toll-like receptors and Type I interferons*. *J Biol Chem*, 2007. **282**(21): p. 15319-23.

15. Werts, C., et al., *Nod-like receptors in intestinal homeostasis, inflammation, and cancer*. J Leukoc Biol, 2011. **90**(3): p. 471-82.
16. Maekawa, T., T.A. Kufer, and P. Schulze-Lefert, *NLR functions in plant and animal immune systems: so far and yet so close*. Nat Immunol, 2011. **12**(9): p. 817-26.
17. Schroder, K. and J. Tschopp, *The inflammasomes*. Cell, 2010. **140**(6): p. 821-32.
18. Ogura, Y., et al., *Nod2, a Nod1/Apaf-1 family member that is restricted to monocytes and activates NF-kappaB*. J Biol Chem, 2001. **276**(7): p. 4812-8.
19. Strober, W. and T. Watanabe, *NOD2, an intracellular innate immune sensor involved in host defense and Crohn's disease*. Mucosal Immunol, 2011. **4**(5): p. 484-95.
20. Gutierrez, O., et al., *Induction of Nod2 in myelomonocytic and intestinal epithelial cells via nuclear factor-kappa B activation*. J Biol Chem, 2002. **277**(44): p. 41701-5.
21. Rosenstiel, P., et al., *TNF-alpha and IFN-gamma regulate the expression of the NOD2 (CARD15) gene in human intestinal epithelial cells*. Gastroenterology, 2003. **124**(4): p. 1001-9.
22. Park, J.H., et al., *RICK/RIP2 mediates innate immune responses induced through Nod1 and Nod2 but not TLRs*. J Immunol, 2007. **178**(4): p. 2380-6.
23. Inohara, N., et al., *Human Nod1 confers responsiveness to bacterial lipopolysaccharides*. J Biol Chem, 2001. **276**(4): p. 2551-4.
24. Girardin, S.E., et al., *Nod2 is a general sensor of peptidoglycan through muramyl dipeptide (MDP) detection*. J Biol Chem, 2003. **278**(11): p. 8869-72.
25. Inohara, N., et al., *Host recognition of bacterial muramyl dipeptide mediated through NOD2. Implications for Crohn's disease*. J Biol Chem, 2003. **278**(8): p. 5509-12.
26. Inohara, N., et al., *An induced proximity model for NF-kappa B activation in the Nod1/RICK and RIP signaling pathways*. J Biol Chem, 2000. **275**(36): p. 27823-31.
27. Kim, Y.G., et al., *The cytosolic sensors Nod1 and Nod2 are critical for bacterial recognition and host defense after exposure to Toll-like receptor ligands*. Immunity, 2008. **28**(2): p. 246-57.

28. Mo, J., et al., *Pathogen Sensing by Nucleotide-binding Oligomerization Domain-containing Protein 2 (NOD2) Is Mediated by Direct Binding to Muramyl Dipeptide and ATP*. J Biol Chem, 2012. **287**(27): p. 23057-67.
29. Petnicki-Ocwieja, T., et al., *Nod2 is required for the regulation of commensal microbiota in the intestine*. Proc Natl Acad Sci U S A, 2009. **106**(37): p. 15813-8.
30. Biswas, A., et al., *Induction and rescue of Nod2-dependent Th1-driven granulomatous inflammation of the ileum*. Proc Natl Acad Sci U S A, 2010. **107**(33): p. 14739-44.
31. Mizushima, N., et al., *Autophagy fights disease through cellular self-digestion*. Nature, 2008. **451**(7182): p. 1069-75.
32. Sabbah, A., et al., *Activation of innate immune antiviral responses by Nod2*. Nat Immunol, 2009. **10**(10): p. 1073-80.
33. Shaw, M.H., et al., *The ever-expanding function of NOD2: autophagy, viral recognition, and T cell activation*. Trends Immunol, 2011. **32**(2): p. 73-9.
34. van Beelen, A.J., et al., *Stimulation of the intracellular bacterial sensor NOD2 programs dendritic cells to promote interleukin-17 production in human memory T cells*. Immunity, 2007. **27**(4): p. 660-9.
35. Hofmann, K., P. Bucher, and J. Tschopp, *The CARD domain: a new apoptotic signalling motif*. Trends Biochem Sci, 1997. **22**(5): p. 155-6.
36. Kwon, D., et al., *A comprehensive manually curated protein-protein interaction database for the Death Domain superfamily*. Nucleic Acids Res, 2012. **40**(Database issue): p. D331-6.
37. Park, H.H., et al., *The death domain superfamily in intracellular signaling of apoptosis and inflammation*. Annu Rev Immunol, 2007. **25**: p. 561-86.
38. Chou, J.J., et al., *Solution structure of the RAIDD CARD and model for CARD/CARD interaction in caspase-2 and caspase-9 recruitment*. Cell, 1998. **94**(2): p. 171-80.
39. Bouchier-Hayes, L. and S.J. Martin, *CARD games in apoptosis and immunity*. EMBO Rep, 2002. **3**(7): p. 616-21.
40. Proell, M., et al., *The Nod-like receptor (NLR) family: a tale of similarities and differences*. PLoS One, 2008. **3**(4): p. e2119.

41. Tschopp, J., F. Martinon, and K. Burns, *NALPs: a novel protein family involved in inflammation*. *Nat Rev Mol Cell Biol*, 2003. **4**(2): p. 95-104.
42. Manon, F., et al., *Solution structure of NOD1 CARD and mutational analysis of its interaction with the CARD of downstream kinase RICK*. *J Mol Biol*, 2007. **365**(1): p. 160-74.
43. Zhou, P., et al., *Solution structure of Apaf-1 CARD and its interaction with caspase-9 CARD: a structural basis for specific adaptor/caspase interaction*. *Proc Natl Acad Sci U S A*, 1999. **96**(20): p. 11265-70.
44. Rosenstiel, P., et al., *A short isoform of NOD2/CARD15, NOD2-S, is an endogenous inhibitor of NOD2/receptor-interacting protein kinase 2-induced signaling pathways*. *Proc Natl Acad Sci U S A*, 2006. **103**(9): p. 3280-5.
45. Zasloff, M., *Antimicrobial peptides of multicellular organisms*. *Nature*, 2002. **415**(6870): p. 389-95.
46. Steiner, H., et al., *Sequence and specificity of two antibacterial proteins involved in insect immunity*. *Nature*, 1981. **292**(5820): p. 246-8.
47. Zasloff, M., *Magainins, a class of antimicrobial peptides from *Xenopus* skin: isolation, characterization of two active forms, and partial cDNA sequence of a precursor*. *Proc Natl Acad Sci U S A*, 1987. **84**(15): p. 5449-53.
48. Bals, R., *Epithelial antimicrobial peptides in host defense against infection*. *Respir Res*, 2000. **1**(3): p. 141-50.
49. Boman, H.G., *Antibacterial peptides: basic facts and emerging concepts*. *J Intern Med*, 2003. **254**(3): p. 197-215.
50. van 't Hof, W., et al., *Antimicrobial peptides: properties and applicability*. *Biol Chem*, 2001. **382**(4): p. 597-619.
51. Nguyen, L.T., E.F. Haney, and H.J. Vogel, *The expanding scope of antimicrobial peptide structures and their modes of action*. *Trends Biotechnol*, 2011. **29**(9): p. 464-72.
52. Soehnlein, O., *Direct and alternative antimicrobial mechanisms of neutrophil-derived granule proteins*. *J Mol Med (Berl)*, 2009. **87**(12): p. 1157-64.
53. Oudhoff, M.J., et al., *Histatins are the major wound-closure stimulating factors in human saliva as identified in a cell culture assay*. *FASEB J*, 2008. **22**(11): p. 3805-12.

54. Harris, F., S.R. Dennison, and D.A. Phoenix, *Anionic antimicrobial peptides from eukaryotic organisms*. *Curr Protein Pept Sci*, 2009. **10**(6): p. 585-606.
55. Steinstraesser, L., et al., *Host defense peptides and their antimicrobial-immunomodulatory duality*. *Immunobiology*, 2011. **216**(3): p. 322-333.
56. Wong, J.H., L. Xia, and T.B. Ng, *A review of defensins of diverse origins*. *Curr Protein Pept Sci*, 2007. **8**(5): p. 446-59.
57. Verma, C., et al., *Defensins: antimicrobial peptides for therapeutic development*. *Biotechnol J*, 2007. **2**(11): p. 1353-9.
58. Selsted, M.E. and A.J. Ouellette, *Mammalian defensins in the antimicrobial immune response*. *Nat Immunol*, 2005. **6**(6): p. 551-7.
59. Ganz, T., et al., *Defensins. Natural peptide antibiotics of human neutrophils*. *J Clin Invest*, 1985. **76**(4): p. 1427-35.
60. Harwig, S.S., T. Ganz, and R.I. Lehrer, *Neutrophil defensins: purification, characterization, and antimicrobial testing*. *Methods Enzymol*, 1994. **236**: p. 160-72.
61. Ayabe, T., et al., *The role of Paneth cells and their antimicrobial peptides in innate host defense*. *Trends Microbiol*, 2004. **12**(8): p. 394-8.
62. Lehrer, R.I., et al., *Interaction of human defensins with Escherichia coli. Mechanism of bactericidal activity*. *J Clin Invest*, 1989. **84**(2): p. 553-61.
63. Hancock, R.E. and R. Lehrer, *Cationic peptides: a new source of antibiotics*. *Trends Biotechnol*, 1998. **16**(2): p. 82-8.
64. de Leeuw, E. and W. Lu, *Human defensins: turning defense into offense?* *Infect Disord Drug Targets*, 2007. **7**(1): p. 67-70.
65. Kluver, E., K. Adermann, and A. Schulz, *Synthesis and structure-activity relationship of beta-defensins, multi-functional peptides of the immune system*. *J Pept Sci*, 2006. **12**(4): p. 243-57.
66. Tang, Y.Q., et al., *A cyclic antimicrobial peptide produced in primate leukocytes by the ligation of two truncated alpha-defensins*. *Science*, 1999. **286**(5439): p. 498-502.
67. Cole, A.M., et al., *Retrocyclin: a primate peptide that protects cells from infection by T- and M-tropic strains of HIV-1*. *Proc Natl Acad Sci U S A*, 2002. **99**(4): p. 1813-8.

68. Selsted, M.E., *Theta-defensins: cyclic antimicrobial peptides produced by binary ligation of truncated alpha-defensins*. *Curr Protein Pept Sci*, 2004. **5**(5): p. 365-71.
69. Tran, D., et al., *Microbicidal properties and cytotoxic selectivity of rhesus macaque theta defensins*. *Antimicrob Agents Chemother*, 2008. **52**(3): p. 944-53.
70. Welkos, S., et al., *Humanized theta-defensins (retrocyclins) enhance macrophage performance and protect mice from experimental anthrax infections*. *Antimicrob Agents Chemother*, 2011. **55**(9): p. 4238-50.
71. Yamasaki, K. and R.L. Gallo, *Antimicrobial peptides in human skin disease*. *Eur J Dermatol*, 2008. **18**(1): p. 11-21.
72. Brogden, K.A., *Antimicrobial peptides: pore formers or metabolic inhibitors in bacteria?* *Nat Rev Microbiol*, 2005. **3**(3): p. 238-50.
73. Rosado, C.J., et al., *The MACPF/CDC family of pore-forming toxins*. *Cell Microbiol*, 2008. **10**(9): p. 1765-74.
74. Yang, L., et al., *Barrel-stave model or toroidal model? A case study on melittin pores*. *Biophys J*, 2001. **81**(3): p. 1475-85.
75. Chang, W.K., et al., *Characterization of antimicrobial peptide activity by electrochemical impedance spectroscopy*. *Biochim Biophys Acta*, 2008. **1778**(10): p. 2430-6.
76. Wiesner, J. and A. Vilcinskas, *Antimicrobial peptides: the ancient arm of the human immune system*. *Virulence*, 2010. **1**(5): p. 440-64.
77. Bruhn, O., et al., *Antimicrobial peptides and proteins of the horse - insights into a well-armed organism*. *Vet Res*, 2011. **42**(1): p. 98.
78. McKenzie, H.A. and D.C. Shaw, *The amino acid sequence of equine milk lysozyme*. *Biochem Int*, 1985. **10**(1): p. 23-31.
79. Skerlavaj, B., et al., *Structural and functional analysis of horse cathelicidin peptides*. *Antimicrob Agents Chemother*, 2001. **45**(3): p. 715-22.
80. Oliveira Filho, J.P., et al., *Cloning, sequencing and expression analysis of the equine hepcidin gene by real-time PCR*. *Vet Immunol Immunopathol*, 2010. **135**(1-2): p. 34-42.
81. Couto, M.A., et al., *Identification of eNAP-1, an antimicrobial peptide from equine neutrophils*. *Infect Immun*, 1992. **60**(8): p. 3065-71.

82. Davis, E.G., et al., *Molecular cloning and characterization of equine NK-lysin*. *Vet Immunol Immunopathol*, 2005. **105**(1-2): p. 163-9.
83. Kuiper, H., et al., *Assignment of the PAX6 gene to bovine chromosome 15q25-->q27 by fluorescence in situ hybridization and confirmation by radiation hybrid mapping*. *Cytogenet Genome Res*, 2005. **109**(4): p. 533.
84. Davis, E.G., Y. Sang, and F. Blecha, *Equine beta-defensin-1: full-length cDNA sequence and tissue expression*. *Vet Immunol Immunopathol*, 2004. **99**(1-2): p. 127-32.
85. Looft, C., et al., *Sequence analysis of a 212 kb defensin gene cluster on ECA 27q17*. *Gene*, 2006. **376**(2): p. 192-8.
86. Bruhn, O., et al., *A novel horse alpha-defensin: gene transcription, recombinant expression and characterization of the structure and function*. *Biochem J*, 2007. **407**(2): p. 267-76.
87. Bruhn, O., et al., *The repertoire of equine intestinal alpha-defensins*. *BMC Genomics*, 2009. **10**: p. 631.
88. Schlüsselhuber, M., et al., *In vitro potential of equine DEFA1 and eCATH1 as alternative antimicrobial drugs in rhodococcosis treatment*. *Antimicrob Agents Chemother*, 2012.
89. Purcell, E.M., H.C. Torrey, and R.V. Pound, *Resonance Absorption by Nuclear Magnetic Moments in a Solid*. *Physical Review*, 1946. **69**(1-2): p. 37-38.
90. Bloch, F., W.W. Hansen, and M. Packard, *Nuclear Induction*. *Physical Review*, 1946. **69**(3-4): p. 127-127.
91. Wuthrich, K., *Protein structure determination in solution by NMR spectroscopy*. *J Biol Chem*, 1990. **265**(36): p. 22059-62.
92. Keeler, J., *Understanding NMR Spectroscopy 2010*, London: Wiley.
93. F. Lottspeich, H.Z., *Bioanalytik*. 1998, Heidelberg, Berlin: Spektrum Akademischer Verlag.
94. wuthrich, K., *NMR of Proteins and Nucleic Acids*. 1986, New York, Chichester, Brisbane, Toronto, Singapore: A Wiley-Interscience Publication, John Wiley and Sons.
95. Lehman, I.R., *DNA ligase: structure, mechanism, and function*. *Science*, 1974. **186**(4166): p. 790-7.

96. Douglas, H., *Studies on transformation of Escherichia coli with plasmids*. Journal of Molecular Biology, 1983. **166**(4): p. 557-580.
97. Mandel, M. and A. Higa, *Calcium-dependent bacteriophage DNA infection*. J Mol Biol, 1970. **53**(1): p. 159-62.
98. Mullis, K., et al., *Specific enzymatic amplification of DNA in vitro: the polymerase chain reaction*. Cold Spring Harb Symp Quant Biol, 1986. **51 Pt 1**: p. 263-73.
99. Gill, S.C. and P.H. von Hippel, *Calculation of protein extinction coefficients from amino acid sequence data*. Analytical Biochemistry, 1989. **182**(2): p. 319-326.
100. Laemmli, U.K., *Cleavage of structural proteins during the assembly of the head of bacteriophage T4*. Nature, 1970. **227**(5259): p. 680-5.
101. Meierhenrich, U.J., et al., *Circular dichroism of amino acids in the vacuum-ultraviolet region*. Angew Chem Int Ed Engl, 2010. **49**(42): p. 7799-802.
102. Chen, Y.H. and J.T. Yang, *A new approach to the calculation of secondary structures of globular proteins by optical rotatory dispersion and circular dichroism*. Biochem Biophys Res Commun, 1971. **44**(6): p. 1285-91.
103. Nobbmann, U., et al., *Dynamic light scattering as a relative tool for assessing the molecular integrity and stability of monoclonal antibodies*. Biotechnol Genet Eng Rev, 2007. **24**: p. 117-28.
104. Delaglio, F., et al., *NMRPipe: a multidimensional spectral processing system based on UNIX pipes*. J Biomol NMR, 1995. **6**(3): p. 277-93.
105. Johnson, B.A., *Using NMRView to Visualize and Analyze the NMR Spectra of Macromolecules*. 2004. p. 313-352.
106. Guntert, P., C. Mumenthaler, and K. Wuthrich, *Torsion angle dynamics for NMR structure calculation with the new program DYANA*. J Mol Biol, 1997. **273**(1): p. 283-98.
107. Koradi, R., M. Billeter, and K. Wuthrich, *MOLMOL: a program for display and analysis of macromolecular structures*. J Mol Graph, 1996. **14**(1): p. 51-5, 29-32.
108. Petrey, D. and B. Honig, *GRASP2: visualization, surface properties, and electrostatics of macromolecular structures and sequences*. Methods Enzymol, 2003. **374**: p. 492-509.
109. Ramachandran, G.N., C. Ramakrishnan, and V. Sasisekharan, *Stereochemistry of polypeptide chain configurations*. J Mol Biol, 1963. **7**: p. 95-9.

110. Qin, H., et al., *Structural basis of procaspase-9 recruitment by the apoptotic protease-activating factor 1*. Nature, 1999. **399**(6736): p. 549-57.
111. Fridh, V. and K. Rittinger, *The tandem CARDs of NOD2: intramolecular interactions and recognition of RIP2*. PLoS One, 2012. **7**(3): p. e34375.
112. Szyk, A., et al., *Crystal structures of human alpha-defensins HNP4, HD5, and HD6*. Protein Sci, 2006. **15**(12): p. 2749-60.
113. de Leeuw, E., et al., *Structure-dependent functional properties of human defensin 5*. FEBS Letters, 2007. **581**(3): p. 515-520.
114. Jing, W., et al., *Solution structure of cryptdin-4, a mouse paneth cell alpha-defensin*. Biochemistry, 2004. **43**(50): p. 15759-66.
115. Wanniarachchi, Y.A., et al., *Human defensin 5 disulfide array mutants: disulfide bond deletion attenuates antibacterial activity against Staphylococcus aureus*. Biochemistry, 2011. **50**(37): p. 8005-17.
116. Jung, S., et al., *Hydramacin-1, structure and antibacterial activity of a protein from the basal metazoan Hydra*. J Biol Chem, 2009. **284**(3): p. 1896-905.
117. Satchell, D.P., et al., *Quantitative interactions between cryptdin-4 amino terminal variants and membranes*. Peptides, 2003. **24**(11): p. 1795-805.
118. Damiano, J.S. and J.C. Reed, *CARD proteins as therapeutic targets in cancer*. Curr Drug Targets, 2004. **5**(4): p. 367-74.
119. Ogura, Y., et al., *A frameshift mutation in NOD2 associated with susceptibility to Crohn's disease*. Nature, 2001. **411**(6837): p. 603-6.
120. Hugot, J.P., et al., *Association of NOD2 leucine-rich repeat variants with susceptibility to Crohn's disease*. Nature, 2001. **411**(6837): p. 599-603.
121. Ragnar Norrby, M.P., Bo Aronsson, Dominique, L. Monnet, Irja Lutsar, Ioan Stelian Bocsan, Otto Cars, Helen Giamarellou, Inge C. Gyssens. *The bacterial challenge: time to react*. 2009; Available from: http://www.emea.europa.eu/docs/en_GB/document_library/Report/2009/11/WC500008770.pdf.
122. Jung, S., et al., *Human beta-defensin 2 and beta-defensin 3 chimeric peptides reveal the structural basis of the pathogen specificity of their parent molecules*. Antimicrob Agents Chemother, 2011. **55**(3): p. 954-60.

8 Appendix

8.1 Abbreviations

µg	Microgram
1D	One-dimensional
2D	Two-dimensional
3D	Three-dimensional
A	Alanine
Å	Angstrom
AD	Acid transactivation domain
AI	After induction
Ala	Alanine
Aliph.	Aliphatic
AMP	Antimicrobial peptide
APS	Ammonium peroxydisulphate
Arg	Arginine
Asn	Asparagine
ATP	Adenosine-5'-triphosphate
B	Before treatment
BIR	Baculoviral inhibitory repeat
Bo	Magnetic field
bp	Base pairs
C	Cysteine
CARD	Caspase recruitment domain
CD	Circular dichroism
cDNA	Complementary DNA

CIITA	MHC class II transactivator
Cys	Cysteine
D	Aspartic acid
DAMP	Danger associated molecular pattern
DC	Dendritic cells
DD	Death domain superfamily
DED	Death effector domain
DEFA1	Alpha-defensin 1
DEFB	Beta-defensin
DLS	Dynamic light scattering
DNA	Deoxyribonucleic acid
dNTP	Deoxyribonucleotide
E	Glutamic acid
E 1, E 2	Elution steps
E.coli	Escherichia coli
F	Fraction
FID	Free induction decay
FIIND	Function-to-find domain
G	Glycine
Gdn ·	HCl Guanidine hydrochloride
Gln	Glutamine
Glu	Glutamic acid
H	Histidine
HBD	Human beta-defensin
HD	Human defensin
HDP	Host defense peptide

HEPES	4-(2-hydroxyethyl)-1-piperazineethanesulphonic acid
His	Histidine
HNP	Human neutrophil peptide
H α	Alpha-proton
H β	Beta-proton
H γ	Gama-proton
I	Isoleucine
I	Spin
IB	Inclusion body
IBD	Inflammatory bowel disease
IFN	Type I interferon
Ile	Isoleucine
IPTG	Isopropyl- β -D-1-thiogalactopyranoside
IRF3	Interferon regulatory factor 3
K	Lysine
kDa	Kilo Dalton
L	Leucine
LB	Luria Broth
Leu	Leucine
LPS	Lipopolysaccharides
LRR	Leucine rich repeat
MALDI-TOF	Matrix-assisted laser desorption/ionisation-time of flight
MAPK	Mitogen-activated protein kinase
MAMP	Microbial associated molecular pattern
MAVS	Mitochondrial antiviral-signaling protein
MDP	Muramyl dipeptide

ms	Millisecond
MS	Mass spectrometry
MW	Molecular weight
MWCO	Molecular-weight cutoff
N	Asparagine
NAIP	Neuronal apoptosis inhibitor protein
NF-Kappa B	Nuclear factor kappa B
Ni ²⁺ -NTA	Nickel-nitrilotriacetic acid
NK cells	Natural killer cells
NLR	NOD-like receptors
NLRC	CARD-containing subfamily
NLRP	Pyrin containing
NMR	Nuclear magnetic resonance
NOD	Nucleotide binding and oligomerization domain
NOD1 1	Nucleotide-binding oligomerization domain containing protein 1
NOD2 2	Nucleotide-binding oligomerization domain containing protein 2
NOESY	Nuclear Overhauser and exchange spectroscopy
OD	Optical density
P	Proline
P	Pellet
PAMPs	Pathogen-associated molecular patterns
PC	Phosphatidylcholine
PCR	Polymerase Chain Reaction
PE	Phosphatidylethanolamine

ppm	Parts per milion
Pro	Proline
PRR	Pattern-recognition receptors
PYD	Pyrin domain
Q	Glutamine
R	Arginine
R. equi	Rhodococcus equi
RF	Radio frequency
RF	Radio-frequency electromagnetic radiation
RICK	Serine threonine kinase
rmsd	Root mean square deviation
RNA	Ribonucleic acid
ROS	Reactive oxygen species
RP-HPLC	Reverse Phase-High Performance Liquid Chromatography
rpm	Round per minute
S	Serine
S	Supernatant
S. zooepidemicus	Streptococcus zooepidemicus
SDS	Sodium dodecyl sulphate
SDS-PAGE	Sodium dodecyl sulphate polyacrylamide gel electrophoresis
Ser	Serine
T	Threonine
T1	Longitudinal relaxation time
T2	Transverse relaxation time
TBA	Tris-borate-EDTA buffer
TEMED	N, N, N', N'- tetramethylethylenediamine

TEV	Tobacco Etch Virus
TFA	Trifluoroacetic acid
TLR	Toll-like receptors
TMS	Tetramethylsilane
TOCSY	Total correlation spectroscopy
TRIS	Trishydroxymethylaminomethane
U	Unit
UV	Ultraviolet
V	Volt
V/V	Volume per volume
W	Washing step
Y	Tyrosine
δ	Chemical shift
μ	Magnetic moment

8.2 Curriculum Vita

Name:	Mohammad Rasool Shomali
Date of Birth:	29.08.1973
Place of Birth:	Irbid (Jordan)
Nationality:	German/Jordanian
04/2008 – present:	PhD student at the Institute of Biochemistry, Christian Albrechts University of Kiel Supervisor: Prof. Dr. J. Grötzinger
04/2005 – 03/2008:	Head of Biotechnology Lab, Gulf Pharmaceutical Industries (Julphar)/United Arab Emirates
09/2004 – 03/2005:	Analyst: Department of plant viral disease: LUFA Company/Kiel, Germany
01/2004 – 08/2004:	Research assistance at the Institute of Biochemistry, Christian Albrechts University of Kiel, Prof. Dr. Saftig's group
03/2003 – 01/2004:	Diploma thesis in biochemistry and molecular Supervisor: Prof. Dr. Paul Saftig
03/1999 – 03/2003:	Study of biochemistry and molecular biology at Christian Albrechts University of Kiel
12/1996 – 06/1998:	Study of German language
08/1995 – 10/1996:	Biology teacher
10/1991 – 06/1995:	Study of applied biology at Jordan University of Science and Technology (Bachelor)

8.3 Posters and Publications

Publications:

Marischen, L., D. Wesch, H. H. Oberg, P. Rosenstiel, A. Trad, **M. Shomali**, J. Grotzinger, O. Janssen, V. Tchikov, S. Schutze & D. Kabelitz (2011) Functional expression of NOD2 in freshly isolated human peripheral blood gammadelta T cells. *Scand J Immunol*, 74, 126-34.

Trad, A., N. Hedemann, **M. Shomali**, V. Pawlak, J. Grotzinger & I. Lorenzen (2011) Development of sandwich ELISA for detection and quantification of human and murine a disintegrin and metalloproteinase17. *J Immunol Methods*, 371, 91-6.

Trad, A., H. P. Hansen, **M. Shomali**, M. Peipp, K. Klausz, N. Hedemann, K. Yamamoto, A. Mauermann, C. Desel, I. Lorenzen, H. Lemke, S. Rose-John & J. Grotzinger (2012) ADAM17-overexpressing breast cancer cells selectively targeted by antibody-toxin conjugates. *Cancer Immunol Immunother*.

Ahmad Trad, Michel Riese, **Mohammad Shomali**, Nina Hedemann, Joachim Grötzinger Inken Lorenzen (**submitted**). The disintegrin domain of ADAM17 antagonises fibroblast-carcinoma cell interactions.

Posters:

Pawlak, V., Lorenzen, I., Spudy, B., Mohr, M., **Shomali, M.**, Sönnichsen, F., Grötzinger, J., "The disintegrin and EGF-like domain of ADAM17," Fourth International Symposium of the SFB 415 „Signal Transduction Research – Basic Principles and clinical Perspectives“, Hamburg, Germany, August 10-12, 2009

Pawlak, V., Lorenzen, I., Spudy, B., Mohr, M., **Shomali, M.**, Sönnichsen, F., Grötzinger, J., "The disintegrin and EGF-like domain of ADAM17", First International Symposium on Structural Systems Biology, Hamburg, Germany, September 24-25, 2009

8.4 Acknowledgments

Firstly I would like to thank my supervisor Prof. Dr. Joachim Grötzinger for that he trusted me with these exciting projects and for his dedicated supervision. I am very grateful for his suggestions, advice, criticism and the patience support during my doctoral studies.

I thank Prof. Dr. Stefan Rose-John for the reception at the Institute of Biochemistry and for his support.

I'd also like to thank Prof. Dr. Matthias Leippe for the acceptance to be the second referee.

A big thank for Prof. Dr. Frank D. Sönnichsen for the recording of NMR-spectra and for Prof. Dr. Andreas Tholey for the performing of mass spectrometry.

Specifically, I would like to thank Dr. Sascha Jung for constant support in analysis of NMR-spectra and Dr. Inken Lorenzen for her critical discussions and advices.

I thank Dr. Björn Spudy for initial training as I started with my doctoral study. I thank Dr. Marwan Tayeh and Dr. Ahmad Trad for the prompt and thorough proofreading.

I thank all current and former members of the Grötzinger's group for motivating work environment, friendly atmosphere and technical suggestions.

Finally a very big thank to my wife, children and parents for putting up with me during my studies and tireless support.

8.5 Declaration

I hereby declare, Mohammad Rasool Shomali, that this thesis, and the research it describes, is entirely my own work; except for scientific advices given by my doctoral supervisor Prof. Dr. Joachim Grötzinger and the work was done according to good scientific practice. In addition, no other aids were used besides those that were stated.

Moreover, the present thesis has not been presented in part or whole, for any other degree or award and I have not been terminated other doctoral studies.

Kiel,

Mohammad Rasool Shomali